The Effect of Topography on Surface Behavior of *Pseudomonas aeruginosa*

Yow-Ren Chang

Dissertation submitted to the faculty of the Virginia Polytechnic Institute and State University in partial fulfillment of the requirements for the degree of

Doctor of Philosophy In

Chemical Engineering

William A. Ducker (chair)

Eric R. Weeks

Joseph O. Falkinham

Richey M. Davis

Michael J. Bortner

September 6, 2019

Blacksburg, Virginia

Keywords: surface topography, *Pseudomonas aeruginosa*, biofilms, tracking, microscopy, colloidal crystals

ABSTRACT

The Effect of Topography on Surface Behavior of *Pseudomonas aeruginosa*

Yow-Ren Chang

Bacterial biofilms are communities of micro-organisms encased a self-produced extracellular matrix. While they form readily in a nature, biofilm formation in man-made systems have economic and health consequences. Prior research demonstrated that topographical features comprised of uniform, micro-meter sized particles hindered the biofilm formation of *Pseudomonas aeruginosa* (*P. aeruginosa*), an opportunistic human pathogen. The goal of the present work is to 1) further develop a potential anti-biofilm coating by improving its robustness and 2) study the mechanism(s) by which surface topography hinders biofilm formation. The robustness of a topographical coating comprised of an array of silica particles is improved by the introduction of silica bridges through a sol-gel reaction. To study the mechanism(s), specifically, we hypothesized that the motion, or surface motility, of *P. aeruginosa* is hindered by the presence of micro-meter scale obstacles via physical obstruction. To test this, we analyzed the behavior of single *P. aeruginosa* cells at micron-scale spatial resolutions using time-lapse fluorescence microscopy, image analysis, and particle tracking techniques. We fabricated various types of micron-scale topography with curvature (particle arrays) and recti-linear features (vertical steps) and varied the critical dimension within the range of 0.5 – 10 μm which spans the dimensions of a typical *P. aeruginosa* cell. We found that there was a threshold feature size of 1-2 μm at which bacterial surface motility is drastically impacted.

On positively curved topography (particle arrays), we found that the frequent obstacles reduced the average speed of a bacterium from 6.2 $\pm$ 0.3 μm per 5 min on a flat surface to 2.1 $\pm$ 0.3 μm per 5 min on an array of 2 μm particles. Furthermore, we observed that bacteria often move in-between particles, suggesting that bacteria have difficulty climbing over tall obstacles. To further investigate *P. aeruginosa*'s ability to cope with topography, we examined the effect of recti-linear features (vertical steps) on surface motility. We found that step heights > 0.9 μm drastically reduced the probability of crossing and that the average speed when approaching the step is reduced by a factor of 2. Interestingly, we find that bacteria have a slight preference to traverse down which is against the direction of gravity in our system. In summary, these results offer insights into how a surface motile bacterium copes with a topographical surface. Our data indicate that the topography of a surface can impede the surface motility of bacterium and thus, may be an important mechanism by which topography prevents biofilm formation.

ABSTRACT (GENERAL AUDIENCE)

The Effect of Topography on Surface Behavior of *Pseudomonas aeruginosa*

Yow-Ren Chang

Bacteria and other micro-organisms can grow on surfaces such as medical devices and cause infections. Other examples of where bacteria can grow are on drains and pipes causing clogging, and on the hulls of ships, thus increasing drag. The goal of the current work is to investigate material coatings that resist the attachment and growth of bacteria on surfaces. We demonstrate that changing the roughness of the surface can reduce the number of bacteria found on the surface. More specifically, we have made surfaces covered with spheres that are approximately the same size as a bacterium, about 1 micrometer (10x smaller than the diameter of hair). We find that the spheres act as physical obstacles that block bacteria from moving on a surface. These results suggest that changing the micro-scale geometry of a surface may reduce the rate of infections on medical devices or hinder the growth of bacteria in other systems.

ACKNOWLEGEMENTS

I will like to take the opportunity to thank the many people who have helped me during my time at Virginia Tech. Thank you to all my fellow group members for their support: Prudvi Gaadam, Zechen Zhang, Jimmy Ritter, Lt. Alex Kriegel, Htwe Mon, and Jon Hittel. In addition, I would like to acknowledge fellow graduate students: Devon Albert, Travis Murphy, Ethan Smith, Mick Williams, Ami Jo, Han Chen, and Jimmy Dickmann. I would also like to thank my committee members for their helpful discussions and suggestions while working on this dissertation. Specifically, I'd like to thank Joe Falkinham for helping me get started with micro-biological experiments. Without his help, this work would not be possible. I'd also like to thank Eric Weeks for being an inquisitive collaborator and excellent mentor. He has given me an appreciation for image and data analysis and I have learned much while working with him. I want to especially thank my adviser, William Ducker. He is an adviser who is generous with his time and knowledge and strives to challenge you to be become a better and more rigorous scientist. Finally, I'd like to thank my parents for their courage to immigrate to the United States in hopes of a better future. My opportunity to purse higher education is a direct consequence of their hard work and sacrifice.

TABLE OF CONTENTS

TABLE OF FIGURES

ATTRIBUTION

This dissertation contains copies of manuscripts that have been published or submitted for publication. The papers that constitute Chapters 2, 3, and 4 are listed below along with details on author contribution to the work. All manuscripts are reproduced with permission.

Chapter 2

Full citation: Chang, Y.R.; Taylor, S.; Duncan, S.; Mazilu, D. A.; Ritter, A. L.; Ducker, W. A., Fabrication of stabilized colloidal crystal monolayers. *Colloids and Surfaces A: Physicochemical and Engineering Aspects* **2017,** *514*, 185-191.

DOI: https://doi.org/10.1016/j.colsurfa.2016.11.050

Author contribution: Y.C. and W.A.D designed experiments. Y.C., A.L.R., and W.A.D. analyzed the results. S.T. and S.D. were undergraduates working under the supervision of Y.C. and performed peel test experiments. A.L.R. performed abrasion tests of layer-by-layer samples. D.A.M. provided silica layer-by-layer samples. Y.C. performed all remaining experiments.

Chapter 3

Full citation: Chang, Y.R.; Weeks, E. R.; Ducker, W. A., Surface Topography Hinders Bacterial Surface Motility. *ACS Applied Materials & Interfaces* **2018,** *10* (11), 9225-9234.

DOI: https://doi.org/10.1021/acsami.7b16715

Author contribution: Y.C., E.R.W., and W.A.D. designed experiments, analyzed results and discussed results. Y.C. performed all experiments.

Chapter 4

Full citation: Chang, Y.R.; Weeks, E. R.; Barton, D.; Dobnikar, J.; Ducker, W. A., Effect of Topographical Steps on the Surface Motility of the Bacterium *Pseudomonas aeruginosa*. Submitted to *ACS Biomaterials Science and Engineering* 2019.

Author contriubtions: Y.C., E.R.W., and W.A.D. designed experiments and analyzed results. All authors discussed results. Y.C. performed all experiments.

The following are additional publications in which I have made contributions to but are not included in this dissertation.

1. **Full citation:** Kargar, M.; Chang, Y.R.; Hoseinabad, H. K.; Pruden, A.; Ducker, W. A., Colloidal Crystals Delay Formation of Early Stage Bacterial Biofilms. *ACS Biomater Sci Eng* **2016,** *2* (6), 1039-1048.
2. **Full citation:** Mon, H.; Chang, Y.R.; Ritter, A. L.; Falkinham, J. O.; Ducker, W. A., Effects of Colloidal Crystals, Antibiotics, and Surface-Bound Antimicrobials on Pseudomonas aeruginosa Surface Density. *ACS Biomater Sci Eng* **2018,** *4* (1), 257-265.
3. **Full citation:** Hittel, J; Chang, Y.R.; Ducker, W.A. Effect of Solid Wettability and Young's Modulus on Pseudomonas Aeruginosa Surface Motility. *In preparation*.

Chapter 1 Introduction

Bacterial biofilms are communities of micro-organisms encased in a self-secreted polymeric matrix and are readily found in nature.[1-3] However, in man-made systems, biofilms often pose serious engineering challenges. For example, the side of ship hulls can be fouled by the attachment and growth of micro-organisms, thus causing drag and increasing the cost of operation and maintenance.[4] Biofilms can also form on the inside of industrial pipes,[5] thereby obstructing or disturbing flow. Finally, in medical settings, biofilms are a source of chronic and persistent infections.[6] Hospital acquired infections kill nearly 100,000 patients each year in the United States[7] and cost nearly $17 billion to treat and manage.[8]

While antibiotics are traditionally used to kill bacteria causing infections in patients, they are ineffective against cells in biofilms due to diffusional barriers conferred by the extracellular matrix,[9] the existence of persister cells, and the recent rise in antibiotic resistant strains.[10-11] Indeed, antibiotics have been shown to be less effective against bacteria in a biofilm than individual cells.[12-13] Thus, alternative engineering solutions are required to reduce the incidence of infections.

Recent examples of antibiofilm strategies include the use of liquid-infused surfaces,[14-15] surface chemical modifications,[16-18] modulation of material mechanical properties,[19-25] dynamic systems,[26-28] and the use of topographical surfaces.[29-38] Our research group has recently demonstrated that arrays of micron-scale colloidal particles (colloidal crystals) hinders the growth of biofilms formed by various micro-organisms.[39-42] Colloidal crystals made from silica particles reduced the number of the opportunistic

human pathogen *Pseudomonas aeruginosa* by up to 99% when compared to a flat silica plate.[41] These results suggest that altering the topography of a surface may be an effective method of preventing bacterial biofilm formation on medical device surfaces.

The goal of the present body of work is to investigate the mechanisms by which surface topography hinders bacterial biofilm formation. By understanding how topography inhibits biofilm formation, we can better design topographical surfaces for future anti-biofilm applications. The remaindering of this Introduction will first review the steps in bacterial biofilm formation (**Chapter 1.1**). Then, the current literature on the effects of surface topography on biofilm formation will be covered (**Chapter 1.2**). We will see in **Chapter 1.2** that there is a current knowledge gap in understanding the mechanisms of how surface topography impacts biofilm formation. As will be discussed, an understudied aspect of biofilm formation is bacterial surface motility. In **Chapter 1.3**, the current literature on how bacteria achieve surface motility is reviewed. It is hypothesized that surface topography may impact the motility of bacteria and subsequently biofilm formation.

1.1. Bacterial biofilm formation

Many micro-organisms can form biofilms but one of the best studied biofilm-forming organisms is *Pseudomonas aeruginosa* (*P. aeruginosa*) and the process has been extensively reviewed. [3, 6, 43-48] *P. aeruginosa* is a rod-shaped bacterium, whose body is approximately 3 μm long and 1 μm wide. It is an opportunistic human pathogen and is a common cause of nosocomial infections such as burn wounds and urinary tract infections.[49] Furthermore, *P. aeruginosa* commonly causes respiratory tract infections in cystic fibrosis patients.[50] Due to its medical relevance, the experimental work in

subsequent chapters will focus on *P. aeruginosa*. In order to investigate how topography impacts biofilm formation, we briefly review different processes in forming biofilms.

Figure 1-1 depicts the biofilm formation process. The steps include: surface attachment, motility, reproduction, micro-colony growth, communication, production of extracellular matrix, colony maturation, and dispersion. Prior to surface attachment, bacteria are transported to a surface by convection or active motion. Individual bacteria first can attach to a surface (reversibly or irreversibly) from bulk liquid onto a solid surface.[46, 51-53] Various factors such as hydrodynamics[54], presence of pre-conditioning films,[55-57] surface topography,[30, 58-61] and surface chemistry may all have an effect on the transport of bacteria to an interface. In addition to these physical factors, specific motility appendages or surface adhesives may also assist with transport to a surface and subsequent attachment. To date, there is no known single adhesin for *P. aeruginosa*.[62]

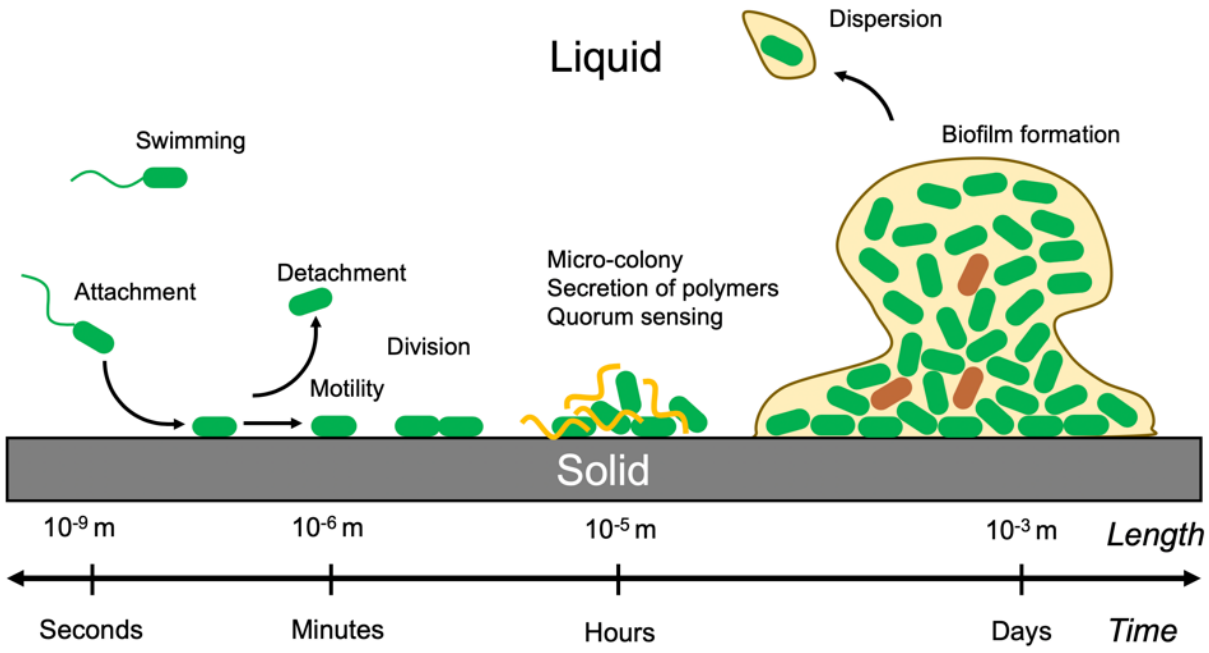

Figure 1-1. Schematic of the biofilm formation process. Biofilm formation involves several steps over various time and length scales.

Once on the surface, bacteria can use a variety of mechanisms to move. One mechanism that *P. aeruginosa* uses is twitching motility, which is achieved through the extension and retraction of thin (~10 nm) polymer strands known as type IV pili.[63] The type IV pilus is an appendage made of pilin subunits[64-65] and has been shown to exert up to 100 pN of force.[66] The type IV pilus has been shown to influence the progression into a biofilm.[67-68] Surface motility is a focus of this work and will be further discussed later in this Chapter.

After attachment, bacteria can move on the surface to organize and multiply by growth and division. *P. aeruginosa* has been shown to leave behind polymeric trails as it explores the surface; these trails guides new cells and may be a mechanism by which cells self-organize on a surface.[69] Bacteria can also multiply and divide to form structures. In *Vibrio cholerae*, a rod-shaped organism that causes cholera, it has been shown that micro-colonies form from a single parent cell and that colony formation is driven by cell division.[70-71]

As these micro-colonies form, an important component of biofilms that is produced is the extracellular matrix, or EPS. It confers protection from environmental stresses, holds groups of bacteria together, and provides a large diffusional barrier against harmful chemicals such as antibiotics.[9] In fact, the EPS matrix can comprise up to ~90% of the dry mass in a bacterial biofilm.[9] While the exact composition of the EPS is still being actively researched, it is believed that the EPS generally contains exopolysaccharides, proteins, and extracellular DNA.[9] Note that the composition of the EPS may change from species to species.

For *P. aeruginosa,* there are three exopolysaccharides: alginate, *Psl,* and *Pel*.[72] Alginate is commonly found in *P. aeruginosa* biofilms involved with cystic fibrosis.[73] Studies have demonstrated that alginate overproduction in *P. aeruginosa* results in increased resistance to the antibiotic tobramycin[74] and is thus believed to act as a protective barrier for the organism. However, alginate is not essential for biofilm formation: *algD* mutants of *P. aeruginosa* PAO1 (alginate-defective mutants) still formed biofilms albeit with more heterogenous architecture when compared to the wild-type strain.[75] Furthermore, different strains of *P. aeruginosa* may have different compositions of exopolysaccharides; alginate is not a major component of the EPS of the *P. aeruginosa* PA14 strain.[76]

Intracellular (between bacteria) communication is an important aspect of the social behaviors for bacteria when forming a biofilm. This is achieved by a process known as quorum sensing, which may modulate biomolecular processes associated with biofilm formation.[77-81] *P. aeruginosa* uses acyl homoserine lactones (AHLs) as a quorum sensing molecule.[82] Quorum sensing has been shown to impact behaviors such as swarming motility,[83] the release of extracellular DNA,[84] synthesis of exopolysaccharides,[85] and complete biofilm formation.[86] The study of quorum sensing networks has led to researchers to suggest the possibly of targeted drug therapy for the prevention of bacterial biofilm formation.[87] O'Loughlin et al. demonstrated that the synthetic molecule meta-bromo-thiolactone disrupts quorum sensing in *P. aeruginosa* and biofilm formation.[88] In a study by Ueda and Wood, quorum sensing was demonstrated to lower levels of the intercellular signaling molecule c-di-GMP (discussed below) and therefore lowering production of *Pel*.[89]

There are also intercellular (within a cell) communication processes that occur during biofilm formation. It has demonstrated that the molecule 3',5'-cyclic diguanylic acid (c-di-GMP) is an important messenger involved in *P. aeruginosa* biofilm formation.[62] In general, high levels of c-di-GMP are associated with biofilm formation and low c-di-GMP levels are associated with planktonic bacteria.[62] Very recent research suggests that *P. aeruginosa* use type IV pili in conjunction with cAMP signaling[90] to sense a surface. Furthermore, this signaling is passed down to subsequent generations of bacteria, thus adapting bacteria to surface attachment.[91]

Finally, biofilm dispersion can refer to several processes of detachment whereby individual cells or clusters of biofilm cells detach from the surface to enable other surfaces to be colonized.[92] Dispersion can be triggered by environmental[93] or nutritional conditions[94] or by phenotypic changes actively made by the organism.[95] Furthermore, quorum sensing and intra-cellular communication may play roles in biofilm dispersion.[82] Quorum sensing in *P. aeruginosa* regulates the production of *Pel*, an important matrix component that holds cells together; this influences the dispersion of cells.[82]

1.2. Current engineered methods to prevent biofilm formation

Engineering methods to prevent biofilm formation can be very broadly categorized into two types: chemical and physical methods. Chemical modifications of surfaces are well studied in the literature and may offer promising avenues towards preventing biofilm formation on surfaces. Examples include the use of silver nanoparticles,[16] surface-bound antimicrobials,[17] and polyethylene glycol (PEG) modification.[18] However, bacteria excrete extracellular matrix components such as polysaccharides, extracellular DNA, and

proteins.[9] These molecules excreted by bacteria, along with other molecules in the environment, can rapidly adsorb onto surfaces and could mask any engineered surface chemistries. Chemical treatments also actively kill micro-organisms whereas physical methods do not. Any chemical surface may provide an evolutionary selective pressure. Thus, it may be possible that bacteria evolve to overcome such surfaces.

One example of a physical method is the modification of the elastic modulus of a material. A huge body of literature has demonstrated that the mechanical properties of an underlying substrate influences the behavior of mammalian cells.[96-100] However, the effect of substrate stiffness on bacterial behaviors has not been extensively studied. Song and Ren found that the bacterial area coverage of *E. coli* RP437 and *P. aeruginosa* PAO1 was lower on a stiffer (~2.6 MPa) polydimethylsiloxane (PDMS) substrate than softer substrates.[24] In contrast however, Kolewe et al. demonstrated that fewer bacteria (*E. coli* MG1655 and *S. aureus* SH1000) adhered to softer (~40 kPa) poly(ethylene glycol) dimethacrylate hydrogels when compared to stiffer (~6.5 MPa) substrates at both 2 h and 24 h.[25] In another study, it was demonstrated that fewer *S. epidermidis* and *E. coli* cells adhere to softer polyelectrolyte multilayer substrates (~1 MPa to ~ 100 MPa).[21]

The different results reported in the literature may be due to different behaviors of the different organisms tested, the different mechanical properties investigated, the different magnitudes of elastic moduli tested, the different methods of characterizing mechanical properties, and the vastly different materials used. Hydrogels,[19-20] polyelectrolyte multilayers,[21-22] polymer brushes,[23] and PDMS are examples of materials used to study the effect of modulus on bacterial attachment.

While different studies have reported different correlations between modulus and bacterial attachment, it is still unclear by what mechanism modulus affects bacterial attachment and surface behavior. One hypothesis by Epstein et al. is that softer materials, which deform more under stresses, are unstable surfaces for bacteria to form biofilms on.[101] In an experiment with the organism *Neisseria gonorrhoeae* (type IV pili mediated motion), researchers found that that the average velocity of bacteria depended on the fluidity of the underlying phospholipid membrane.[57] Specifically, they found that the average velocity of bacteria reduced on more fluid-like surfaces and suggested that after pilus attachment, the bacteria were unable to pull the body along the surface due to slipping of the phospholipid membranes. The inability for the bacterium to move and explore the surface may serve as a disadvantage towards biofilm formation. Very recently, it was demonstrated that the surface motility of *E. coli* was affected by substrate modulus however the authors attributed the effect to motility via the flagellum.[102] It was hypothesized that the reduction in motility could be due to the cells sensing a favorable surface for biofilm formation during the initial attachment. In other words, if the cells found the surface favorable when they first attached, then they will begin to form a biofilm immediately rather than migrate on the surface to search for a favorable location for biofilm formation.

Liquid films immobilized on a solid surface is another promising physical method for the prevention of biofilm formation on surfaces.[14, 103-104] It is hypothesized that a liquid layer can act as mobile interface to which bacteria are not able to attach to or move via cell appendages. Epstein et al. demonstrated that oil-infused surfaces prevented the colonization of *P. aeruginosa* PA14, *S. aureus* SC01, and *E. coli* ZK2686 for up to 7 days.

Crystal violet staining was used to show that for all species of bacteria tested, there were at least 95% less biofilm on the oil-infused surfaces than on a state-of-the-art PEG antimicrobial surface. This method of using a liquid film on a solid surface is an extremely promising method of prevent biofilm formation on surfaces and has been recent implemented for marine anti-biofouling.[105]

Dynamic surfaces are recent responsive materials and systems that have shown great promise for antibiofilm applications. Recent work showed that shape changing topographic patterns triggered by temperature changes were shown to remove *P. aeruginosa* biofilms[26] and that this action also sensitized biofilms to subsequent antibiotic treatment.[27] Soft robotics have been used to mechanically strain tubing to remove biofilms.[28] Finally, pH changes have been utilized to alter the dispersity and thickness of poly(acrylic acid) brushes; these changes affected the attachment of *Staphylococcus epidermidis*.[106]

1.2.1. Surface topography may prevent bacterial biofilms

Modifying the topography of a surface is another promising engineering route to prevent biofilm formation. Here I focus on topographic dimensions that are about 1μm in size, which is much greater than the thickness of chemical films. Thus, topography can potentially act independently of the surface chemistry, and avoids the problem of conditioning films covering up an engineered surface chemical coating. The remainder of this literature review will focus entirely on topographic treatments and the current understanding of the mechanisms of action.

In the following discussion, it is important to distinguish between nanometer-scale roughness (features much smaller than the dimensions of a bacterium) and micrometer-scale topography (features on the size order of a bacterium, a typical *P. aeruginosa* cell is approximately 3 μm in length and 1 μm wide). Both the micrometer and nanometer length scales are important as bacteria have appendages that are nanoscopic while their bodies are microscopic.

1.2.2. The effect of nanoscale roughness on bacterial attachment is unclear

The attachment of bacteria onto nanoscale features has been extensively studied and recent reviews can be found in references.[107-110] It is apparent that the literature is divided on the effects of nanoscale topography on bacterial adhesion; some studies have reported that an increase in surface roughness increases cell attachment and other studies have reported the opposite. Interestingly, some studies have suggested that while the number density of attached bacteria was unaffected by nanoscale features, there were differences in bio-molecular response.[111-112]

It is often hypothesized that an increase in surface area leads to an increase in contact area for microorganisms but due to the conflicting reports in the literature, this hypothesis remains to be validated. A recent review attributes the ambiguity of the effect of nanoscale roughness on bacterial adhesion to the simplistic metrics used to characterize roughness.[113] Often, the RMS roughness of a surface is the sole characterization reported. This review calls for more rigorous characterization of surface nano-topography.[113]

Nanoscale features may be “covered up” by adsorption of molecules thus potentially rendering nanoscale roughness inconsequential. Indeed, studies have demonstrated that the nanoscale roughness effects are mitigated by the adsorption of protein films.[114-115] Our research efforts do not include the investigation of the effect of nanoscale roughness on bacterial attachment, yet we acknowledge that it may have some significance.

1.2.3. Bacteria may have preferential attachment sites

The effect of microscale topography on bacterial adhesion and biofilm formation is still under active investigation. However, a review of the current literature does reveal common experimental observations. In the attachment phase, many researchers have observed that bacterial preferentially attach to certain locations on a topographical surface, suggesting there are more favorable locations that others. While the understanding of why some attachment sites are more or less favorable than others is not completely known, some studies have proposed predictive models for the attachment of microorganisms to a topographical surface that may offer insights into this question.

In several studies by Diaz, the occupancy of *Pseudomonas fluorescens* in certain topographic features was greater than in other features under static conditions.[116-117] Atomic force microscopy images showed that the bacteria were situated on trenches, aligned to the long axis of the trenches. The length of the bacteria was also shortened on the trenches when compared to flat surfaces.[116]

Ling et al. found that micro-fabricated PDMS surfaces impacted the attachment pattern and biofilm development when tested in a natural environment.[36] Surfaces

showed reduction in biovolume over the course of 28 days and bacteria clearly aligned to the topography and attached in parallel lines (see Figure 1-2). The alignment of bacteria to the local topography has been observed under other experimental conditions as well.[39] The authors attribute the observed results to the "shelter" effect, where the topography shields microorganisms from environmental stress.[118] Other studies have supported this "shelter" effect hypothesis.[119]

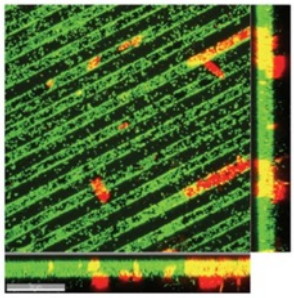

Figure 1-2. Confocal scanning laser microscopy image of a biofilm. Biofilms were grown on topographical ridges. Micro-organisms appear to have preferred attachment sites. Image reproduced from Ref [36] with permission.

1.2.4. Models of bacterial attachment onto surface topography

To date, there is no complete theory on how bacteria attach to topographical surfaces. As described above, there is not even a complete understanding of how bacteria adhere to a flat solid. In this section, we review some of the concepts in the literature that may lead to a theory in the future.

It is generally hypothesized that bacteria tend to maximize their attachment surface area. For example, Mei et al. found that the adhesion force of *S. aureus* increased with increasing surface roughness and this effect was attributed to the increase in available attachment area.[120] Ling et al. found that bacteria adhere to trenches.[36] They attributed

this to the “shelter” effect where microorganisms may choose to adhere to locations that shield them from hydrodynamic stresses,[118] but a trench also provides walls for additional attachment area. This concept is complicated by the fact that bacteria attach not only via their bodies, but also via pili, which are often more than 10 μm long, compared to the 3 μm body length for *P. aeruginosa*.

Some studies in the literature suggest a possible relationship between surface wetting/superhydrophobicity and anti-bacterial fouling. For example, Carman et al. correlated the wettability of a surface to cell attachment.[121] For superhydrophobic surfaces in the Cassie state[122] there are air pockets at the surface that may prevent attachment. Ma et al., studied how *P. aeruginosa* attached to taro leaves, which have a cone-like surface texture with dimensions on the order of 10 μm.[32] Ma et al found that fewer bacteria adhered to the surface in a non-wetted state than a wetted state.[32] Interestingly, the authors found of the bacteria that did attach, most were located at the base of the cone-like structures.

One well studied topographical system is the Sharklet topography, which is a development of the Brennan group designed to mimic shark skin.[121, 123-124] In one study, this group examined the effect of the aspect ratio of micro-topographical features, defined as the feature height divided by the feature width, on the attachment of microorganisms.[125] The data showed that, for multiple species, there were fewer attached microorganisms on the surfaces with the largest topographical aspect ratio (tall and narrow feature). This relationship held only when the topographical features were similar in dimensions to the sizes of the microorganisms.

The Brennan group has also proposed that the engineered roughness index (ERI), a dimensionless quantity, could be used to characterize a topographical surface and predict a surface's anti-fouling capability.[126] The ERI factor is defined as $(r \times d_f)/f_D$ where r is the Wenzel's roughness factor, f_D is the depressed surface fraction, and d_f is the degree of freedom of movement.[126] The ERI is a dimensionless quantity that was motivated by Wenzel and Cassie-Baxter wetting theories but was not rigorously derived. The Wenzel's roughness factor describes the ratio of the actual surface area (total surface area available) to the projected surface area (surfaces viewed from top-down). The settlement of zoospores was tested on the Sharklet topography and several other topographical patterns such as pillars, ridges, and triangles.[126] The area density of attached microorganisms was determined by microscopy, and the authors found a correlation between the ERI and the mean spore density on the solid. The greater the ERI value for a surface topography, the fewer attached microorganisms there were on the surface. However, this simple predictive theory may not work for larger topographical spacing greater than 2 μm and cannot describe curved surfaces. In addition, as pointed out in a recent review article,[110] the ERI does not take into consideration the size of the microorganism.

The Brennan group has also argued that when an organism settles between two protrusions on a topographical surface, the surface features may bend, thus producing stress gradients (termed nano-force gradients by the authors).[127] They hypothesized that there is a correlation between the magnitude of nano-force gradients and the attachment of microorganisms. The settlement of zoospores onto different variations of the Sharklet design was studied. The force required to deflect these features ranged from effectively

0 nN up to ~ 400 nN. The researchers found that the greater the force gradient, the fewer attached microorganisms (up to ~50% reduction compared to a flat surface). They hypothesized that microorganisms may be seeking a location with lower gradients as it may require less energy to stabilize itself and attach to the surface. A downside to this predictive theory was that the Sharklet design had the fewest attached microorganisms, but not the highest nano-force gradient. The authors speculate that the Sharklet topography may be more complex and more tortuous than other designed surfaces and its anti-microbial feature cannot be fully explained by the nano-force gradient hypothesis alone.

More recently, the Brennan group presented an energetic model that predicted the attachment of microorganisms to different surface topographies.[128] For a given surface topography, a lattice was overlaid and the number of attachment sites was assigned to each point. Decker et al. derived an equation that would predict the settlement density of microorganisms.[128] Comparison between Monte Carlo simulations and experimental results showed qualitative agreement. However, like the ERI, this model does not consider the size of the bacterium and it is unclear if it can explain how organisms attach to curved surfaces.

Kargar et al. studied how topographical cues influenced the adhesion of *P. aeruginosa* PAO1 and interpreted the results based on thermodynamic principles of vesicle-rigid surface interaction.[129] Specifically, the authors looked at polystyrene fibers with diameters of 70 to 1100 nm and spacing of sub-100 nm to microns (see Figure 1-3). Samples were tested in static conditions for 2.5 h and the minimum density of attached cells was found when the spacing of the fibers was less than the diameter of the bacterium,

and the diameter of the fiber was approximately the diameter of the bacterium. Four different adhesion states were analyzed: (AS) bacterium aligned with spacing, (CS) bacterium crossed the spacing, (CF) bacterium crossed the fiber, and (AF) bacterium aligned with the fiber (see Figure 1-3). For the range where the spacing of the fibers was less than diameter of the bacterium, the frequency of CS adhesions decreased with increasing fiber diameter while the AS mode increased with increasing fiber diameter. The results were interpreted in context of minimizing total free energy of adhesion to the surface. In order to attach, the bacterium must contact and deform to increase the contact area. The deformation energy must come from bending of membrane, tension energy, and pressure with increased volume. Less deformation is required to attach to a larger radius of curvature fiber. Bacteria tend to adsorb in the gaps between fibers (AS) when the gap is similar to the bacterial diameter.

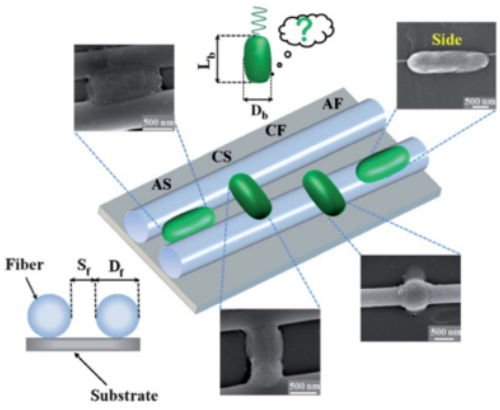

Figure 1-3. Schematic of the effects of curvature on bacterial attachment. Diagram of different ways *P. aeruginosa* attaches onto fibers with curvature similar to the scale of a bacterium. Image is reproduced from Ref [129] with permission.

1.2.5. Topography may act as a physical barrier to prevent colony formation

Several studies have suggested that bacterial attachment and growth is affected when a critical scale of the topographical features is similar to the size scale of the bacterium. A leading hypothesis is that the topography acts as a physical barrier to prevent or at least delay continued colonization of a surface.

In a study by Hochbaum and Aizenberg, it was shown how the dimensions of nano-post spacing could influence bacterial attachment, demonstrating the importance of topographical cues.[61] The authors found that when the dimensions of the post spacing approached the dimensions of *P. aeruginosa*, cells attach to posts and regularly align to achieve a high contact area as shown by fluorescent images (see Figure 1-4). Microscopy showed that bacteria were still able to freely move on and among the posts, and that mutants lacking flagella and pili also exhibited the same attachment behavior. Experiments with *S. aureus* and *E. coli* showed similar results, however the transition to strong alignment changed with the size of the bacteria species.

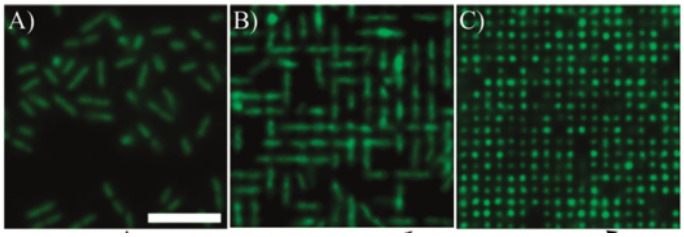

Figure 1-4. Fluorescence micrographs of *P. aeruginosa* attached to nanopost arrays with different post spacing. The spacing in the grids are a) 2.2, b) 0.9, and c) 0.7 μm. Reprinted with permission from Ref [61]. Copyright 2010 American Chemical Society.

Similar pillar structures have been shown to delay biofilm formation. Xu and Siedlecki studied how *S. epidermidis* and *S. aureus* attached and grew on polyurethane

films with submicron (400 to 500 nm in diameter) pillars.[34] Bacterial adhesion (1 or 2 h) or long term biofilm growth (2 to 5 days) was tested using a rotating disk system to mimic physiological shear stresses. The 400 nm pillars reduce *S. epidermidis* adhesion by average of 80% compared to flat over a range of shear stresses. Notably, the addition of serum reduced bacterial adhesion. However, the effect of shear stress on adhesion was mixed. In some cases, adhesion increased with increasing shear stress, and in others adhesion decreased with increasing shear stress, or simply did not change appreciably. Microscopy of biofilm samples showed the presence of more EPS and cells on flat surfaces than on pillars, suggesting these pillars do delay biofilm formation. Importantly, only individual cells could be seen on pillared structures suggesting a mechanism by which biofilm delay was achieved.

Diaz et al. studied how gold surfaces submicron topographical features affect the colonization and spreading rate of *P. fluorescens.*[130] They compared flat gold surfaces (50 – 100 nm grains and a RMS of 2 – 3 nm) to solid containing ridges that were 750 nm wide and 120 nm deep. Samples were cultured with bacteria for 10 min, 30 min, 1 h, and 2 h. After these time points, samples were removed, dried and imaged by AFM or fluorescent microscopy. From AFM data, the authors found that the “bacterial front” was disrupted on the topographical surface and claim that surface motility was reduced on the topographical surfaces but the data are at discrete time points so motility cannot be directly observed. From light microscopy, authors did find a decrease in the colonized area on a topographical surface compared to the flat control. The authors speculate that the reduction in spreading may be due to the extra energy demand associated with overcoming a physical barrier.

Kargar et al. studied how close-packed arrays of colloidal particles (colloidal crystals) could be used to prevent and delay *P. aeruginosa* colonization.[40] The authors studied how surface curvature affects the attachment of PAO1 after 24 h in a CDC biofilm reactor. Using polystyrene particles with diameter from 250 nm to 1550 nm, colloidal crystals were fabricated and coated with fetal bovine serum. Kargar et al. showed that that up to 80% fewer bacteria were found on colloidal crystals compared to a flat control (see Figure 1-5). It was originally hypothesized that bacteria would adhere less to highly curved surfaces since bacteria would have to bend to form contact but the opposite trend was observed. In unpublished work, I found that the density of *E. coli* increased with increasing particle diameter; in other words, fewer cells adhered to a more highly curved surface.

In other work of Kargar et al,[40] bacteria appeared to prefer to attach to interstitial sites which may offer more available attachment area. Increased spacing between favorable sites may then be a physical barrier for colony formation. Biofilm formation after two days was indeed delayed more on 1500 nm colloidal crystals than on flat surfaces.[39]

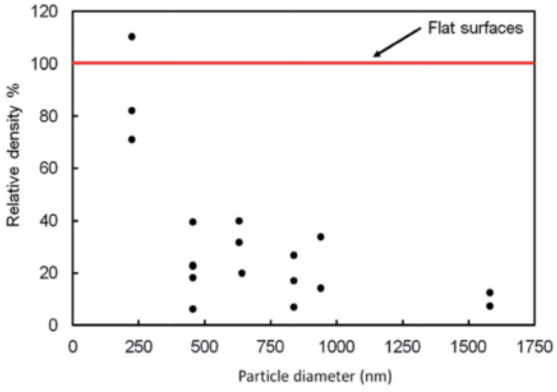

Figure 1-5. The attachment of *P. aeruginosa* is reduced by colloidal crystals. *P. aeruginosa* was cultured in a CDC Biofilm Reactor for 24 hours. There were fewer bacteria on colloidal crystals formed from larger

diameter particles. Image is reproduced from Ref [40] which is licensed under Creative Commons Attribution-Non Commercial 3.0 Unported License.

The effect of Sharklet surfaces on algae-related microorganisms was reviewed earlier, but Brennan's group have also examined the effect on bacteria. Chung et al. studied how *S. aureus* grew on the Sharklet topography (see Figure 1-6).[29] The notable difference in these studies and previous Sharklet studies is that the bacteria could attach in the grooves within the topographical features. On flat surfaces, *S. aureus* was found to have colonized up to 70% of the surface area after 21 days of culture. In comparison the Sharklet surface was only 35% covered after 21 days of culture. The authors hypothesize that the Sharklet topography provides a physical barrier for the bacteria to actually form colonies.

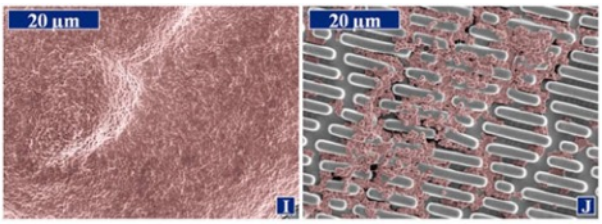

Figure 1-6. Scanning electron micrographs of *S. aureus* biofilms. Biofilms were grown on a flat surface (left) and a Sharklet surface (right), showing a dramatic reduction in biomass on the Sharklet surface. Images are reproduced from Ref [29] which is published under an open access license.

In a related work, Reddy et al. examined how uropathogenic *E. coli* behaved on flat surfaces versus the Sharklet topography.[131] The authors performed CFU counts, area coverage analysis by SEM, and migration assays. They found that the Sharklet surface reduced the CFU by ~80% on a Sharklet topography when compared to a flat control. While the study did show that cell migration perpendicular to the long axis of the

topographical features of Sharklet was reduced compared to a flat control, the bacterial strain used in these studies oddly did not have swimming or swarming motility. Both these studies highlight the potential for application of the Sharklet topography to medical devices as both *S. aureus* and pathogenic *E. coli* are more relevant in a medical setting. However, both these studies used non-motile species and a motile bacterium may not hindered by the Sharklet topography. The Sharklet design is an excellent example of how nature has inspired engineering efforts to achieve a certain goal (in this case, prevention of bacterial adhesion and growth). Many other research groups have taken inspiration from nature to design functional materials for the prevention of biofilm formation and their recent efforts are reviewed in references.[132-133]

Ling et al. have studied how *P. aeruginosa* attaches to and forms biofilms on different micron-sized surface topographies.[37] Here, features sizes around 500 nm to 2 μm and different shapes made from PDMS were used to test the adhesion of *P. aeruginosa* in a flow cell and static culture conditions. For flow experiments, cells were pumped through the chamber for 1 h to determine adhesion or for 24 h with media to study biofilm formation. Interestingly, the authors found for initial attachment the topographical surfaces performed no better than a flat surface. Indeed, even the Sharklet topography did not have a statistically significant reduction in cell attachment compared to a flat surface. Interesting, experiments showed little to no biomass on the flat surface which questions the effect of surface micro-topography on biofilm formation. However, it is possible that the positioning of samples in a flow chamber may have an impact on how *P. aeruginosa* attaches onto the surface and subsequently, how a biofilm develops.

A follow-up study by the same group however showed that *E. coli* may behaves very differently on topographical surfaces.[134] Graham et al., first studied how *E. coli* attached to different materials and found that fewer bacteria adhered to surfaces with the lowest surface energy. While they found that nanoscale features did not significantly impact the adhesion of *E. coli*, they did find an effect of microscale topographical features under both static and flow conditions. The topographical features used in this study were not the same as the previous study, but are still molded from PDMS. Clearly, *E. coli* attachment was reduced on topographical features when compared to a flat surface, most notably on circular patterns rather than linear patterns. It is highly likely that the difference in observed trends in attachment between this study and the previous study is due to differences between *P. aeruginosa* and *E. coli*.

So far, we have seen several examples that suggest surface micro-topography hinders bacterial biofilm formation via physical obstruction. Another example of a physical interaction between surface topography and micro-organisms that is of interest is the use of nanopillars. Ivanova et al. found that the wings of cicadas are antimicrobial surfaces and that the effect was attributed to physical rupture of bacterial membranes (see Figure 1-7).[135] Furthermore, it has been demonstrated that the effect is mechanical; weaker cell membranes resulted in more efficient antimicrobial properties.[136] The high aspect ratio nano-pillar geometry was replicated using black silicon and this material had similar antimicrobial properties as the cicada wings.[137] These examples suggest that physical rupture of cells is another potential role of surface topography in preventing biofilm formation.

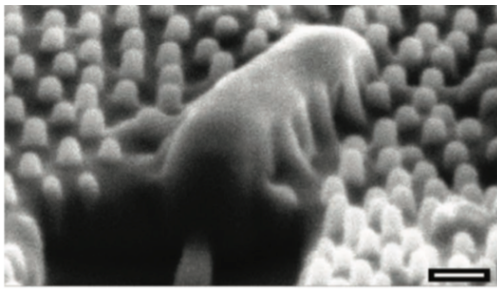

Figure 1-7. Cicada wings are antimicrobial. SEM image of a *P. aeruginosa* cell ruptured after contact with the nano-pillar topography found on cicada wings. Image is reproduced from Ref [135] with permission from John Wiley & Sons.

Overall, the results from experiments with micro-scale topography and bacterial biofilms indicate that there is a critical scale specific to the dimensions of the bacteria that is required in order to control cell attachment. However, this may limit broader applicability of surface topography in preventing bacterial adhesion if there are multiple species of different sizes colonizing a surface. The role of topography in bacterial surface attachment and biofilm formation is still not completely understood. To date, many studies have described the phenomenological effects of surface topography on biofilm formation and some have hypothesized a mechanism of action. Future studies are required to test these hypothesized mechanisms. One of the hypotheses that will be examined in this dissertation is that surface motility is impacted by topography, thus I will review current literature on how bacteria achieve surface motility through type IV pili.

1.3. Surface motility

In Chapters 3 and 4, we focus on how surface topography influences the motility of *P. aeruginosa*. The ability of an organism to move on a surface may assist it in finding nutrients,[138] participate in social behaviors, organize into micro-colonies,[69] and to explore

and colonize new areas on a surface.[139] Thus, the inhibition of surface motility by topographical features may be a mechanism by which topography delays biofilm formation.

Surface motility of *P. aeruginosa* is achieved by the extension and retraction of type IV pili.[63, 66] Recent experiments utilizing a combination of high-resolution microscopy and particle tracking techniques have demonstrated that this motility is comprised of many complex behaviors.[140] Figure 1-8 is data from our research lab, showing the trajectory of the leading (blue) and trailing (red) ends of a single *P. aeruginosa* cell over the course of approximately 1 minute.

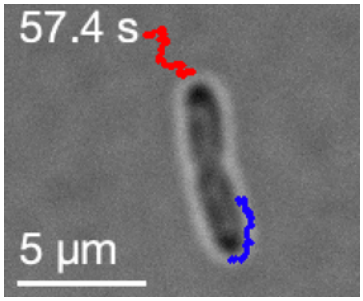

Figure 1-8. Brightfield image of a single *P. aeruginosa* cell and its trajectory. The trajectory shows the position of the leading (blue) and trailing (red) ends of the bacterium over the course of approximately 1 minute at 100 ms time resolution.

Jin et al. demonstrated that the motion of single cells of *P. aeruginosa* can be decomposed into slow and fast motions.[141] In background work that is not reported in the papers assembled for this dissertation, I used Jin et al.'s procedures to calculated the instantaneous velocity of a bacterium based on denoised positional data (see Figure 1-9. For the conditions used in the dissertation, I find that there are rare, large instantaneous velocity values that Jin et al. termed slingshots. Recent simulation work demonstrated

that just two pili are required to obtain the motility behaviors of *P. aeruginosa* observed experimentally.[142]

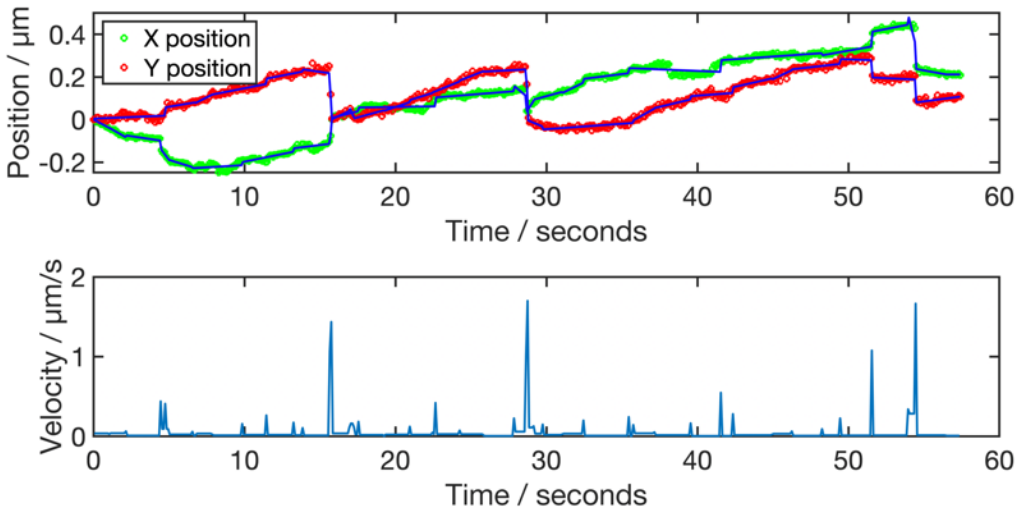

Figure 1-9. Denoised position of a cell and its instantaneous velocity. The large vertical steps in the top frame are high velocity events.

The detailed mechanisms of *P. aeruginosa* surface motility may offer important insights into how surface motile bacteria adapt to different surfaces and environmental conditions. In the following discussion, it should be noted that it is currently unclear if any changes in motility are due to responses from active sensors that bacteria may have or changes are simply due to the biophysical effects of the environment. Jin et al. suggests that the slingshot mechanism may be a way for bacteria to efficiently navigate through viscous environments.[141] In fact, recent research suggests that *P. aeruginosa* slingshot more often on soft surfaces,[23] suggesting that bacteria may adapt their motility in response to surface moduli. Furthermore, the motion of *P. aeruginosa* was shown to be more unidirectional under nutrient deficient conditions and that motion was more stalled under nutrient rich conditions.[138] It was demonstrated that stalled motion was correlated

with symmetric localization of FimX, a protein involved in type IV pili assembly, suggesting that bacteria may adaptive their motility in response to available nutrients.[138] This behavior is distinctly different that chemotaxis, where an organism may respond to a gradient in chemical concentration. Recent research demonstrates that *P. aeruginosa* can rapidly alter their surface twitching motility in response to chemical gradients; specifically, single cells were found to reverse direction more often when moving away from attractants.[143]

Recent research has also demonstrated that the type IV pilus may act as a force sensor that the bacterium uses to know when it is on a surface and to trigger biofilm formation. In *P. aeruginosa*, pilus retraction was shown to be involved in the Chp chemosensory system, which controls cAMP production, a signaling molecule implicated in virulence.[90] cAMP levels were monitored through fluorescence reporters; increased fluorescence intensities were associated with contact with a solid surface and pilus retraction.[90] In the organism *Caulobacter crescentus*, the lack of tight adherence (tad) pili retraction have been shown to stimulate the synthesis of adhesive compounds called holdfasts.[144] This work suggests this bacterium senses that it is on a surface when the pilus is unable to fully retract due to attachment to the surface; this action then triggers the attachment to a surface.[144]

Type IV pili have conferred a variety of behaviors that may assist a bacterium in adapting to life on a surface. It has been shown that *P. aeruginosa* can adopt different motility modes termed walking where the long axis of the cell body is perpendicular or tilted relative to an interface or crawling, where the body is parallel to an interface.[139] Different orientations leads to different surface motilities; the walking mode has been

shown to be more diffusive whereas the crawling mode leads to directed, persistent motion.[139] The distribution of pili at one end of the bacterium also allows the bacterium to travel upstream under high shear fluid conditions; high shear re-orients the body such that type IV pili pull the body upstream.[54]

1.4. Goals of the Dissertation

The literature review demonstrates that topography affects biofilm formation. The major goal of the current work is to investigate the mechanism(s) by which surface topography hinders bacterial biofilm formation. Understanding these mechanism(s) will help inform the design of future anti-biofilm topographical surfaces. Specifically, the work focuses on how surface motility is impacted by topography. The work is presented in three Chapters. First, I present a methods paper (Chapter 2) where I developed a method to fabricate a set of coatings each consisting of packed spheres of a different radius. The critical issue was to make a film that was sufficiently robust to be used as an antibiofilm coating, that is the particles were firmly attached. This coating was used in Chapter 3. In Chapters 3 and 4, I discuss work that investigates how curved and rectilinear topographical features respectively impact the surface motility of *Pseudomonas aeruginosa*. The central hypothesis is that topography of a micrometer sizes will hinder the motility. Chapter 4 also further explores the mechanism.

References

1. Costerton, J. W.; Lewandowski, Z.; Caldwell, D. E.; Korber, D. R.; Lappin-Scott, H. M., Microbial biofilms. *Annual Reviews in Microbiology* **1995,** *49* (1), 711-745.

2. Bjarnsholt, T.; Alhede, M.; Alhede, M.; Eickhardt-Sørensen, S. R.; Moser, C.; Kühl, M.; Jensen, P. Ø.; Høiby, N., The in vivo biofilm. *Trends in Microbiology* **2013,** *21* (9), 466-474.

3. Stoodley, P.; Sauer, K.; Davies, D.; Costerton, J. W., Biofilms as complex differentiated communities. *Annual Reviews in Microbiology* **2002,** *56* (1), 187-209.

4. Schultz, M.; Bendick, J.; Holm, E.; Hertel, W., Economic impact of biofouling on a naval surface ship. *Biofouling* **2011,** *27* (1), 87-98.

5. Percival, S.; Walker, J., Potable water and biofilms: a review of the public health implications. *Biofouling* **1999,** *14* (2), 99-115.

6. Hall-Stoodley, L.; Costerton, J. W.; Stoodley, P., Bacterial biofilms: from the natural environment to infectious diseases. *Nature Reviews Microbiology* **2004,** *2* (2), 95-108.

7. Klevens, R. M.; Edwards, J. R.; Richards, C. L.; Horan, T. C.; Gaynes, R. P.; Pollock, D. A.; Cardo, D. M., Estimating Health Care-Associated Infections and Deaths in U.S. Hospitals, 2002. *Public Health Reports* **2007,** *122* (2), 160-166.

8. Hassan, M.; Tuckman, H. P.; Patrick, R. H.; Kountz, D. S.; Kohn, J. L., Cost of hospital-acquired infection. *Hospital topics* **2010,** *88* (3), 82-89.

9. Flemming, H.-C.; Wingender, J., The biofilm matrix. *Nature Reviews Microbiology* **2010,** *8* (9), 623-633.

10. Mah, T.-F.; Pitts, B.; Pellock, B.; Walker, G. C.; Stewart, P. S.; O'Toole, G. A., A genetic basis for Pseudomonas aeruginosa biofilm antibiotic resistance. *Nature* **2003,** *426* (6964), 306-310.

11. Mah, T.-F. C.; O'Toole, G. A., Mechanisms of biofilm resistance to antimicrobial agents. *Trends in Microbiology* **2001,** *9* (1), 34-39.

12. Stewart, P. S.; Costerton, J. W., Antibiotic resistance of bacteria in biofilms. *The lancet* **2001,** *358* (9276), 135-138.

13. Anderl, J. N.; Franklin, M. J.; Stewart, P. S., Role of Antibiotic Penetration Limitation in Klebsiella pneumoniae Biofilm Resistance to Ampicillin and Ciprofloxacin. *Antimicrob. Agents Chemother.* **2000,** *44* (7), 1818-1824.

14. Epstein, A. K.; Wong, T.-S.; Belisle, R. A.; Boggs, E. M.; Aizenberg, J., Liquid-infused structured surfaces with exceptional anti-biofouling performance. *Proceedings of the National Academy of Sciences* **2012,** *109* (33), 13182-13187.

15. Howell, C.; Grinthal, A.; Sunny, S.; Aizenberg, M.; Aizenberg, J., Designing Liquid-Infused Surfaces for Medical Applications: A Review. *Adv. Mater.* **2018,** *30* (50), 1802724.

16. Agarwal, A.; Weis, T. L.; Schurr, M. J.; Faith, N. G.; Czuprynski, C. J.; McAnulty, J. F.; Murphy, C. J.; Abbott, N. L., Surfaces modified with nanometer-thick silver-impregnated polymeric films that kill bacteria but support growth of mammalian cells. *Biomaterials* **2010,** *31* (4), 680-690.

17. Iarikov, D. D.; Kargar, M.; Sahari, A.; Russel, L.; Gause, K. T.; Behkam, B.; Ducker, W. A., Antimicrobial surfaces using covalently bound polyallylamine. *Biomacromolecules* **2014,** *15* (1), 169-176.

18. Park, K. D.; Kim, Y. S.; Han, D. K.; Kim, Y. H.; Lee, E. H. B.; Suh, H.; Choi, K. S., Bacterial adhesion on PEG modified polyurethane surfaces. *Biomaterials* **1998,** *19* (7), 851-859.

19. Tuson, H. H.; Renner, L. D.; Weibel, D. B., Polyacrylamide hydrogels as substrates for studying bacteria. *Chem. Commun.* **2012,** *48* (10), 1595-1597.

20. Guégan, C.; Garderes, J.; Le Pennec, G.; Gaillard, F.; Fay, F.; Linossier, I.; Herry, J. M.; Fontaine, M. N. B.; Réhel, K. V., Alteration of bacterial adhesion induced by the substrate stiffness. *Colloids and Surfaces B: Biointerfaces* **2014,** *114*, 193-200.

21. Lichter, J. A.; Thompson, M. T.; Delgadillo, M.; Nishikawa, T.; Rubner, M. F.; Van Vliet, K. J., Substrata Mechanical Stiffness Can Regulate Adhesion of Viable Bacteria. *Biomacromolecules* **2008,** *9* (6), 1571-1578.

22. Saha, N.; Monge, C.; Dulong, V.; Picart, C.; Glinel, K., Influence of Polyelectrolyte Film Stiffness on Bacterial Growth. *Biomacromolecules* **2013,** *14* (2), 520-528.

23. Zhang, R.; Ni, L.; Jin, Z.; Li, J.; Jin, F., Bacteria slingshot more on soft surfaces. *Nature Communications* **2014,** *5*, 5541.

24. Song, F.; Ren, D., Stiffness of Cross-Linked Poly(Dimethylsiloxane) Affects Bacterial Adhesion and Antibiotic Susceptibility of Attached Cells. *Langmuir : the ACS journal of surfaces and colloids* **2014,** *30* (34), 10354-10362.

25. Kolewe, K. W.; Peyton, S. R.; Schiffman, J. D., Fewer Bacteria Adhere to Softer Hydrogels. *ACS Applied Materials & Interfaces* **2015**.

26. Gu, H.; Lee, S. W.; Buffington, S. L.; Henderson, J. H.; Ren, D., On-Demand Removal of Bacterial Biofilms via Shape Memory Activation. *ACS Applied Materials & Interfaces* **2016,** *8* (33), 21140-21144.

27. Lee, S. W.; Gu, H.; Kilberg, J. B.; Ren, D., Sensitizing bacterial cells to antibiotics by shape recovery triggered biofilm dispersion. *Acta Biomaterialia* **2018,** *81*, 93-102.

28. Levering, V.; Wang, Q.; Shivapooja, P.; Zhao, X.; López, G. P., Soft Robotic Concepts in Catheter Design: an On-Demand Fouling-Release Urinary Catheter. *Advanced Healthcare Materials* **2014,** *3* (10), 1588-1596.

29. Chung, K. K.; Schumacher, J. F.; Sampson, E. M.; Burne, R. A.; Antonelli, P. J.; Brennan, A. B., Impact of engineered surface microtopography on biofilm formation of Staphylococcus aureus. *Biointerphases* **2007,** *2* (2), 89-94.

30. Díaz, C.; Schilardi, P. L.; dos Santos Claro, P. C.; Salvarezza, R. C.; Fernández Lorenzo de Mele, M. A., Submicron Trenches Reduce the Pseudomonas fluorescens Colonization Rate on Solid Surfaces. *ACS Applied Materials & Interfaces* **2009,** *1* (1), 136-143.

31. Epstein, A. K.; Hong, D.; Kim, P.; Aizenberg, J., Biofilm attachment reduction on bioinspired, dynamic, micro-wrinkling surfaces. *New Journal of Physics* **2013,** *15* (9), 095018.

32. Ma, J.; Sun, Y.; Gleichauf, K.; Lou, J.; Li, Q., Nanostructure on taro leaves resists fouling by colloids and bacteria under submerged conditions. *Langmuir : the ACS journal of surfaces and colloids* **2011,** *27* (16), 10035-10040.

33. Perni, S.; Prokopovich, P., Micropatterning with conical features can control bacterial adhesion on silicone. *Soft Matter* **2013,** *9* (6), 1844-1851.

34. Xu, L.-C.; Siedlecki, C. A., Submicron-textured biomaterial surface reduces staphylococcal bacterial adhesion and biofilm formation. *Acta Biomaterialia* **2012,** *8* (1), 72-81.

35. Lin, J.; Wen, G.; Peihong, X.; Hainan, G.; Ming, Z.; Chen, Z.; Yali, Z.; Dong, H., Quantitative assay for the colonization ability of heterogeneous bacteria on controlled nanopillar structures. *Nanotechnology* **2015,** *26* (5), 055702.

36. Ling, G. C.; Low, M. H.; Erken, M.; Longford, S.; Nielsen, S.; Poole, A. J.; Steinberg, P.; McDougald, D.; Kjelleberg, S., Micro-fabricated polydimethyl siloxane (PDMS) surfaces regulate the development of marine microbial biofilm communities. *Biofouling* **2014,** *30* (3), 323-335.

37. Ling III, J. F.; Graham, M. V.; Cady, N. C., Effect of topographically patterned poly (dimethylsiloxane) surfaces on pseudomonas aeruginosa adhesion and biofilm formation. *Nano LIFE* **2012,** *2* (04), 1242004.

38. Bhattacharjee, A.; Khan, M.; Kleiman, M.; Hochbaum, A. I., Effects of Growth Surface Topography on Bacterial Signaling in

Coculture Biofilms. **2017,** *9*, 18531−18539.

39. Kargar, M.; Chang, Y. R.; Hoseinabad, H. K.; Pruden, A.; Ducker, W. A., Colloidal Crystals Delay Formation of Early Stage Bacterial Biofilms. *ACS Biomater Sci Eng* **2016,** *2* (6), 1039-1048.

40. Kargar, M.; Pruden, A.; Ducker, W. A., Preventing bacterial colonization using colloidal crystals. *Journal of Materials Chemistry B* **2014,** *2* (36), 5962-5971.

41. Mon, H.; Chang, Y.-R.; Ritter, A. L.; Falkinham, J. O.; Ducker, W. A., Effects of Colloidal Crystals, Antibiotics, and Surface-Bound Antimicrobials on Pseudomonas aeruginosa Surface Density. *ACS Biomater Sci Eng* **2018,** *4* (1), 257-265.

42. Lagree, K.; Mon, H. H.; Mitchell, A. P.; Ducker, W. A., Impact of surface topography on biofilm formation by Candida albicans. *PLOS ONE* **2018,** *13* (6), e0197925.

43. Percival, S. L.; Malic, S.; Cruz, H.; Williams, D. W., Introduction to biofilms. In *Biofilms and Veterinary Medicine*, Springer: 2011; pp 41-68.

44. Monds, R. D.; O'Toole, G. A., The developmental model of microbial biofilms: ten years of a paradigm up for review. *Trends in microbiology* **2009,** *17* (2), 73-87.

45. Walker, J.; Marsh, P., A review of biofilms and their role in microbial contamination of dental unit water systems (DUWS). *International biodeterioration & biodegradation* **2004,** *54* (2), 87-98.

46. Petrova, O. E.; Sauer, K., Sticky situations: key components that control bacterial surface attachment. *J. Bacteriol.* **2012,** *194* (10), 2413-2425.

47. O'Toole, G.; Kaplan, H. B.; Kolter, R., Biofilm Formation as Microbial Development. *Annual Review of Microbiology* **2000,** *54* (1), 49-79.

48. Harmsen, M.; Yang, L.; Pamp, S. J.; Tolker-Nielsen, T., An update on Pseudomonas aeruginosa biofilm formation, tolerance, and dispersal. *FEMS Immunology & Medical Microbiology* **2010,** *59* (3), 253-268.

49. Bodey, G. P.; Bolivar, R.; Fainstein, V.; Jadeja, L., Infections Caused by Pseudomonas aeruginosa. *Clinical Infectious Diseases* **1983,** *5* (2), 279-313.

50. Davies, J. C., Pseudomonas aeruginosa in cystic fibrosis: pathogenesis and persistence. *Paediatric Respiratory Reviews* **2002,** *3* (2), 128-134.

51. Palmer, J.; Flint, S.; Brooks, J., Bacterial cell attachment, the beginning of a biofilm. *Journal of Industrial Microbiology & Biotechnology* **2007,** *34* (9), 577-588.

52. Persat, A.; Nadell, C. D.; Kim, M. K.; Ingremeau, F.; Siryaporn, A.; Drescher, K.; Wingreen, N. S.; Bassler, B. L.; Gitai, Z.; Stone, H. A., The Mechanical World of Bacteria. *Cell* **2015,** *161* (5), 988-997.

53. Conrad, J. C., Physics of bacterial near-surface motility using flagella and type IV pili: implications for biofilm formation. *Res. Microbiol.* **2012,** *163* (9–10), 619-629.

54. Lecuyer, S.; Rusconi, R.; Shen, Y.; Forsyth, A.; Vlamakis, H.; Kolter, R.; Stone, H. A., Shear stress increases the residence time of adhesion of Pseudomonas aeruginosa. *Biophys. J.* **2011,** *100* (2), 341-350.

55. Gómez-Suárez, C.; Pasma, J.; van der Borden, A. J.; Wingender, J.; Flemming, H.-C.; Busscher, H. J.; van der Mei, H. C., Influence of extracellular polymeric substances on deposition and redeposition of Pseudomonas aeruginosa to surfaces. *Microbiology* **2002,** *148* (4), 1161-1169.

56. Schwarz-Linek, J.; Winkler, A.; Wilson, L. G.; Pham, N. T.; Schilling, T.; Poon, W. C., Polymer-induced phase separation in Escherichia coli suspensions. *Soft Matter* **2010,** *6* (18), 4540-4549.

57. Holz, C.; Opitz, D.; Mehlich, J.; Ravoo, B. J.; Maier, B., Bacterial motility and clustering guided by microcontact printing. *Nano Lett.* **2009,** *9* (12), 4553-4557.

58. Díaz, C.; Cortizo, M. C.; Schilardi, P. L.; Saravia, S. G. G. d.; Mele, M. A. F. L. d., Influence of the nano-micro structure of the surface on bacterial adhesion. *Materials Research* **2007,** *10*, 11-14.

59. Díaz, C.; Schilardi, P.; Salvarezza, R.; de Mele, M. F. L., Have flagella a preferred orientation during early stages of biofilm formation?: AFM study using patterned substrates. *Colloids and Surfaces B: Biointerfaces* **2011,** *82* (2), 536-542.

60. Meel, C.; Kouzel, N.; Oldewurtel, E. R.; Maier, B., Three-Dimensional Obstacles for Bacterial Surface Motility. *Small* **2012,** *8* (4), 530-534.

61. Hochbaum, A. I.; Aizenberg, J., Bacteria pattern spontaneously on periodic nanostructure arrays. *Nano Lett.* **2010,** *10* (9), 3717-3721.

62. Ha, D.-G.; O'Toole, G. A., c-di-GMP and its effects on biofilm formation and dispersion: a Pseudomonas aeruginosa review. *Microbiology spectrum* **2015,** *3* (2), 10.1128/microbiolspec.MB-0003-2014.

63. Skerker, J. M.; Berg, H. C., Direct observation of extension and retraction of type IV pili. *Proc Natl Acad Sci U S A* **2001,** *98* (12), 6901-6904.

64. Maier, B.; Wong, G. C. L., How Bacteria Use Type IV Pili Machinery on Surfaces. *Trends in Microbiology*.

65. Parge, H. E.; Forest, K. T.; Hickey, M. J.; Christensen, D. A.; Getzoff, E. D.; Tainer, J. A., Structure of the fibre-forming protein pilin at 2.6 A resolution. *Nature* **1995,** *378* (6552), 32-38.

66. Maier, B.; Potter, L.; So, M.; Seifert, H. S.; Sheetz, M. P., Single pilus motor forces exceed 100 pN. *Proceedings of the National Academy of Sciences* **2002,** *99* (25), 16012-16017.

67. O'Toole, G. A.; Kolter, R., Flagellar and twitching motility are necessary for Pseudomonas aeruginosa biofilm development. *Mol. Microbiol.* **1998,** *30* (2), 295-304.

68. Klausen, M.; Aaes-Jørgensen, A.; Molin, S.; Tolker-Nielsen, T., Involvement of bacterial migration in the development of complex multicellular structures in Pseudomonas aeruginosa biofilms. *Mol. Microbiol.* **2003,** *50* (1), 61-68.

69. Zhao, K.; Tseng, B. S.; Beckerman, B.; Jin, F.; Gibiansky, M. L.; Harrison, J. J.; Luijten, E.; Parsek, M. R.; Wong, G. C., Psl trails guide exploration and microcolony formation in Pseudomonas aeruginosa biofilms. *Nature* **2013,** *497* (7449), 388-391.

70. Beroz, F.; Yan, J.; Meir, Y.; Sabass, B.; Stone, H. A.; Bassler, B. L.; Wingreen, N. S., Verticalization of bacterial biofilms. *Nature Physics* **2018,** *14* (9), 954-960.

71. Yan, J.; Sharo, A. G.; Stone, H. A.; Wingreen, N. S.; Bassler, B. L., Vibrio cholerae biofilm growth program and architecture revealed by single-cell live imaging. *Proceedings of the National Academy of Sciences* **2016,** *113* (36), E5337-E5343.

72. Ryder, C.; Byrd, M.; Wozniak, D. J., Role of polysaccharides in Pseudomonas aeruginosa biofilm development. *Current Opinion in Microbiology* **2007,** *10* (6), 644-648.

73. Govan, J. R.; Deretic, V., Microbial pathogenesis in cystic fibrosis: mucoid Pseudomonas aeruginosa and Burkholderia cepacia. *Microbiological Reviews* **1996,** *60* (3), 539-574.

74. Hentzer, M.; Teitzel, G. M.; Balzer, G. J.; Heydorn, A.; Molin, S.; Givskov, M.; Parsek, M. R., Alginate Overproduction Affects Pseudomonas aeruginosa Biofilm Structure and Function. *J. Bacteriol.* **2001,** *183* (18), 5395-5401.

75. Stapper, A. P.; Narasimhan, G.; Ohman, D. E.; Barakat, J.; Hentzer, M.; Molin, S.; Kharazmi, A.; Høiby, N.; Mathee, K., Alginate production affects Pseudomonas aeruginosa biofilm development and architecture, but is not essential for biofilm formation. *Journal of medical microbiology* **2004,** *53* (7), 679-690.

76. Wozniak, D. J.; Wyckoff, T. J. O.; Starkey, M.; Keyser, R.; Azadi, P.; O'Toole, G. A.; Parsek, M. R., Alginate is not a significant component of the extracellular polysaccharide matrix of PA14 and PAO1 Pseudomonas aeruginosa biofilms. *Proceedings of the National Academy of Sciences* **2003,** *100* (13), 7907-7912.

77. Miller, M. B.; Bassler, B. L., Quorum Sensing in Bacteria. *Annual Review of Microbiology* **2001,** *55* (1), 165-199.

78. Nealson, K. H.; Hastings, J. W., Bacterial bioluminescence: its control and ecological significance. *Microbiological Reviews* **1979,** *43* (4), 496-518.

79. Waters, C. M.; Bassler, B. L., Quorum sensing: cell-to-cell communication in bacteria. *Annu. Rev. Cell Dev. Biol.* **2005,** *21*, 319-346.

80. Ng, W.-L.; Bassler, B. L., Bacterial quorum-sensing network architectures. *Annual review of genetics* **2009,** *43*, 197.

81. Whitehead, N. A.; Barnard, A. M. L.; Slater, H.; Simpson, N. J. L.; Salmond, G. P. C., Quorum-sensing in Gram-negative bacteria. *FEMS Microbiology Reviews* **2001,** *25* (4), 365-404.

82. Solano, C.; Echeverz, M.; Lasa, I., Biofilm dispersion and quorum sensing. *Current Opinion in Microbiology* **2014,** *18*, 96-104.

83. Shrout, J. D.; Chopp, D. L.; Just, C. L.; Hentzer, M.; Givskov, M.; Parsek, M. R., The impact of quorum sensing and swarming motility on Pseudomonas aeruginosa biofilm formation is nutritionally conditional. *Mol. Microbiol.* **2006,** *62* (5), 1264-1277.

84. Allesen-Holm, M.; Barken, K. B.; Yang, L.; Klausen, M.; Webb, J. S.; Kjelleberg, S.; Molin, S.; Givskov, M.; Tolker-Nielsen, T., A characterization of DNA release in Pseudomonas aeruginosa cultures and biofilms. *Mol. Microbiol.* **2006,** *59* (4), 1114-1128.

85. Sakuragi, Y.; Kolter, R., Quorum-Sensing Regulation of the Biofilm Matrix Genes (pel) of Pseudomonas aeruginosa. *J. Bacteriol.* **2007,** *189* (14), 5383-5386.

86. Davies, D. G.; Parsek, M. R.; Pearson, J. P.; Iglewski, B. H.; Costerton, J. W.; Greenberg, E. P., The Involvement of Cell-to-Cell Signals in the Development of a Bacterial Biofilm. *Science* **1998,** *280* (5361), 295-298.

87. Kalia, V. C., Quorum sensing inhibitors: An overview. *Biotechnol. Adv.* **2013,** *31* (2), 224-245.

88. O'Loughlin, C. T.; Miller, L. C.; Siryaporn, A.; Drescher, K.; Semmelhack, M. F.; Bassler, B. L., A quorum-sensing inhibitor blocks Pseudomonas aeruginosa virulence and biofilm formation. *Proceedings of the National Academy of Sciences* **2013,** *110* (44), 17981-17986.

89. Ueda, A.; Wood, T. K., Connecting Quorum Sensing, c-di-GMP, Pel Polysaccharide, and Biofilm Formation in <italic>Pseudomonas aeruginosa</italic> through Tyrosine Phosphatase TpbA (PA3885). *PLoS Pathog* **2009,** *5* (6), e1000483.

90. Persat, A.; Inclan, Y. F.; Engel, J. N.; Stone, H. A.; Gitai, Z., Type IV pili mechanochemically regulate virulence factors in Pseudomonas aeruginosa. *Proceedings of the National Academy of Sciences* **2015,** *112* (24), 7563-7568.

91. Lee, C. K.; de Anda, J.; Baker, A. E.; Bennett, R. R.; Luo, Y.; Lee, E. Y.; Keefe, J. A.; Helali, J. S.; Ma, J.; Zhao, K.; Golestanian, R.; O'Toole, G. A.; Wong, G. C. L., Multigenerational memory and adaptive adhesion in early bacterial biofilm communities. *Proceedings of the National Academy of Sciences* **2018,** *115* (17), 4471.

92. Kim, S.-K.; Lee, J.-H., Biofilm dispersion in Pseudomonas aeruginosa. *Journal of Microbiology* **2016,** *54* (2), 71-85.

93. Applegate, D. H.; Bryers, J. D., Effects of carbon and oxygen limitations and calcium concentrations on biofilm removal processes. *Biotechnol. Bioeng.* **1991,** *37* (1), 17-25.

94. Sauer, K.; Cullen, M. C.; Rickard, A. H.; Zeef, L. A.; Davies, D. G.; Gilbert, P., Characterization of nutrient-induced dispersion in Pseudomonas aeruginosa PAO1 biofilm. *J. Bacteriol.* **2004,** *186* (21), 7312-7326.

95. Sauer, K.; Camper, A. K.; Ehrlich, G. D.; Costerton, J. W.; Davies, D. G., Pseudomonas aeruginosa displays multiple phenotypes during development as a biofilm. *J. Bacteriol.* **2002,** *184* (4), 1140-1154.

96. Wood, J. A.; McKee, C. T.; Thomasy, S. M.; Fischer, M. E.; Shah, N. M.; Murphy, C. J.; Russell, P., Substratum compliance regulates human trabecular meshwork cell behaviors and response to latrunculin B. *Investigative ophthalmology & visual science* **2011,** *52* (13), 9298-9303.

97. Engler, A. J.; Sen, S.; Sweeney, H. L.; Discher, D. E., Matrix elasticity directs stem cell lineage specification. *Cell* **2006,** *126* (4), 677-689.

98. Discher, D. E.; Janmey, P.; Wang, Y.-l., Tissue cells feel and respond to the stiffness of their substrate. *Science* **2005,** *310* (5751), 1139-1143.

99. Dalby, M. J.; Gadegaard, N.; Tare, R.; Andar, A.; Riehle, M. O.; Herzyk, P.; Wilkinson, C. D.; Oreffo, R. O., The control of human mesenchymal cell differentiation using nanoscale symmetry and disorder. *Nature materials* **2007,** *6* (12), 997-1003.

100. Fletcher, D. A.; Mullins, R. D., Cell mechanics and the cytoskeleton. *Nature* **2010,** *463* (7280), 485-492.

101. Epstein, A.; Hochbaum, A.; Kim, P.; Aizenberg, J., Control of bacterial biofilm growth on surfaces by nanostructural mechanics and geometry. *Nanotechnology* **2011,** *22* (49), 494007.

102. Song, F.; Brasch, M. E.; Wang, H.; Henderson, J. H.; Sauer, K.; Ren, D., How bacteria respond to material stiffness during attachment: a role of Escherichia coli flagellar motility. *ACS Applied Materials & Interfaces* **2017,** *9* (27), 22176-22184.

103. Chen, J.; Howell, C.; Haller, C. A.; Patel, M. S.; Ayala, P.; Moravec, K. A.; Dai, E.; Liu, L.; Sotiri, I.; Aizenberg, M.; Aizenberg, J.; Chaikof, E. L., An immobilized liquid interface prevents device associated bacterial infection in vivo. *Biomaterials* **2017,** *113*, 80-92.

104. Kovalenko, Y.; Sotiri, I.; Timonen, J. V. I.; Overton, J. C.; Holmes, G.; Aizenberg, J.; Howell, C., Bacterial Interactions with Immobilized Liquid Layers. *Advanced Healthcare Materials* **2016**, 1600948-n/a.

105. Amini, S.; Kolle, S.; Petrone, L.; Ahanotu, O.; Sunny, S.; Sutanto, C. N.; Hoon, S.; Cohen, L.; Weaver, J. C.; Aizenberg, J.; Vogel, N.; Miserez, A., Preventing mussel adhesion using lubricant-infused materials. *Science* **2017,** *357* (6352), 668.

106. Yadav, V.; Jaimes-Lizcano, Y. A.; Dewangan, N. K.; Park, N.; Li, T.-H.; Robertson, M. L.; Conrad, J. C., Tuning Bacterial Attachment and Detachment via the Thickness and Dispersity of a pH-Responsive Polymer Brush. *ACS Applied Materials & Interfaces* **2017,** *9* (51), 44900-44910.

107. Anselme, K.; Davidson, P.; Popa, A. M.; Giazzon, M.; Liley, M.; Ploux, L., The interaction of cells and bacteria with surfaces structured at the nanometre scale. *Acta Biomaterialia* **2010,** *6* (10), 3824-3846.

108. Gharechahi, M.; Moosavi, H.; Forghani, M., Effect of Surface Roughness and Materials Composition. *Journal of Biomaterials and Nanobiotechnology* **2012,** *3* (04), 541.

109. Hasan, J.; Chatterjee, K., Recent advances in engineering topography mediated antibacterial surfaces. *Nanoscale* **2015,** *7* (38), 15568-15575.

110. Graham, M. V.; Cady, N. C., Nano and microscale topographies for the prevention of bacterial surface fouling. *Coatings* **2014,** *4* (1), 37-59.

111. Rizzello, L.; Galeone, A.; Vecchio, G.; Brunetti, V.; Sabella, S.; Pompa, P. P., Molecular response of Escherichia coli adhering onto nanoscale topography. *Nanoscale research letters* **2012,** *7* (1), 1-8.

112. Rizzello, L.; Sorce, B.; Sabella, S.; Vecchio, G.; Galeone, A.; Brunetti, V.; Cingolani, R.; Pompa, P. P., Impact of Nanoscale Topography on Genomics and Proteomics of Adherent Bacteria. *ACS Nano* **2011,** *5* (3), 1865-1876.

113. Crawford, R. J.; Webb, H. K.; Truong, V. K.; Hasan, J.; Ivanova, E. P., Surface topographical factors influencing bacterial attachment. *Adv. Colloid Interface Sci.* **2012,** *179–182* (0), 142-149.

114. Preedy, E.; Perni, S.; Nipiĉ, D.; Bohinc, K.; Prokopovich, P., Surface Roughness Mediated Adhesion Forces between Borosilicate Glass and Gram-Positive Bacteria. *Langmuir : the ACS journal of surfaces and colloids* **2014,** *30* (31), 9466-9476.

115. Singh, A. V.; Vyas, V.; Patil, R.; Sharma, V.; Scopelliti, P. E.; Bongiorno, G.; Podestà, A.; Lenardi, C.; Gade, W. N.; Milani, P., Quantitative Characterization of the Influence of the Nanoscale Morphology of Nanostructured Surfaces on Bacterial Adhesion and Biofilm Formation. *PLoS ONE* **2011,** *6* (9), e25029.

116. Díaz, C.; Schilardi, P.; De Mele, M. F. L., Influence of Surface Sub-micropattern on the Adhesion of Pioneer Bacteria on Metals. *Artificial Organs* **2008,** *32* (4), 292-298.

117. Díaz, C.; Schilardi, P.; Salvarezza, R.; Fernández Lorenzo de Mele, M., Nano/microscale order affects the early stages of biofilm formation on metal surfaces. *Langmuir : the ACS journal of surfaces and colloids* **2007,** *23* (22), 11206-11210.

118. Scardino, A.; Guenther, J.; De Nys, R., Attachment point theory revisited: the fouling response to a microtextured matrix. *Biofouling* **2008,** *24* (1), 45-53.

119. Scheuerman, T. R.; Camper, A. K.; Hamilton, M. A., Effects of Substratum Topography on Bacterial Adhesion. *J. Colloid Interface Sci.* **1998,** *208* (1), 23-33.

120. Mei, L.; Busscher, H. J.; van der Mei, H. C.; Ren, Y., Influence of surface roughness on streptococcal adhesion forces to composite resins. *Dent. Mater.* **2011,** *27* (8), 770-778.

121. Carman, M. L.; Estes, T. G.; Feinberg, A. W.; Schumacher, J. F.; Wilkerson, W.; Wilson, L. H.; Callow, M. E.; Callow, J. A.; Brennan, A. B., Engineered antifouling microtopographies--correlating wettability with cell attachment. *Biofouling* **2006,** *22* (1-2), 11-21.

122. Berg, J. C., *An introduction to interfaces & colloids: the bridge to nanoscience*. World Scientific: 2010.

123. Decker, J. T.; Sheats, J. T.; Brennan, A. B., Engineered antifouling microtopographies: surface pattern effects on cell distribution. *Langmuir : the ACS journal of surfaces and colloids* **2014,** *30* (50), 15212-15218.

124. Hoipkemeier-Wilson, L.; Schumacher, J. F.; Carman, M. L.; Gibson, A. L.; Feinberg, A. W.; Callow, M. E.; Finlay, J. A.; Callow, J. A.; Brennan, A. B., Antifouling potential of lubricious, micro-engineered,

PDMS elastomers against zoospores of the green fouling alga Ulva (Enteromorpha). *Biofouling* **2004,** *20* (1), 53-63.

125. Schumacher, J. F.; Aldred, N.; Callow, M. E.; Finlay, J. A.; Callow, J. A.; Clare, A. S.; Brennan, A. B., Species-specific engineered antifouling topographies: correlations between the settlement of algal zoospores and barnacle cyprids. *Biofouling* **2007,** *23* (5-6), 307-317.

126. Schumacher, J. F.; Carman, M. L.; Estes, T. G.; Feinberg, A. W.; Wilson, L. H.; Callow, M. E.; Callow, J. A.; Finlay, J. A.; Brennan, A. B., Engineered antifouling microtopographies - effect of feature size, geometry, and roughness on settlement of zoospores of the green alga Ulva. *Biofouling* **2007,** *23* (1-2), 55-62.

127. Schumacher, J. F.; Long, C. J.; Callow, M. E.; Finlay, J. A.; Callow, J. A.; Brennan, A. B., Engineered nanoforce gradients for inhibition of settlement (attachment) of swimming algal spores. *Langmuir : the ACS journal of surfaces and colloids* **2008,** *24* (9), 4931-4937.

128. Decker, J. T.; Kirschner, C. M.; Long, C. J.; Finlay, J. A.; Callow, M. E.; Callow, J. A.; Brennan, A. B., Engineered antifouling microtopographies: an energetic model that predicts cell attachment. *Langmuir : the ACS journal of surfaces and colloids* **2013,** *29* (42), 13023-13030.

129. Kargar, M.; Wang, J.; Nain, A. S.; Behkam, B., Controlling bacterial adhesion to surfaces using topographical cues: a study of the interaction of Pseudomonas aeruginosa with nanofiber-textured surfaces. *Soft Matter* **2012,** *8* (40), 10254-10259.

130. Díaz, C.; Schilardi, P. L.; dos Santos Claro, P. C.; Salvarezza, R. C.; Fernández Lorenzo de Mele, M. n. A., Submicron trenches reduce the Pseudomonas fluorescens colonization rate on solid surfaces. *ACS applied materials & interfaces* **2009,** *1* (1), 136-143.

131. Reddy, S. T.; Chung, K. K.; McDaniel, C. J.; Darouiche, R. O.; Landman, J.; Brennan, A. B., Micropatterned surfaces for reducing the risk of catheter-associated urinary tract infection: an in vitro study on the effect of sharklet micropatterned surfaces to inhibit bacterial colonization and migration of uropathogenic Escherichia coli. *Journal of endourology / Endourological Society* **2011,** *25* (9), 1547-1552.

132. Malshe, A.; Rajurkar, K.; Samant, A.; Hansen, H. N.; Bapat, S.; Jiang, W., Bio-inspired functional surfaces for advanced applications. *CIRP Annals-Manufacturing Technology* **2013,** *62* (2), 607-628.

133. Bhushan, B., Bioinspired structured surfaces. *Langmuir : the ACS journal of surfaces and colloids* **2012,** *28* (3), 1698-1714.

134. Graham, M. V.; Mosier, A. P.; Kiehl, T. R.; Kaloyeros, A. E.; Cady, N. C., Development of antifouling surfaces to reduce bacterial attachment. *Soft Matter* **2013,** *9* (27), 6235-6244.

135. Ivanova, E. P.; Hasan, J.; Webb, H. K.; Truong, V. K.; Watson, G. S.; Watson, J. A.; Baulin, V. A.; Pogodin, S.; Wang, J. Y.; Tobin, M. J., Natural bactericidal surfaces: mechanical rupture of Pseudomonas aeruginosa cells by cicada wings. *Small* **2012,** *8* (16), 2489-2494.

136. Pogodin, S.; Hasan, J.; Baulin, Vladimir A.; Webb, Hayden K.; Truong, Vi K.; Phong Nguyen, The H.; Boshkovikj, V.; Fluke, Christopher J.; Watson, Gregory S.; Watson, Jolanta A.; Crawford, Russell J.; Ivanova, Elena P., Biophysical Model of Bacterial Cell Interactions with Nanopatterned Cicada Wing Surfaces. *Biophys. J.* **2013,** *104* (4), 835-840.

137. Ivanova, E. P.; Hasan, J.; Webb, H. K.; Gervinskas, G.; Juodkazis, S.; Truong, V. K.; Wu, A. H. F.; Lamb, R. N.; Baulin, V. A.; Watson, G. S.; Watson, J. A.; Mainwaring, D. E.; Crawford, R. J., Bactericidal activity of black silicon. *Nat Commun* **2013,** *4*.

138. Ni, L.; Yang, S.; Zhang, R.; Jin, Z.; Chen, H.; Conrad, J. C.; Jin, F., Bacteria differently deploy type-IV pili on surfaces to adapt to nutrient availability. *npj Biofilms and Microbiomes* **2016,** *2*, 15029.

139. Conrad, Jacinta C.; Gibiansky, Maxsim L.; Jin, F.; Gordon, Vernita D.; Motto, Dominick A.; Mathewson, Margie A.; Stopka, Wiktor G.; Zelasko, Daria C.; Shrout, Joshua D.; Wong, Gerard C. L., Flagella and Pili-Mediated Near-Surface Single-Cell Motility Mechanisms in P. aeruginosa. *Biophys. J.* **2011,** *100* (7), 1608-1616.

140. Burrows, L. L., Pseudomonas aeruginosa Twitching Motility: Type IV Pili in Action. *Annual Review of Microbiology* **2012,** *66* (1), 493-520.

141. Jin, F.; Conrad, J. C.; Gibiansky, M. L.; Wong, G. C., Bacteria use type-IV pili to slingshot on surfaces. *Proceedings of the National Academy of Sciences* **2011,** *108* (31), 12617-12622.

142. Brill-Karniely, Y.; Jin, F.; Wong, G. C.; Frenkel, D.; Dobnikar, J., Emergence of complex behavior in pili-based motility in early stages of P. aeruginosa surface adaptation. *Scientific Reports* **2017,** *7*.

143. Oliveira, N. M.; Foster, K. R.; Durham, W. M., Single-cell twitching chemotaxis in developing biofilms. *Proceedings of the National Academy of Sciences* **2016,** *113* (23), 6532-6537.

144. Ellison, C. K.; Kan, J.; Dillard, R. S.; Kysela, D. T.; Ducret, A.; Berne, C.; Hampton, C. M.; Ke, Z.; Wright, E. R.; Biais, N.; Dalia, A. B.; Brun, Y. V., Obstruction of pilus retraction stimulates bacterial surface sensing. *Science* **2017,** *358* (6362), 535.

Chapter 2 Fabrication of stabilized colloidal crystal monolayers

Yow-Ren Chang[1], Shane Taylor[1], Scott Duncan[1], Dan A. Mazilu[2], A. L. Ritter[1], William A. Ducker[1]*

[1.] Department of Chemical Engineering, and Center for Soft Matter and Biological Physics, Virginia Tech, Blacksburg, VA 24061, USA.

[2.] Department of Physics and Engineering, Washington and Lee University, Lexington, VA 24450, USA

2.1. Abstract

A recent report described a very simple and rapid method to prepare colloidal crystal monolayers by rubbing spherical particles between two rubber plates [C. Park *et al.*, Advanced Materials, 26 (2014) 4633]. Here we describe a commensurately simple extension of Park's procedure to prepare films that are much more robust, yet retain the overall structure of the colloidal crystal monolayer. The procedure produces solid necks that connect pairs of particles and also connect particles to the solid. These connections between particles are achieved by first forming liquid capillaries between the particles and then solidifying those necks by exposure to gas phase reactant and catalyst. We show that the stabilized films are more resistant to removal of particles during a peel test. We also show that the stabilization method is effective on silica layer-by-layer films.

2.2. Introduction

Colloidal crystal monolayers (CCMs) are films consisting of monolayers of organized particles. CCMs have a variety of applications, including anti-reflective coatings [1-2], surface enhanced Raman scattering films [3], and sensors [4], and are also used as templates for the production of patterned films. Ye and Qi have written a comprehensive review describing the many applications of colloidal crystals [5].

A recent article by Park et al. described an extremely simple method, "the rubbing method", for making CCMs [6]. In brief, spherical micro-particles are simply rubbed onto a rubber material or film. This extremely facile procedure can be used to very quickly coat large areas of objects and may be useful in many applications. Of particular interest to us is that CCMs affect the ability of bacteria to adsorb and colonize surfaces [7-8]. However, for this and some other applications, the particle film must be robust. For example, if the colloidal crystal is used to coat a catheter that is inserted into a human body, then the particles must remain on the catheter during handling, insertion, and subsequent use, both to be effective against bacteria and to avoid unwanted distribution of micro-particles within the body. Unfortunately, our experience is that the particles in CCMs produced by the rubbing method (and also by the convective [1] and surface deposition [9] methods) are very easily removed simply by wiping a tissue or a hand against the solid. This makes them impractical for some applications.

The objective of this work is to develop a simple extension to the rubbing method in which CCMs are made robust (more stable) while maintaining the essential shape and organization of the constituent particles. The increased stability is assessed by a standard peel test. The lack of stability of the particles in colloidal crystals is due to the

weak forces that hold the particles together. In the case of the rubbing methods, these forces are probably capillary forces and van der Waals forces. Stronger forces and therefore greater stability can be achieved by increasing the contact area between the spheres (the formation of necks) as shown in Figure 2-1. Several prior methods have been explored for increasing the stability of particles in the film. The most obvious method is to heat the film above the softening point such that molecular mobility is increased. This facilitates deformation of the particles and migration of molecules to form necks between particles and between particles and the underlying substrate. Necks can be developed between polymer particles with low chain melting temperatures (T_g), simply by heating above T_g [8] as is done for latex paints [10], but for a shorter time such that the particle shape is not lost. For high-melting inorganic materials, such as SiO_2, sintering requires a high temperature (>1000 °C) which may damage other components and introduce stresses that cause cracking [11].

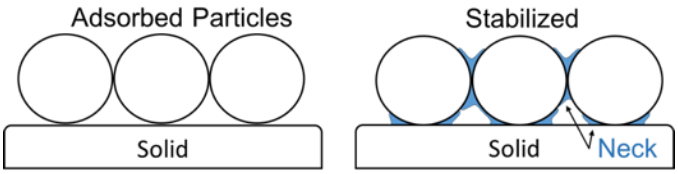

Figure 2-1. Schematic of stabilization. Our objective is to introduce solid necks between particles and between the particles and the solid.

Other methods for stabilizing colloidal crystals are hydrothermal treatment [12] and vapor deposition – either chemical vapor deposition (CVD) [13] or atomic layer deposition (ALD) [14]. Both CVD and ALD are very effective at stabilization and offer good control of

thickness, but require strictly anhydrous conditions [12] and may be time consuming to produce strong and therefore thick connections.

Here we describe a method of stabilization (see Figure 2-2) that is based on the widely-implemented sol-gel process [15]. This method is similar to that used previously by Vossen *et al.* to control the pore size in colloidal masks for creating metallic nanoparticle arrays [16]. After the particle array is formed, we clean the sample with O_2 plasma, which also creates hydroxyl groups that are the reaction sites for the sol-gel process. A small droplet of liquid tetraethylorthosilicate (TEOS) solution is infused into the surface film to produce capillaries between particles, and then the film is exposed to a vapor consisting of NH_4OH, H_2O, and ethanol to form a sol-gel, and then finally heat treated to form solid necks. Separate delivery of liquid and gas components allows us to first create the desired structure of necks by capillary forces in the liquid phase and then to maintain the neck structure by reaction gas-phase reactants only. This procedure is very simple and rapid and has only one liquid-phase step. We find that it dramatically increases the stability of particles within the colloidal crystal monolayer.

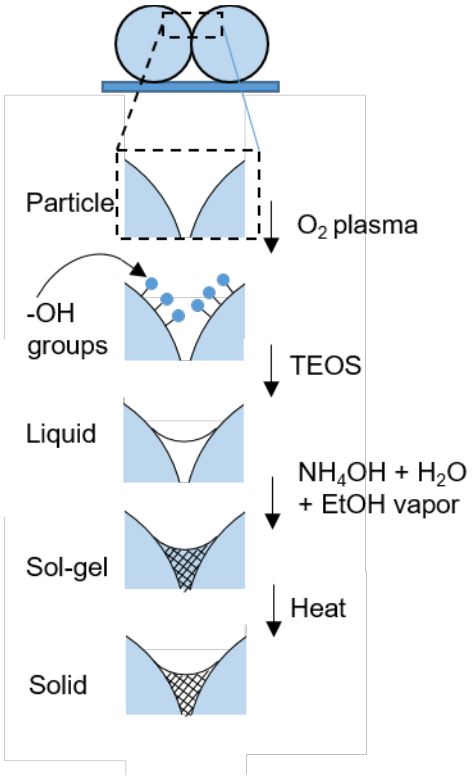

Figure 2-2. Schematic of the TEOS method.

We also applied our method to silica layer-by-layer (LbL) films. LbL deposition has found application in pressure sensors [17], catalysis [18], biosensors [19-21], electrochromism [22-23], second harmonic generation [24-25], photovoltaics [26-27], and narrow [28-29] and broadband [30] anti-reflection coatings. But in common with colloidal crystal monolayers, there is a significant challenge in making robust particle films via LbL deposition. While films of alternating polycation and polyanion layers are quite stable due to significant interleaving of the oppositely charged flexible polymer chains [31], films made of alternating polyelectrolyte and colloid layers can be removed with gentle abrasion [12]. This may be a consequence of reduced electrostatic interaction between the polyion and the rigid colloid [32].

2.3. Material and Methods

2.3.1. TEOS treatment

A schematic of the TEOS treatment is shown in Figure 2-2. Samples were O_2 plasma treated (SPI Supplies, PA) at 100 W for 1 minute to form reactive hydroxyl groups on silica surfaces. TEOS (Sigma Aldrich, MO) was diluted in ethanol as a carrier solvent. One concentration (5 % (v/v)) was used for colloidal crystal samples and two concentrations (5% and 20 % (v/v)) were used for silica LbL samples. Twenty microliters of this solution per 1 cm^2 area were pipetted onto the sample. The solution wetted the sample surface and then the ethanol was allowed to evaporate at room temperature. The TEOS should form capillary necks between particles and between the particle and substrate as the ethanol evaporates. Samples were then placed in a sealed chamber with two separate solutions, 7M ammonium hydroxide (Fisher Scientific, NH) and 8M water in ethanol (Decon Labs, PA). Lower concentration of TEOS (5 % (v/v)) samples were left in the chamber for approximately 16 h and higher concentration of TEOS (20 % (v/v)) samples were left in the chamber for approximately 40 h. Finally, the film was cured by heating at 200°C for 1 h.[15]

2.3.2. Preparation of silica colloidal crystal monolayers

Silica CCMs were fabricated using the rubbing method [6]. Polydimethylsiloxane (PDMS, Sylgard 184, Dow Corning, MI) was mixed at a 10:1 base to curing agent ratio, degassed, poured into 100 mm polystyrene petri dishes and cured at 60°C overnight. Silica particles (Fiber Optic Center Inc., MA) were sandwiched between a large sheet of PDMS, which was retained as the sample, and a small piece, which was later discarded,

and then rubbed manually in a uni-directional manner. The quality of the colloidal crystal was assessed by shining a 523 nm laser through the sample and observing the scattering pattern. Particles in excess of a monolayer were removed by rinsing with ethanol. We believe that the particle monolayer is held to the polymer surface by PDMS meniscii formed from the rubbing method (See Figure 2-3).

2.3.3. Preparation of silica LbL films

Silica LbL films consisted of 16 bilayers of alternating poly(diallyldimethylammonium chloride) (PDDA) and negatively-charged silica (SiO_2) nanoparticles on glass substrates. The PDDA was from Sigma-Aldrich and was diluted to 10 mM with deionized water. The silica nanoparticles (SNOWTEX ST-20L, Nissan Chemical) have a nominal particle size of 40–50 nm and were in a colloidal suspension at pH = 10.3 and room temperature (21° C). The glass substrates were premium microscope slides from Fisher Scientific that were cleaned according to a procedure similar to the one described in [30]. The cleaning was done under sonication in three successive twenty-minute steps, with LABTONE detergent, 1N sodium hydroxide solution, and deionized water. The cleaned slides were subsequently dried under a flow of dry nitrogen gas prior to dipping.

The dipping was done using a Stratosequence VI dipping machine from nanoStrata Inc. The microscope slides were dipped for three minutes each into the PDDA solution and the colloidal silica suspension, with three one-minute rinsing dips in deionized water between the PDDA-SiO_2 dipping steps. The slides were slowly stirred during both dipping and rinsing. After the final dip in the SiO_2 colloidal suspension, the

slides were dried under a flow of dry nitrogen gas and stored at room temperature until used for experiments. This procedure produces LbL films on both sides of the microscope slide.

2.3.4. Scanning Electron Microscopy (SEM) sample preparation and imaging

Sample structure was investigated by SEM. For cross-section imaging, samples were submerged in liquid nitrogen for at least 5 minutes, then snapped in half to expose a cross-section. All samples were sputter coated with a 5 nm layer of iridium (Leica EM ACE600) and further grounded using graphite conductive adhesive. Imaging was performed using a Zeiss LEO 1550 at 5 kV and approximately 10 mm working distance.

2.3.5. Film Robustness

Peel test

The mechanical robustness of silica CCMs was evaluated by a peel test (a variant of ASTM D1876). Standardized peel tests usually involve pre-scratching the sample with a cross-hatch pattern. This was not performed in our tests. The remaining CCMs was quantified microscopically after a peel test. A piece of Scotch tape was placed on top of a sample and pressed down onto the sample by a 100 g weight. The tape was then peeled slowly by hand such that the tape made a 90° angle with the sample surface. This was done to maintain peeling consistency from sample to sample. The samples were then imaged in brightfield with a Zeiss Imager M2 microscope. The percent area coverage by the CCM film was quantified using ImageJ. We defined a perfectly close-

packed CCM to have 100% area coverage, that is, the minimum interstitial space was included as part of the film area.

The peel test was performed for CCMs made from four different particle diameters: 1, 2, 4, and 8 μm. For each particle diameter, the percent area coverage was measured before and after TEOS treatment. Three samples of each condition were imaged at three random locations. The fraction of the film remaining after a peel test was calculated from:

$$\frac{\%\ \text{area after peel}}{\%\ \text{area before peel}}, \quad (1)$$

and the effect of the TEOS treatment on the fraction of the film remaining after a peel test was analyzed by Student's *t*-test for each colloidal crystal size.

Abrasion test

The mechanical stability of the LbL colloidal films was tested by the following abrasion procedure. A ball (diameter = 4 cm) was glued to a Petri dish cover and covered with a lens cleaning cloth (Zeiss). The Petri dish cover in turn was attached to a Mini Shaker (VWR). The sample, a 3 x 1 inch microscope slide coated with the colloidal film, rested on the cloth covered ball. A 60 gram mass was placed and on top of the slide to apply a load and create friction. The shaker then was run for 30 seconds at a speed of 400 rpm in an orbital motion, diameter, 3 mm. From the diameter of the wear spot (~ 4 mm), we estimate that the average pressure of the lens cleaning cloth on the colloidal film was greater than 10^5 N/m^2.

In order to characterize the consequence of abrading the films, we measured the UV-Vis reflectance of the films before and after abrasion (Filmetrics F-20 thin-film measurement system and a PerkinElmer Lambda 25 UV/VIS spectrophotometer (λ = 300

to 1100 nm)). The abrasion test was applied to one side of the microscope slide leaving an intact film on the opposite side of the slide. We attempted to wipe this intact film off the back side in order to enhance the changes in the reflection spectrum arising from the abrasion test. But the films on one set of treated samples (those prepared by Method 2) were so robust that we were unable to wipe them off the back side. We could correct for this difference (whether the film was wiped off the back side or not) in the analysis as discussed below.

We applied the abrasion test to sets of 16 bilayer films prepared by one of three methods: (1) Method 1: 5 % (v/v) TEOS and 16 h reaction time; (2) Method 2: 20 % (v/v) TEOS and 40 h reaction time or (3) no TEOS treatment. Each method was replicated six times. For no-TEOS and Method 1, the abrasion resistance was measured on two spots on each of three slides. One of the three fabricated Method 2 samples broke. In order to maintain six replicates for each method, the abrasion resistance was measured on three spots on each of those two Method 2 slides. Thus, the experimental design was one categorical factor with three levels (treatment by Method 1, treatment by Method 2 and no treatment) and six replications of each level. The experimental design and the statistical analysis of the results were done using the software application Design Expert from StatEase.

2.4. Results and Discussion

2.4.1. TEOS does not significantly alter the structure of colloidal crystals

Figure 2-3 contains SEM images and laser diffraction patterns showing the effect of the TEOS treatment on the morphology of films produced by the rubbing method using

1 μm microspheres. The first point to note is that the TEOS treatment did not affect the crystalline arrangement of the microspheres, or the crown (curved portion opposite the solid) of the sphere. Thus, the treatment preserved the useful features of the film. Figure 2-3d shows that the bottom half of each particle is engulfed in silica after the TEOS treatment.

It is interesting to note that, even before TEOS treatment, there were necks both between the particles and between the particles and the solid (see Figure 2-3a&c and Figure 5-5). These necks were not reported in the original work described by Park et al. [6], and they did not provide sufficient strength to maintain the film against even casual rubbing. We speculate that these necks are monomer or low-molecular-weight PDMS that was transferred to the particles when they rolled across the PDMS during the rubbing procedure. It is possible that at least some part of the PDMS necks remain after the TEOS treatment.

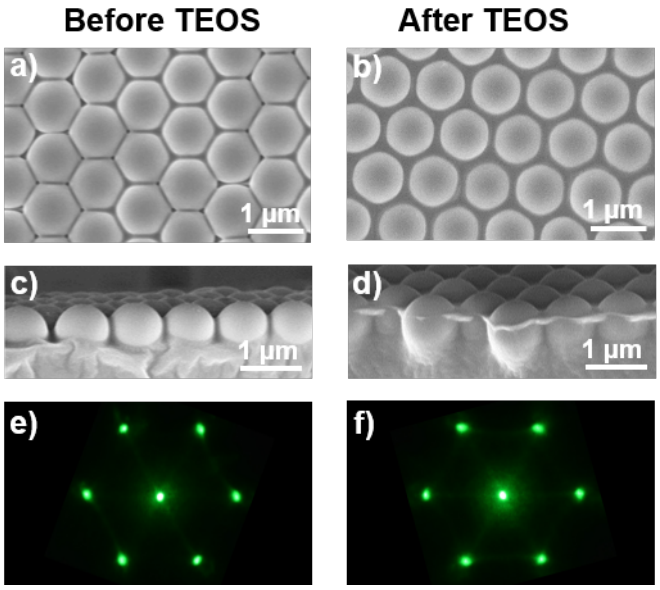

Figure 2-3. Effect of TEOS treatment on CCMs fabricated from 1 μm diameter silica microspheres on PDMS. (a-d) Top-down and cross-section SEM images. Particles appear partially embedded in PDMS. (e)

and (f) Laser scattering patterns showing that the hexagonal close packing of the spheres on the length scale of the beam diameter (~millimeter scale) is not altered by the TEOS.

The effect of the TEOS on 4 μm particles is shown in Figure 2-4. As for the 1 μm particles, SEM images show that necks were already present before the TEOS treatment, and that the arrangement of the particles was unaffected by the TEOS treatment. SEM and scattering patterns of additional particles sizes (see Figure 5-6 and Figure 5-8) show much the same effect of TEOS treatment for other particle sizes.

Comparing the 1 μm and 4 μm images we see that whereas the bottom half of the 1 μm particle CCM was engulfed in TEOS, the 4 μm particles are joined by distinct necks. We attribute this to the fact that we added the same amount of TEOS for both particle sizes, so the ratio of TEOS volume to film height is smaller for the 4 μm particles. It is interesting that the neck width on the 4 μm particles does not increase after TEOS treatment. The alteration of the neck is however manifest from two features: (1) a complex residue remains after fracture of the sample (Figure 2-4d), suggesting the neck is now brittle and (2) the increase in stability of the film described in the following section.

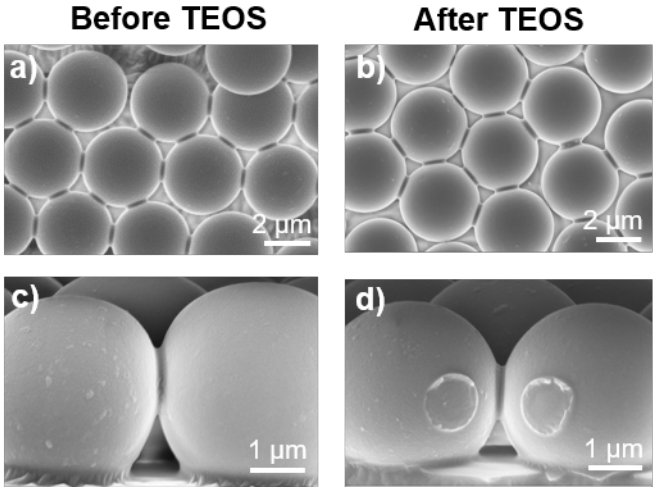

Figure 2-4. Effect of TEOS treatment on CCMs fabricated from 4 μm diameter silica microspheres on PDMS. SEM imaging again shows that TEOS does not significantly alter the organization of the particles, and that there are necks between particles before TEOS treatment.

2.4.2. TEOS increases the robustness of colloidal crystals

We assessed the robustness of CCMs formed by the rubbing method with a peel test. Without the TEOS treatment, it was clear by visual inspection that much of the CCM was removed by the peel test. Quantification of microscopic images showed that the fraction of the colloidal crystal film remaining on the surface after a peel test increased significantly with TEOS treatment (Figure 2-5). Less than 10% of the untreated film remained after a peel test, whereas nearly 100% of the TEOS treated film remained bound to the surface after peel test, which was a dramatic improvement. Confirming the obvious, a Student's t-test resulted in $p < 0.001$ for the null hypothesis that the TEOS treatment does not affect the fraction of film remaining. Considering each particle size separately, p was also less than 0.001.

Our peel-test data also allowed us to test whether the particle size had a significant effect on the film robustness. We did not find a significant effect. As stated above, we added the same amount of TEOS for each particle size. In a practical application, one might want to simply reduce the amount added for the 1 μm particle (to reduce engulfment) or increase the amount added to increase the robustness of CCMs fabricated from larger particles.

We considered how the total adhesion (A_T) of particles to the solid substrate in a given area would scale with particle radius (see Supplementary Materials for full analysis). The total adhesion would depend on the number of particles in a given area (N [=] 1), the

contact area of the particles with the solid substrate (A_c [=] length^2), and the work of adhesion between a particle and the substrate (W_{12} [=] energy/length^2). We assume that W_{12} is constant with respect to particle radius. The number of particles in a given area simply scales as $N \sim 1/r^2$. The scaling relationship between the contact area and the particle radius can be obtained from JKR theory of a particle adhering to an elastic substrate [33]; this analysis gave that $A_c \sim R^{4/3}$ and therefore A_T scales with $R^{-2/3}$. This result suggests that given equal peel tests of TEOS treated colloidal crystals, there is a weak dependence of particle radius on the fraction of particles remaining after a peel test. More specifically, the fraction of particles remaining should decrease with increasing particle radius.

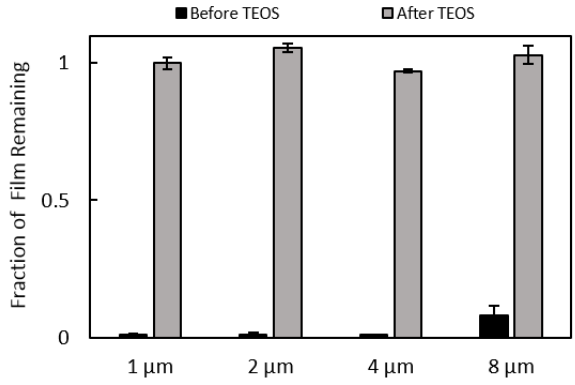

Figure 2-5. Peel-test results for silica colloidal crystal monolayers before and after the TEOS treatment. The fraction of the CCM film remaining after a peel test is much greater for TEOS-treated films treatment. The error bars are the standard error.

2.4.3. Structure and optical properties of silica LbL was not altered by TEOS

Due to the simplicity and success of the TEOS method for silica colloidal crystals, we next studied whether this method could increase the robustness of LbL silica particle films. Figure 2-6 shows SEM images of silica LbL films before and after TEOS treatment.

The film thickness was approximately 300 nm and discrete particles were visible. The discrete particles remain visible after TEOS treatment and the film thickness does not appear to be altered. If necks existed between the particles, as observed between the larger colloidal particles in the CCMs, they would be on the order of a few nanometers in diameter and may not be observable. This issue is compounded by the addition of a 5 nm iridium coating on the samples to prevent charging in the SEM measurement.

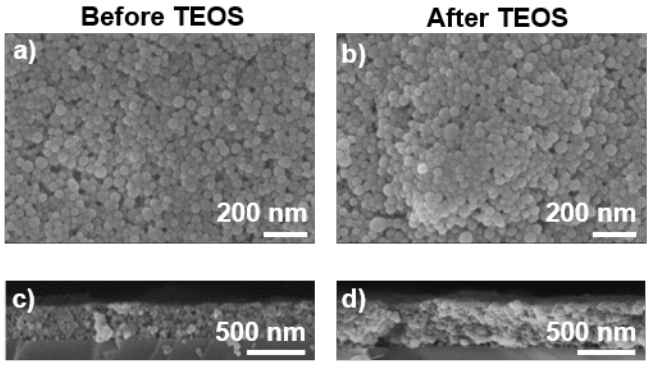

Figure 2-6. SEM images of silica LbL films before and after TEOS. (a) and (b) are top-down SEM images of silica LbL films before and after TEOS treatment. (c) and (d) are cross-section SEM images of silica LbL films before and after TEOS treatment. The film structure is not greatly altered by the TEOS treatment and the particles remain discrete.

The influence of the TEOS treatment on the optical properties of LbL silica films was studied by UV-Vis spectrophotometry. The percent spectral reflectance from normal incident light versus wavenumber (inverse wavelength) of silica LbL films before and after TEOS treatment is shown in Figure 2-7. We found that the amplitude and period of the fringes did depend weakly on the concentration of TEOS (data not shown) suggesting that the silica created by the TEOS treatment filled in void spaces between colloidal particles and, as a consequence, changed the average film index of refraction. Our initial results indicate that, in addition to improving the stability of LbL films, the TEOS treatment

can be used to tune the average index of refraction to the ideal value, $\sqrt{n_{glass}n_{air}} \approx 1.22$ [29], for a narrow-band antireflection coating.

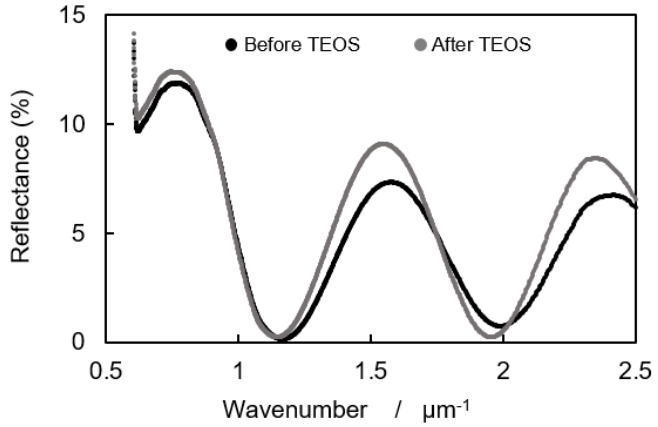

Figure 2-7. UV-VIS reflectance spectrum of silica LbL films before and after TEOS treatment. The wavenumber is equal to inverse wavelength. The TEOS treatment does not greatly alter the reflectance spectrum of the silica LbL film.

2.4.4. TEOS treatment increases abrasion resistance of LbL film

The results of the abrasion test fell into three categories, as shown in Figure 2-8a: (1) the film was removed entirely and the reflectance spectrum of the glass slide was observed, (2) the film was partially removed and there were features in the reflectance spectrum of both the glass slide and the film, or (3) the film was left fully intact after abrasion and the thin-film interference fringes are observed. All six replications for the films produced using Method 2 produced the spectrum of fully intact film in Figure 2-8a, which showed that the film was present on *both* sides of the slide at the end of the test. Most of the untreated samples looked like the fully removed film in Figure 2-8a. Together these results showed that Method 2 greatly increases the robustness of the film.

We quantified the fraction of film remaining after the abrasion test by assuming that the fraction remaining was proportional to the difference in reflectance between $k \approx 1.5\ \mu m^{-1}$ and $k \approx 2.0\ \mu m^{-1}$ (i.e. the fringe amplitude, see arrows in Figure 2-8a). The amplitude of the fringe for the glass slide without any LbL film was zero. We needed to make a correction to the measured amplitudes for the Method 2 slides because the film unexpectedly remained intact on both sides. The interference fringes on each side make equal contributions to the fringe amplitude, so for comparison to the other methods, we halved the amplitude of the Method 2 samples .

The fringe amplitudes versus TEOS treatment are plotted in Figure 2-8b. The squares in the figure are the means of the six replications and the error bars are confidence intervals for the means (Fisher's least significant difference) based on Analysis of Variance (ANOVA). Tukey's test was applied to the difference between the means. The difference between the no-treatment and Method 1 means is clearly not statistically significant ($p = 0.11$). The difference between the means of no-treatment and Method 2 (greater volume of TEOS and more time) is statistically significant ($p < 0.0001$). The observation that Method 1 did not improve the mechanical stability while Method 2 did improve stability serves as a warning that the exact conditions for TEOS treatment (time and concentration) for LbL films would need to be adjusted for different LbL constructs.

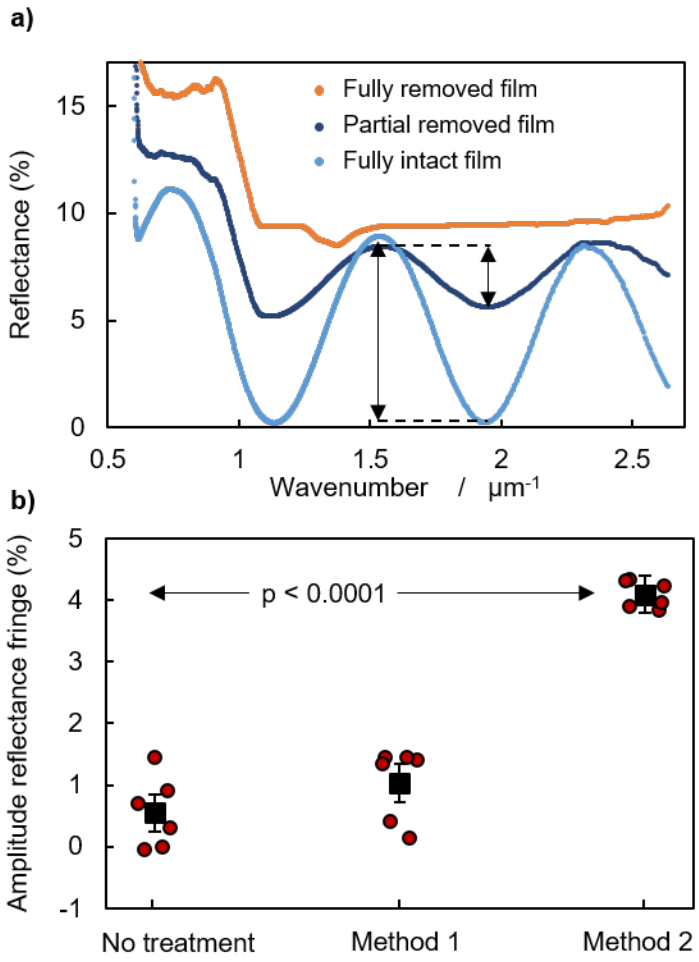

Figure 2-8. Abrasion testing of silica LbL films with no treatment and with TEOS treatment. (a) UV-VIS reflectance spectra of silica LbL films after abrasion test showing three types of outcomes described in the text. (b) Amplitudes of the reflectance spectra for samples with and without TEOS treatment. The amplitudes for Method 2 have been halved (from ≈8 to ≈4). The arrows in (a) show examples of the measured amplitudes. Samples were not treated, treated by Method 1 (5 % (v/v) and 16 h reaction time), or treated by Method 2 (20 % (v/v) TEOS and 40 h reaction time). The error bars are confidence intervals for the means (Fisher's least significant difference) based on Analysis of Variance (ANOVA). $p < 0.0001$ for the null hypothesis that TEOS treatment (Method 2) does not improve the abrasion resistance of the silica LbL films.

2.5. Conclusions

We developed a simple method to transform fragile colloidal crystal monolayers formed by the rubbing method into robust colloidal crystal monolayers. The method was based on the widely used sol-gel reaction of TEOS. Despite making the films more robust, the method did not significantly alter the organization of the colloidal crystal monolayer film, and left the shape of the top of the particles intact, thereby maintaining the desirable properties of the film. The method also improved the mechanical robustness of silica LbL films and provided a process for tuning the average index of refraction to the ideal value for a narrow-band antireflection coating.

2.6. Acknowledgments

The authors thank the Institute for Critical Technology and Applied Science (ICTAS) at Virginia Tech and the Virginia Commonwealth Commercialization Fund (CRCF) for funding and support. We also thank the ICTAS Nanoscale Characterization and Fabrication Laboratory (NCFL) for the use of facilities and equipment.

2.7. Supplementary Material

Supplementary material is contained in Appendix A. Supplementary material contains SEM images and scattering patterns of colloidal crystal monolayers fabricated from 1 μm, 2 μm, 4 μm, and 8 μm silica microparticles. We have also included a scaling analysis on the dependence of the total adhesion of particles in a colloidal crystal to the substrate on particle size.

References

1. Prevo, B. G.; Velev, O. D., Controlled, rapid deposition of structured coatings from micro- and nanoparticle suspensions. *Langmuir* **2004,** *20* (6), 2099-2107.

2. Prevo, B. G.; Hon, E. W.; Velev, O. D., Assembly and characterization of colloid-based antireflective coatings on multicrystalline silicon solar cells. *J. Mater. Chem.* **2007,** *17* (8), 791-799.

3. Christie, D.; Lombardi, J.; Kretzschmar, I., Two-Dimensional Array of Silica Particles as a SERS Substrate. *Journal of Physical Chemistry C* **2014,** *118* (17), 9114-9118.

4. Cai, Z. Y.; Zhang, J. T.; Xue, F.; Hong, Z. M.; Punihaole, D.; Asher, S. A., 2D Photonic Crystal Protein Hydrogel Coulometer for Sensing Serum Albumin Ligand Binding. *Anal. Chem.* **2014,** *86* (10), 4840-4847.

5. Ye, X. Z.; Qi, L. M., Two-dimensionally patterned nanostructures based on monolayer colloidal crystals: Controllable fabrication, assembly, and applications. *Nano Today* **2011,** *6* (6), 608-631.

6. Park, C.; Lee, T.; Xia, Y.; Shin, T. J.; Myoung, J.; Jeong, U., Quick, Large-Area Assembly of a Single-Crystal Monolayer of Spherical Particles by Unidirectional Rubbing. *Adv. Mater.* **2014,** *26* (27), 4633-4638.

7. Kargar, M.; Chang, Y. R.; Hoseinabad, H. K.; Pruden, A.; Ducker, W. A., Colloidal Crystals Delay Formation of Early Stage Bacterial Biofilms. *ACS Biomater Sci Eng* **2016,** *2* (6), 1039-1048.

8. Kargar, M.; Pruden, A.; Ducker, W. A., Preventing bacterial colonization using colloidal crystals. *Journal of Materials Chemistry B* **2014,** *2* (36), 5962-5971.

9. Lu, Z. C.; Zhou, M., Fabrication of large scale two-dimensional colloidal crystal of polystyrene particles by an interfacial self-ordering process. *Journal of Colloid and Interface Science* **2011,** *361* (2), 429-435.

10. Visschers, M.; Laven, J.; van der Linde, R., Film formation from latex dispersions. *Journal of Coatings Technology* **2001,** *73* (916), 49-55.

11. Zhang, D.; Xu, Y.; Feng, G.; Huang, Y.-R.; Lee, D., Comparing sintering and atomic layer deposition as methods to mechanically reinforce nanocolloidal crystals. *J. Mater. Res.* **2015,** *30* (23), 3717-3727.

12. Gemici, Z.; Shimomura, H.; Cohen, R. E.; Rubner, M. F., Hydrothermal Treatment of Nanoparticle Thin Films for Enhanced Mechanical Durability. *Langmuir : the ACS journal of surfaces and colloids* **2008,** *24* (5), 2168-2177.

13. Miguez, H.; Tetreault, N.; Hatton, B.; Yang, S. M.; Perovic, D.; Ozin, G. A., Mechanical stability enhancement by pore size and connectivity control in colloidal crystals by layer-by-layer growth of oxide. *Chem. Commun.* **2002,** (22), 2736-2737.

14. Zhang, L.; Prosser, J. H.; Feng, G.; Lee, D., Mechanical properties of atomic layer deposition-reinforced nanoparticle thin films. *Nanoscale* **2012,** *4* (20), 6543-6552.

15. Hench, L. L.; West, J. K., THE SOL-GEL PROCESS. *Chem. Rev.* **1990,** *90* (1), 33-72.

16. Vossen, D. L. J.; Penninkhof, J. J.; van Blaaderen, A., Chemical modification of colloidal masks for nanolithography. *Langmuir : the ACS journal of surfaces and colloids* **2008,** *24* (11), 5967-5969.

17. Markutsya, S.; Jiang, C. Y.; Pikus, Y.; Tsukruk, V. V., Freely suspended layer-by-layer nanomembranes: Testing micromechanical properties. *Adv. Funct. Mater.* **2005,** *15* (5), 771-780.

18. Yan, W. F.; Mahurin, S. M.; Overbury, S. H.; Dai, S., Nanoengineering catalyst supports via layer-by-layer surface functionalization. *Top. Catal.* **2006,** *39* (3-4), 199-212.

19. CampÃ s, M. n.; O'Sullivan, C., Layer-by-Layer Biomolecular Assemblies for Enzyme Sensors, Immunosensing, and Nanoarchitectures. In *Anal. Lett.*, Taylor & Francis Ltd: 2003; Vol. 36, p 2551.

20. Gifford, E. L., *Sensitivity control of optical fiber biosensors utilizing turnaround point long period gratings with self-assembled polymer coatings*. University Libraries, Virginia Polytechnic Institute and State University: [Blacksburg, Va. :, 2008.

21. Wang, Z.; Heflin, J. R.; Van Cott, K.; Stolen, R. H.; Ramachandran, S.; Ghalmi, S., Biosensors employing ionic self-assembled multilayers adsorbed on long-period fiber gratings. *Sensors and Actuators B: Chemical* **2009,** *139* (2), 618-623.

22. Janik, J. A.; Heflin, J. R.; Marciu, D.; Miller, M. B.; Davis, R. M., Electrochromic Behavior of Ionically Self-Assembled Thin Films. *MRS Symp. Proc.* **2001,** *660* (JJ8.20), 1-6.

23. DeLongchamp, D. M.; Kastantin, M.; Hammond, P. T., High-contrast electrochromism from layer-by-layer polymer films. *Chem. Mater.* **2003,** *15*, 1575-1586.

24. Heflin, J. R.; Liu, Y.; Figura, C.; Marciu, D.; Claus, R. O., Thickness Dependence of Second Harmonic Generation in Thin Films Fabricated from Ionically Self-Assembled Monolayers. *Appl. Phys. Lett.* **1999,** *74*, 495-497.

25. Chen, K.; Durak, C.; Heflin, J. R.; Robinson, H. D., Plasmon-Enhanced Second Harmonic Generation from Ionic Self-Assembled Multilayer Films. *Nano Lett.* **2007,** *7*, 254-258.

26. Cao, T. B.; Wei, L. H.; Yang, S. M.; Zhang, M. F.; Huang, C. H.; Cao, W. X., Self-assembly and photovoltaic property of covalent-attached multilayer film based on highly sulfonated polyaniline and diazoresin. *Langmuir : the ACS journal of surfaces and colloids* **2002,** *18* (3), 750-753.

27. Piok, T.; Brands, C.; Neyman, P. J.; Erlacher, A.; Soman, C.; Murray, M. A.; Schroeder, R.; Graupner, W.; Heflin, J. R.; Marciu, D.; Drake, A.; Miller, M. B.; Wang, H.; Gibson, H.; Dorn, H. C.; Leising, G.; Guzy, M.; Davis, R. M. In *Photovoltaic cells based on ionically self-assembled nanostructures*, 4th International Topical Conference on Optical Probes on Pi-Conjugated Polymers and Photonic Crystals, Salt Lake City, Utah, Feb 15-19; Elsevier Science Sa: Salt Lake City, Utah, 2000; pp 343-347.

28. Ridley, J. I.; Heflin, J. R.; Ritter, A. L. In *Robust antireflection coatings By UV cross-linking of silica nanoparticles and diazo-resin polycation*, 2007; pp 667406-667406-667409.

29. Yancey, S. E.; Zhong, W.; Heflin, J. R.; Ritter, A. L., The influence of void space on antireflection coatings of silica nanoparticle self-assembled films. *J. Appl. Phys.* **2006,** *99* (3), 34313-34323.

30. Shimomura, H.; Gemici, Z.; Cohen, R. E.; Rubner, M. F., Layer-by-Layer-Assembled High-Performance Broadband Antireflection Coatings. *ACS Applied Materials & Interfaces* **2010,** *2* (3), 813-820.

31. Decher, G., Fuzzy Nanoassemblies: Toward Layered Polymeric Multicomposites. *Science* **1997,** *277* (5330), 1232-1237.

32. Lvov, Y.; Ariga, K.; Onda, M.; Ichinose, I.; Kunitake, T., Alternate assembly of ordered multilayers of SiO2 and other nanoparticles and polyions. *Langmuir : the ACS journal of surfaces and colloids* **1997,** *13* (23), 6195-6203.

33. Style, R. W.; Hyland, C.; Boltyanskiy, R.; Wettlaufer, J. S.; Dufresne, E. R., Surface tension and contact with soft elastic solids. *Nature communications* **2013,** *4*.

Chapter 3 Surface topography hinders bacterial surface motility

Yow-Ren Chang[1], Eric R. Weeks[2], and William A. Ducker[1]

[1]Dept. of Chemical Engineering and Center for Soft Matter and Biological Physics, Virginia Tech, VA, 24061, USA

[2]Dept. of Physics, Emory University, GA, 30322, USA

Keywords: biofilm, *Pseudomonas aeruginosa*, surface motility, time-lapse microscopy, surface topography

3.1. Abstract

We demonstrate that the surface motility of the bacterium, *Pseudomonas aeruginosa*, is hindered by a crystalline hemispherical topography with wavelength in the range 2–8 μm. The motility was determined by analysis of time-lapse microscopy images of cells in flowing growth medium maintained at 37°C. The net displacement of bacteria over 5 minutes is much lower on surfaces containing 2–8 μm hemispheres than on flat topography but displacement on the 1 μm hemispheres is not lower. That is, there is a threshold between 1 μm and 2 μm for response to the topography. Cells on the 4 μm hemispheres were more likely to travel parallel to the local crystal axis than in other directions. Cells on the 8 μm topography were less likely to travel across the crowns of the hemispheres and were also more likely to make 30–50º turns than on flat surfaces. These results show that surface topography can act as a significant barrier to surface motility and may therefore hinder surface exploration by bacteria. Because surface exploration can be part of the process whereby bacteria form colonies and seek nutrients, these results help to elucidate the mechanism by which surface topography hinders biofilm formation.

3.2. Introduction

Bacterial biofilms are three-dimensional communities of bacteria encased in a self-secreted extracellular matrix.[1-2] Biofilms are formed when planktonic bacteria adhere to a surface, migrate, reproduce to form micro-colonies, and produce an extracellular matrix.[3] While bacteria often form biofilms in nature, they can be problematic in man-made systems. For example, biofilms can form inside industrial pipes[4] and on the exterior of

ship hulls.[5-6] From a medical perspective, bacterial biofilms are sources of chronic and nosocomial infections,[7-8] causing patient suffering and mortality. It is estimated that hospital acquired infections killed nearly 100,000 patients in the US in 2002 alone[9] and cost $17 billion to treat and manage.[10] Traditional antibiotic treatment of biofilms is difficult because the surrounding matrix provides a barrier and is problematic because of the rise of antibiotic resistance.[11-13] Therefore, there is a growing need to develop methods to prevent bacterial biofilm formation on surfaces. Of particular interest to us are preventative methods that act locally at potential sites of infection, for example at the surface of catheters. Local action is desirable to reduce the incidence of side-effects, and preventative action is desirable to reduce the frequency of patient symptoms.

Several methods of preventing bacterial biofilm formation on surfaces are currently being researched. Notable examples include the use of oil-infused surfaces,[14] modifying the surface chemistry with anti-microbial peptides,[15] and mechanical methods to disrupt biofilms.[16] Recent studies have demonstrated that surface topography with micrometer-scale features also hinders bacterial adhesion and biofilm formation.[17-25] The Brennan group have produced a body of work showing that surface micro-topography mimicking that of shark skin inhibits the adhesion of several micro-organisms.[26-29] Our laboratory recently reported that monolayers of close-packed, hexagonally arranged particles on a solid surface (colloidal crystals) hinder both the initial adhesion[30] and early biofilm formation[31] of the opportunistic human pathogen *Pseudomonas aeruginosa.* Colloidal crystals formed from 1.5 μm diameter particles also reduced the biomass of early-stage *P. aeruginosa* biofilms by ~80% compared to a flat surface.[31]

These results suggest that surface topography could be a useful method for hindering biofilm formation. Yet the *mechanism* behind the action of surface micro-topography inhibiting biofilm growth is not well understood. An understanding of the mechanism would aid in the design of new anti-biofilm surfaces. The development of biofilm is complex; many physical and environmental factors may impact biofilm formation.[32] Along the path to a biofilm, cells must first adhere to the surface, migrate (for surface motile cells), reproduce, and produce a matrix and topography may affect any combination of these processes. Ideas on the mechanism have mainly focused on the effect of topography on adhesion. For example Aizenburg's group has discussed the idea that available *contact area* for adhesion is important,[33] and Brennan's group has considered the *number of contact points* for adhesion.[34] Our group has discussed the importance of *surface curvature* on adhesion.[30]

In this study, we focus on how curved surface micro-topography impacts the surface motility of single *P. aeruginosa* cells within 140 min of exposure to a solid. Previous work by Meel *et al.* examined the effect of rectilinear wall heights on the ability of *Neisseria gonorrhoeae* and *Myxococcus xanthus* to migrate over barriers.[35] Both these organisms and *P. aeruginosa* exhibit twitching motility, a type of surface motility facilitated by Type IV pili.[36-37] It has been shown that twitching motility is required for biofilm formation[38] and can impact biofilm structure.[39] In this paper we assess motility (active motion) using metrics such as the average distance travelled by the cell over a micro-patterned surface. By using a flat surface as our control, our use of the word "motility" does not necessary imply cell "fitness" but includes the effects of the physical environment. This is the same as usage by Meel *et al*. In contrast, an alternative use of "motility" may

exclusively refer to cell fitness that could be changed for example by genetic or regulatory changes.

In this work, we examine how motility is affected by the radius of curvature of the solid surface at constant surface chemistry. So that topography was the only factor, i.e., chemistry was not a factor, we used polymer replicas of micro-topographic solids (Figure 3-1). To enable systematic variation of the radius on a micrometer scale, we first fabricated monolayer colloidal crystals from monodisperse SiO_2 particles of diameter, d = 1, 2, 4, or 8 μm. For the un-curved (flat) control, we used the free surface of polydimethylsiloxane (PDMS). Negative molds were prepared and then replicas were made such that all motility experiments utilized the same polymer, i.e. the same chemistry (Figure 3-1a). The use of replicas meant that the topography is not spherical but rather a spherical cap (Figure 3-1a-b), that is approximately hemispherical. The micro-topography scatters visible light so the cells are difficult to identify on the topography using transmission light microscopy. To enhance contrast for easier visualization, we utilized constitutively fluorescent bacteria and identified the cells from their fluorescent emission. The local topography was identified by phase contrast imaging. As described in the **Results** section, tracking of the motion of these cells show that the topography had a significant impact on motility.

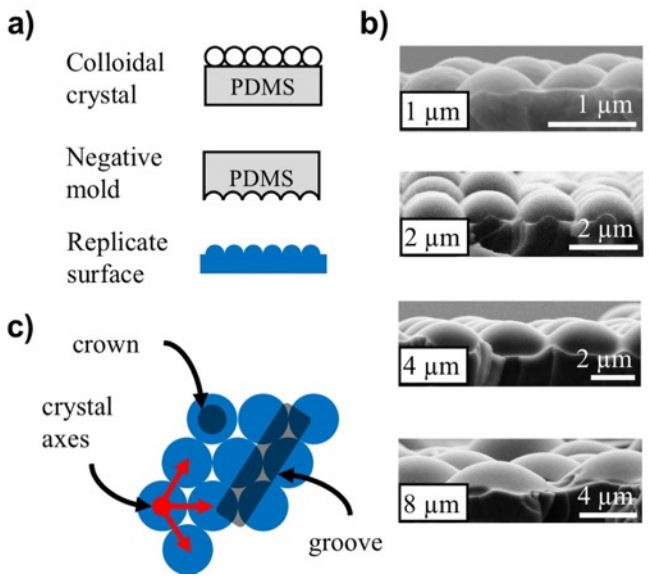

Figure 3-1. Fabrication of NOA textured surfaces. Schematic of the fabrication of NOA textured surfaces. A colloidal crystal made from SiO_2 particles is used as a topographical template. Using PDMS, a negative mold is created from the colloidal crystal, which is then used to create the samples of a single chemistry for the study of bacterial motility. (b) Cross-sectional scanning electron microscopy (SEM) images of the sample surfaces show that the surface features are hemispherical. (c) Schematic describing features of the textured surface.

Our interest is motion of the bacteria on the scale of the topography, that is, over displacements of approximately 1–8 µm. Typically, we find that bacteria traverse approximately 1 µm in 1 min, so we used a frame rate of 30 seconds to enable sampling that was faster that the average traverse time for the smallest feature. An example of a trajectory crossing our topography is shown in Figure 3-2. The intense light required for fluorescence imaging typically produces phototoxicity after about 100-400 frames so we are limited in the number of images that we can capture for each bacterium. We recorded movies that were 120 min long, which enabled sampling of motion at the length scale of the topography (1–8 µm) and for longer travel over multiple repeats of the topography. It

is important to note that there is considerable complexity in surface motility and that some of these features are not examined here. Conrad *et al*. found that P. aeruginosa can crawl with the long axis of its body parallel to the surface or walk with the long axis perpendicular to the surface.[40] We observed that bacteria appear rod-like or circle-like in fluorescence and phase contrast imaging, and following the work of Conrad *et al*.,[40] we attribute this effect to the different cross section of the bacteria that is imaged. We do not distinguish between these orientations in our analysis. When P. aeruginosa is crawling, Jin *et al*. showed that the motion is characterized by a majority of slow movements with rare, rapid jumps, a movement termed as a slingshot.[41] We did not observe the motion during slingshots as our imaging time point intervals (30 s) were far greater than the frame rates at which slingshot events were recorded (10 frames per second[41]).

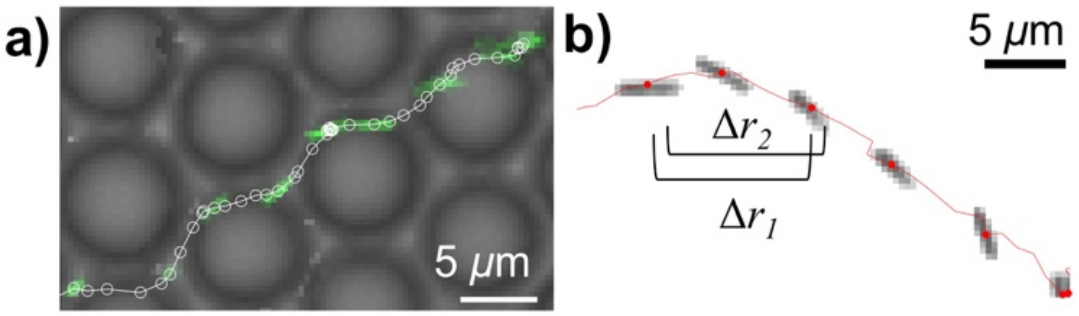

Figure 3-2. Tracking example of bacteria on topographic surface.(a) Time lapse imaging of bacterium (green) traversing an 8 μm textured surface. A time lapse of 30 s was chosen so that the bacterium could cross a large number of repeat features within the 120 exposure limit that we set to minimize phototoxicity. The position of the bacterium at 30 s intervals is indicated by white circles and every 5th image of the bacterium is shown (to limit overlap between images). (b) Time-lapse image of bacterium showing examples of the 5 min. intervals that were used to obtain displacements.

3.3. Materials and Methods

3.3.1. Fabrication of colloidal crystals and topographical replicas

The fabrication of topographical substrates used in this study is schematically shown in Figure 3-1. The templates for the curved features were stabilized colloidal-crystal monolayers that were fabricated as described previously with minor modifications.[42-43] In brief, colloidal crystals were fabricated using a rubbing method[44] in which monodisperse silica microspheres with diameters in the range 1–8 μm (Fiber Optic Center, MA) were rubbed uni-directionally on a sheet of PDMS (Sylgard 184, Dow Corning). The PDMS sheets were prepared by mixing the base and curing agent in a 10:1 mass ratio, degassed, cast into 100 mm petri dishes, and cured at 60ºC for 1 hour. The crystallinity of the colloidal crystals was checked by observing the scattering pattern produced by the colloidal crystal from a 523 nm laser and also by inspection with optical microscopy. The 1 and 2 μm colloidal crystals were stabilized by formation of silica meniscii from a sol-gel reaction of tetraethylorthosilicate (TEOS, Sigma Aldrich).[42] The larger colloidal crystals were more difficult to stabilize using this method[42]; so instead, we spin-coated a pre-hydrolyzed TEOS solution onto the colloidal crystals following previously described methods.[43] To facilitate release of molded polymer from the crystal, an anti-adhesion monolayer was attached to the colloidal crystal by activation with an O_2 plasma followed by immersion in a 1% (v/v) solution of nonafluorohexyltricholorsilane (Gelest) in ethanol. After silane treatment, samples were gently rinsed with ethanol and dried under N_2 gas streams. The negative mold was generated from PDMS. PDMS was mixed, degassed, and poured over the colloidal crystal samples and then cured overnight at 60ºC. An anti-adhesion layer was also created on the stamp, as described above. Flat

stamps were made from PDMS cast into 100 mm petri dishes and cured at 60ºC for 1 hour. The free surface of the PDMS was used as the stamp.

The topographic samples were prepared from Norland Optical Adhesive 81 (NOA, Norland Products) molded by the PDMS stamp. NOA 81, when cured, is a stiff polymer with excellent optical transmittance in the visible light range and has been successfully used as a non-toxic culture substrate for the study of mammalian cells.[45] Cover glass (#1, 25 mm × 50 mm, Fisher Scientific) was cleaned using 10% sodium hydroxide, rinsed thoroughly with deionized water, dried using compressed N_2 gas, and then O_2 plasma treated for 1 min at 100 W (Harrick Plasma). NOA was spin-coated onto the cover glass at 4000 rpm for 10 seconds (Laurell Technologies). Negative molds were placed onto the spin-coated slide and air pockets were gently squeezed out. The NOA was initially cured using an Omnicure Series 1000 UV lamp (Excelitas Technologies) at 400 mW intensity from a distance of 6 inches for 2 minutes and then the negative mold was removed. The NOA underwent a final cure in a UV/ozone cleaner (Bioforce Nanosciences) for 10 minutes. The molded topography was assembled into flow chambers[46] and sealed using PDMS.

The topographies of the NOA replicas were characterized using field emission scanning electron microscopy (FESEM, LEO 1550, Zeiss). For FESEM, samples were fractured in liquid nitrogen and then sputter coated with a 3 nm film of iridium using a Leica EM ACE600 sputter coater. For the 1, 2, and 4 μm particles, the replicates were hemispheres of the same diameter as the particles (Figure 3-1b). For the 8 μm particles, the replicate had the appropriate width (8 μm) but was only about 2 μm high. The root mean square (rms) roughness of the flat surfaces and of the hemispherical particle

features was measured using an Asylum Research Cypher ES atomic force microscope with Bruker ORC8-10 probes. For the textured surfaces, topography was imaged on top of a hemispherical feature and the image was first flattened with a second order plane fit, and then the rms roughness was calculated. The rms roughness of all the surfaces were very similar — in the range of 0.5 to 2 nm — and much smaller than the molded topographic features (~ μm) so we have distinct separation between size scales (see Figure 3-1b for dimensions of topography).

These final NOA samples will be referred to as textured samples as they are replicates of colloidal crystals and not actual colloidal crystals. It is important to note that the replica features are approximately hemispherical (Figure 3-1b). In contrast to actual colloidal crystals, there are no gaps between particles in which bacteria can dwell.

3.3.2. Bacterial growth

The bacteria used in all experiments were *P. aeruginosa* PA01 that were genetically modified to constitutively express tdTomato fluorescent protein.[47] Frozen stocks of bacteria were stored at –80ºC in sterilized 30% glycerol. All solid and liquid media used to culture fluorescent bacteria were supplemented with 30 μg/mL gentamicin (Fisher Scientific). Bacteria were streaked onto tryptic soy agar plates and incubated at 37ºC overnight. A single colony was used to inoculate a 250 mL baffled flask with 50 mL of tryptic soy broth (30 g/L, TSB) capped with a foam stopper to allow air exchange. The flask was incubated at 37ºC and shaken at 300 rpm overnight (211DS, Labnet). Vigorous shaking and air exchange was necessary for good growth. The next day, a fresh culture was started in a 250 mL baffled flask with 50 mL of TSB and was inoculated with 50 μL

of the overnight culture. This culture was grown to the early exponential phase (4 hours) then diluted to OD_{600} = 0.01 in TSB and used to inoculate the flow chamber.

3.3.3. Flow Cell Experiments

Our flow setup is similar to those described in the literature.[40, 48] A home-built heater and microscope enclosure maintained the temperature at 37ºC throughout the experiment. The flow setup consisted of a media bottle containing TSB, a pump, a bubble trap, the flow chamber (1 mm × 4 mm cross section), and a waste container. Components was sterilized by autoclaving and the flow chamber was separately sterilized using ethanol. Media was pre-flowed through the setup for at least 30 minutes prior to inoculation. Immediately before inoculation, flow was stopped and the tubing was clamped to prevent backflow of the inoculum into the media bottle. Using a 26G syringe, 250 µL of the inoculum (diluted early exponential culture, see **Section 2.2.**) was injected into the flow chamber and the chamber was inverted to allow bacteria to attach onto the surface. After 15 minutes, the flow chamber was returned to the topography-down orientation and media flow was resumed at a rate of 4 mL/hour. This flow washes away un-attached cells and provides nutrients for the bacteria attached to the surfaces. Imaging then began immediately, that is, approximately 20 min. after the inoculum was first injected into the flow chamber.

3.3.4. Microscopy

Bacteria were imaged using an upright Zeiss Imager.M2 microscope equipped with a 63x oil immersion objective with a numerical aperture of 1.4 in brightfield and

fluorescence. Owing to the short working distance of high NA lenses and the 1 mm deep fluid cell, the topographic sample was always situated between the image plane and the lens. Images were captured with a Zeiss Axiocam 506 mono camera with 5×5 binning (544 × 440 pixels). The binning reduces the pixel density of images but also decreases the exposure time required to image the bacteria. At these settings, bacteria are about 10 pixels in length and several pixels wide. The bacteria were imaged once every 30 seconds for 2 hours. For flat, 1 μm, and 2 μm surfaces, 2D movies were collected (bacteria were imaged at fixed stage heights). For 4 μm and 8 μm surfaces, *z*-stack movies were collected with 2 μm step intervals. The lamp intensity and exposure times were chosen to reduce phototoxicity. By comparing the motility of bacteria on flat glass surfaces that were imaged using only brightfield or fluorescence (see Figure 5-12), we found that our fluorescence imaging conditions did not impact the motility of the bacteria up to 1 hour (120 exposures). Beyond 1 hour, the speed of the bacteria imaged using fluorescence began to decreased. Therefore, we restricted our analysis of motility to the first hour of data since a bacterium was tracked. We also showed that the motility on flat samples was the same for wild-type and fluorescent bacteria (see Figure 5-13).

Bacteria were automatically tracked using TrackMate,[49] an ImageJ plugin for particle tracking, which has been recently used to successfully track *P. aeruginosa.*[50] Trackmate identifies each cell and determines the centroid, and then the position of the centroid is tracked. The quality of the tracking was checked visually (see Figure 3-2) and by comparing displacement probability distributions for the bacteria on the flat sample that were obtained from TrackMate tracking and from manual tracking (see Figure 5-14).

We did not find a significant difference between the manual and TrackMate tracking for this metric.

Starting about 20 min after the bacteria were first exposed to the solid, we recorded images at intervals of 30 s for a period of 120 min. The 30 s interval allows us to resolve movement through the topography and 120 min of data was enough to track long paths and generate statistics. As described in the **Introduction**, we only included data for the first 60 min. after a bacterium was first tracked. This was so that data was only derived from bacteria that had 120 or fewer exposures to intense light.

In this work, we track all contributions to the movement of the centroid. Uniform growth of the cell does not affect the position of the centroid. Each cell division does affect the position of the centroid, but the effect of division is small because (a) divisions are not that common (we typically observe ~100 divisions out of ~10,000 displacement events), and divisions sometimes increase and sometimes decrease displacement, so there is a high degree of cancellation of the effects of division when calculating average properties.

The surface coverage shown in Table 1 was determined by dividing an image into a 4 μm $\times$ 4 μm grid. If the centroid of a bacterium entered a grid, then that grid was considered to be covered. Note that this considers the projected area of the texture, not the actual contact area between the texture and the solution, which for perfect close-packed hemispheres would be $0.1 \times 1 + 0.91 \times 2 = 1.9$ times greater than the projected area. The area available to the bacteria may be less on the molded topographical surfaces.

3.4. Results

3.4.1. Bacteria trajectories depend on the size scale of the surface texture.

The dimensions of *P. aeruginosa* on flat NOA samples measured by fluorescence microscopy were 2.90 ± 0.07 μm length and 1.21 ± 0.02 μm diameter, where ± refers to the standard error for 40 samples. Therefore, to examine how motility is affected by topography with dimensions similar to the bacteria, we examined motility on NOA samples textured with hemispheres with diameter in the range 1–8 μm.

We captured 120 min time-lapse movies at 30 s intervals for each topography starting 20 min after the solid was first exposed to the bacteria. To obtain a visual impression of the trajectories of *P. aeruginosa* on various textured solids, Figure 3-3 shows the maximum intensity at each pixel for the 120 min time series. If a bacterium passes through a pixel then a high intensity is recorded, and thus the maximum intensity image shows all the locations covered by bacteria. The depth of field of the objective is less than a few micrometers, so on the 4 and 8 μm textured solids, at each time point we rapidly captured a series of images at a series of different focus heights (a "*z*-stack") to sample the entire texture. Each height is given a different false color. Generally speaking, the bacteria do not appear to be moving at random, but often have a persistent overall direction. This effect is most obvious on the flat and 1 μm samples (Figure 3-3).

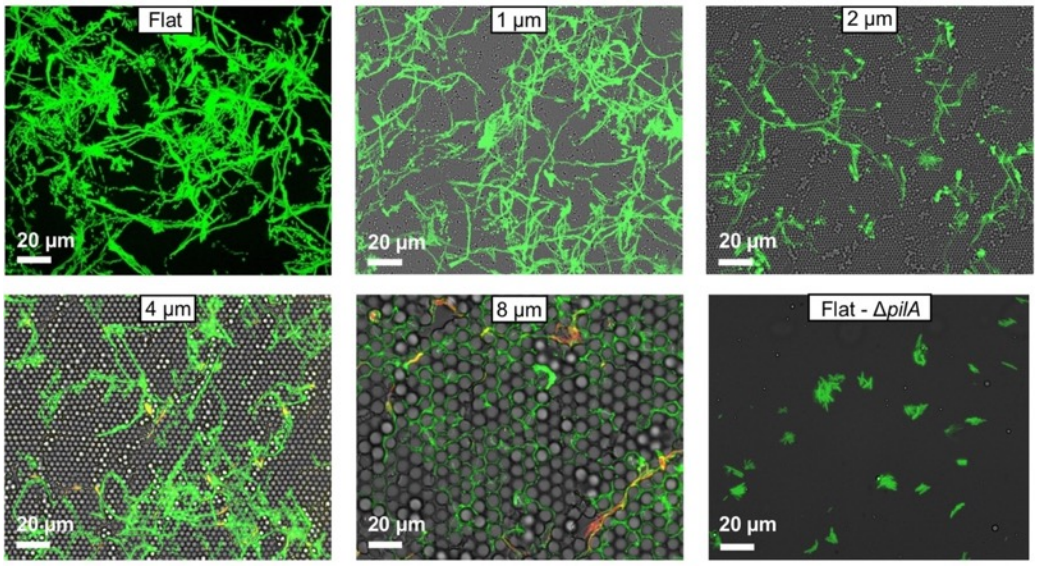

Figure 3-3. Maximum intensity projections of *P. aeruginosa* motility. Intensity maximum in a 120 min. time series of fluorescence images showing all areas of the surface visited by *P. aeruginosa* on a series of textured Norland Optical Adhesive (NOA) solids. The texture is hemispheres made from replicas of colloidal crystals with diameter indicated (1–8 μm, or flat). *P. aeruginosa* appears to explore a smaller fraction of the solid surface when there are features in the 2–8 μm range than for the flatter solids. The average number of bacteria on the images are 53, 51, 61, 46, and 105 for flat–8 μm and 56 for the Δ*pilA* on the flat for 60 min. The measured orientation order parameter for the topographies was ψ_6 = 0.68, 0.87, and 0.80 for 2, 4, and 8 μm. The direction of nutrient flow is from left to right in all images.

The images of the flat and 1 μm textured appear similar to each other, so we conclude that 1 μm hemispheres are too small to have much effect on bacterial motility. A number of qualitative features appear to be different on the 2, 4 and 8 μm textured surfaces compared to the flat and 1 μm solids, so there appears to be a threshold between 1 and 2 μm where motility is affected. If we were to examine even larger scale hemispheres, eventually we would expect that the cells might not be able to discriminate between a very large hemisphere (with low curvature) and a flat surface. Evidently 8 μm is not near such a limit as the behavior on the 8 μm topography was not similar to the flat

topography. Because results on the flat and 1 μm samples are similar we will sometimes refer to them together as the “low textures”.

A number of qualitative features appear to be different on the 2, 4 and 8 μm textured surfaces compared to the flat and 1 μm solids:

1. Images suggest that *P. aeruginosa* explore less of the solid surface when there are features in the 2–8 μm range than for 1 μm or flat surfaces: there is generally more color in the images of the low textures than of the high textures. This could be due to having a greater density of bacteria on the flatter solids, or due to greater average speed on the texture. To reduce the effect of the density, we selected images for Figure 3-3 that had similar numbers of bacteria (see caption) so that it is clear that the effect is due to greater coverage per bacterium.

2. Trajectories on the 4 and 8 μm textures appear to be different: the bacteria tend to move in the valleys between hemispherical features and rarely over the crown of the hemispheres (see Figure 3-1c for an explanation of terms). As a result, some trajectories on these larger scale topographies are characterized by persistent straight runs in the direction of a crystal axis on the 4 μm texture, and some appear to move on a hexagonal grid on the 8 μm texture (Figure 3-4a-b).

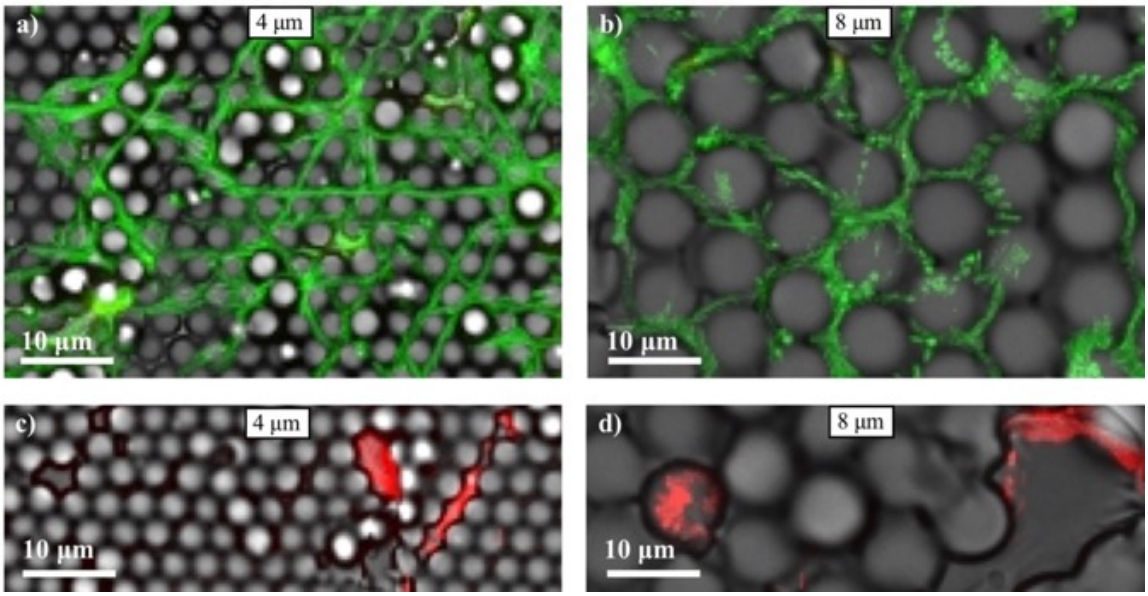

Figure 3-4. Enlarged sections of images showing the behavior of *P. aeruginosa* on the high textures. **(a)** On the 4 µm solid, there is a greater propensity for straight-line motion and **(b)** on the 8 µm solid there is a tendency to move approximately on a hexagonal grid. **(c)** Example of a bacterium moving along a line defect. **(d)** Example of a bacterium interacting with a hole defect. The direction of nutrient flow is from left to right in all images.

3. Defects represent a different topography compared to the surrounding crystalline array of hemispheres. It is possible that such defects inhibit *P. aeruginosa* motility across a surface. Some bacteria do interact with surface defects such as holes (see Figure 3-4c-d) or a second layer of features. Note that because the hemispheres were templated from spheres, some holes in the tested topography are an entire diameter lower that the surrounding crowns (Figure 3-4d). Interactions with hole defects can be seen easily on the images because the bacteria that are on a low z-slice are colored red. Fig. 4d, showing interaction with 8 µm features, indicates that some bacteria execute only small scale excursions within a defect. However, we found that less 10% of the bacteria in a movie interact with lower defects and that a majority of the cells interact with the

hemispherical features. Therefore, our quantitative results are dominated by bacterial interactions with the crystalline array and not with topographical defects. In the following sections, we describe the results of our quantitative analysis of the time series images.

3.4.2. Bacteria have greater displacements on flatter textures

It would be interesting to know the velocity distribution of bacteria, but on inspection of the videos, it is clear that the velocity is highly non-uniform over time; the bacteria dwell, change direction and make sudden jumps, as has been described previously.[40] Therefore, we focus on the distance that the bacteria move over some period that is large enough so that some of this behavior is averaged out. Net distance moved also gives an indication of how much of a surface a bacterium is able to explore. We tracked each bacterium in a 158 μm × 196 μm field of view for 60 minutes and determined its net displacement over five minute intervals. We measured approximately 5,000 displacement events on each surface for one experiment and performed three replicate experiments.

We calculated the displacement (Δr) of a tracked bacterium over a time interval Δt at every tracked time point (t) from the x and y positions according to Eq. 1:

$$\Delta r_t = \sqrt{(x_{t+\Delta t} - x_t)^2 + (y_{t+\Delta t} - y_t)^2} \text{ for all } t < 60 \text{ min.} \quad \text{Eq. 1}$$

We calculated Δr for Δt = 5 min. for the first 60 min. that a bacterium was tracked, i.e. for the interval 0 to 5 min, 0.5 min to 5.5 min, etc. (see Figure 3-2b), with bin size of 1 μm. We chose Δt = 5 min. so that we could sample how far a bacterium has traversed on the scale of the topography. We have also calculated Δr using different Δt and our

conclusions do not change (see Figure 5-15). We did not include data for any bacterium that was tracked for less than 5 min.

The distributions of displacements were clearly non-normal. To test the null hypothesis that the bacterial displacements were not different to each other on different surfaces, we utilized the central limit theorem and took averages of sub-samples of the measurements. For each replicate experiment on each surface, we recorded the average of 100 randomly selected data points and performed this process 100 times. This yielded 100 sub-sampled averaged data points for each experiment. We confirmed that the distributions of these averaged points were indeed normal, and then we average the 100 sub-sampled points to yield an average displacement for each replicate experiment for each experimental condition. We then performed an analysis of variance (ANOVA) followed by Tukey's HSD multiple comparison test (Table 1).

The average displacement was larger (5–6 μm) on the flat and 1 μm samples than on the higher topographies (2–2.5 μm); see Table 1. To test the null hypothesis that the mean displacements of bacteria on all surfaces were the same, we performed an ANOVA. The *p*-value was 9×10^{-5}, hence we reject the null hypothesis. A multiple comparison test showed that indeed bacterial displacements on flat and 1 μm surfaces were similar and that both were statistically different than displacements on higher textured surfaces with the exception that the average displacement on the 1 μm was not statistically different than that on the 4 μm surface (*p*-value 0.07). (see Table 1, displacement data). There was not a significant difference among the results for the 2, 4, and 8 μm surfaces.

Particle Size	Microradius *d*/2 (μm)	Roughness (nm) ± SE	Displacement[a] r_{av} (μm) ± SE	Decay length[b] (μm) ± SE	Coverage per bacterium[c] (μm^2) ± SE	Exponent[d] *n* ± 95% CI
Flat	∞	1.5 ± 0.1	6.2 ± 0.3	16 ± 1.5	0.87 ± 0.19	1.51 ± 0.03
1 μm	0.5	1.4 ± 0.2	5.0 ± 0.6	12 ± 0.5	0.81 ± 0.10	1.47 ± 0.04
2 μm	1.0	1.1 ± 0.1	2.1 ± 0.3*	7 ± 1*	0.44 ± 0.09*	1.24 ± 0.01
4 μm	2.0	1.9 ± 0.2	3.2 ± 0.2*	9 ± 0.5*	0.39 ± 0.03*	1.29 ± 0.04
8 μm	<4 †	0.7 ± 0.1	2.5 ± 0.3*	8 ± 0.8*	0.33 ± 0.01*	1.20 ± 0.04

Table 1. Measured parameters for various topographies

SE – Standard error, CI – confidence interval for replicate experiments

* Indicates significant difference compared to result on flat texture ($p < 0.05$). There was not a significant difference among the results for the 2, 4, and 8 μm surfaces or between the flat and 1 μm surface.

† 8 μm diameter and 2.4 μm height. [a] Average displacement in 5 min. [b] Inverse of the slope of the $\log_{10}(P(\Delta r))$ data in Fig. 5 for $\Delta r > 2\mu m$. [c] Coverage in 100 min. normalized by the average number of bacteria for images in Fig. 3. [d] Fitted value of *a* in $\langle \Delta r^2 \rangle = a \cdot t^n$ for the data presented in Fig. 6.

We also examined the behavior of the Δ*pilA* mutant on the flat surface. The Δ*pilA* mutant does not have a Type IV pilus, and therefore cannot exhibit twitching motility.[51] The average displacement of the Δ*pilA* mutant on the flat surface was 0.54 ± 0.01 μm, which is much less than for the wild-type (6.2 ± 0.3 μm), and less than the length of the bacterium. We also checked that the movement was restored in a complemented *pilA* strain (average displacement was 3.51 ± 0.13 μm, also see Figure 5-16 for maximum

intensity images). This indicates that pilus-mediated motion is responsible for a large fraction of the movement that we observe in the wild-type.

Figure 3-5 shows the distribution of displacements. Displacement measurements were binned into 1 μm bins; the number in each 1 μm interval was normalized by both the total number of Δ*r* and by the bin size, to convert from counts to probability. We then averaged the probability at each interval for three replicate experiments to obtain data in Figure 3-5.

The dispersion of behaviors of the wildtype bacteria suggest that it is also interesting to compare the range of displacements and not just the mean. Figure 3-5 shows, on a log scale, the measured probability distribution of distances traveled in 5 min., averaged across the three experiments. Figure 3-5 indicates a broad distribution of displacements on each texture. The displacement probability distribution of bacteria on a 1 μm textured surface was very similar to that of bacteria on a flat surface. This result suggests that bacterial motion was not strongly influenced by the 1 μm textured surface.

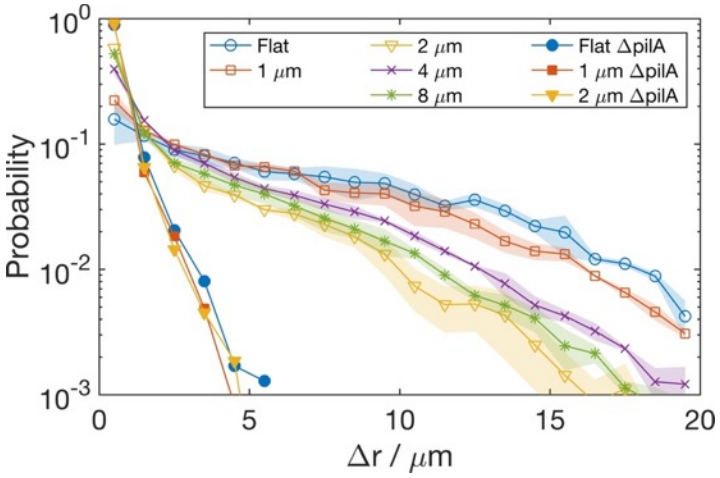

Figure 3-5. Probability/μm of displacement of *P. aeruginosa* over five minutes for a total of 60 min. since tracked on a series of textured solids. The bin width was 1 μm and the vertical scale is logarithmic. The

symbols are the average and the shaded region shows the standard error calculated from the probability at each Δr for the three replicates of the wild-type bacteria and the Δ*pilA* mutant. Note that the shaded regions for the Δ*pilA* mutant are too small to see. The lines are guides to the eye. There is a greater fraction of low-speeds for the 2-8 μm surfaces than for 1 μm or flat surfaces. Fig S4 shows representations of the same data, but the displacement was calculated for intervals of 1, 2, 5, and 10 min. Those figures show that the probability distribution of bacteria on the flat and 1 μm spheres was also shifted to greater displacements for all these time intervals.

The displacement distribution of bacteria on higher textured surfaces (2–8 μm) were similar to each other but distinctly different than that of bacteria on the flat and 1 μm textured surfaces. In this group of higher textures, about 40–60% of the measured displacement events were less than 1 μm, whereas on the lower textures, only 15–25% of displacements were less than 1 μm. On the lower textures about 15–20% of displacements were greater than 10 μm, but only about 5% had displacements this large on the lower surfaces. The distributions are approximately exponential (linear on the log scale of Figure 3-5) for displacements greater than 2 μm. The decay lengths for various topographies are given in Table 1. A Tukey multiple comparison test shows that the decay length for the flat surface is different to that of the 2, 4, and 8 μm topography, but not significantly different from the 1 μm, as expected from Figure 3-5.

Some of the bacteria on the 4 or 8 μm textures are in low defects (colored red in Fig. 3 and 4). 2–10% of the data in Figure 3-5 is from these low areas. Removal of this data does not significantly change Figure 3-5, but if we consider only the subset of data from the low areas, the long displacement (>10μm) data is greatly reduced in probability.

To further quantify the motility of bacteria on the textured surfaces, we calculated the mean square displacement (MSD), $\langle \Delta r^2 \rangle$, of bacteria as a function of time, *t*. For a

random walk (diffusive behavior), $\langle \Delta r^2 \rangle = a \cdot t$, where *a* is a constant. We fitted our data from individual experiments to $\langle \Delta r^2 \rangle = a \cdot t^n$ for comparison (Figure 3-6), and the values of *n* are shown in Table 1. On all topographies, *n* > 1, indicating that bacterial motion was super-diffusive, due to the tendency for bacteria to move in fairly straight lines over short time periods (see Figure 3-3). Again, data for the two topographies fell into two categories. For the flatter textures we found *n* ≈ 1.5 which is very similar to values previously reported for *P. aeruginosa* crawling motility on a flat surface.[40] For the larger-scale topography (> 2 μm), we found *n* ≈ 1.2, i.e. the motion is still super-diffusive but with a smaller exponent, which again indicates that the larger-scale topography hindered motility. The 95% confidence intervals (Table 1) do not overlap, showing that the difference in exponents between the large- and small-scale topographies are significant.

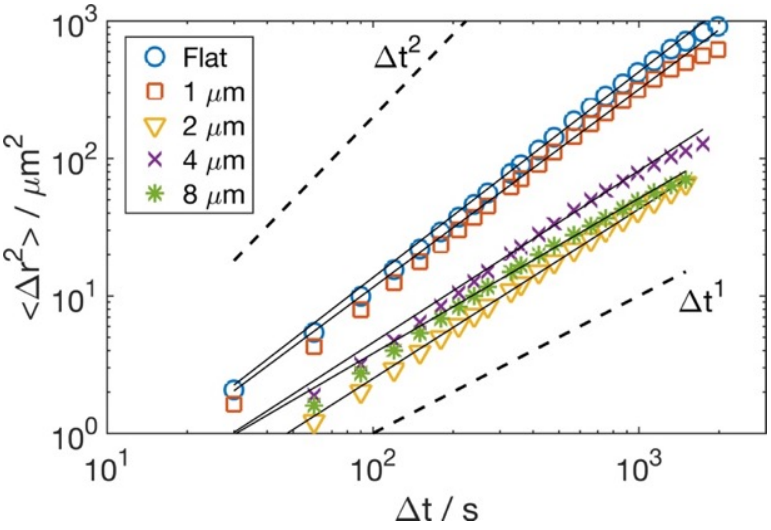

Figure 3-6. Mean square displacement of *P. aeruginosa* on flat and textured surfaces. The solid lines show regression fits to the data for each topography and dotted lines shows MSDs for a random walk ($\Delta t^{1.0}$) and ballistic motion ($\Delta t^{2.0}$) for comparison. *P. aeruginosa* was super-diffusive on all topographies, but *n* was greater on the smaller-scale topography (*n* = 1.5, see Table 1) than on the larger-scale topography (*n* = 1.2-1.3, see Table 1).

All the textured surfaces were fabricated from the same material (NOA); therefore, we conclude that the surface topography hindered the surface motility of *P. aeruginosa*. Furthermore, there appears to be a threshold surface topographical feature size (between 1 and 2 μm) beyond which motility is hindered. This threshold size is similar to the bacterial dimensions (length ≈ 2.90 μm, diameter ≈ 1.21 μm).

Finally, to examine the visual impression from Figure 3-4 that bacteria visit more of the surface on the lower topographies, we also quantified the fraction of the surface that was visited by the set of bacteria in one field of view over 100 min by calculating the area coverage normalized by the average number of bacteria (Table 1). These results indicated that only about 1/2 as much of the surface was covered on the larger-scale topography.

In the next section we analyze why *P. aeruginosa* have shorter displacements on large-scale textures.

3.4.3. The direction of motion is influenced by underlying topography

We first examined whether the *direction* of motion of a single bacterium was influenced by the surface texture. We determined the local crystal orientation (Figure 3-1c) by calculating ψ_6, the bond orientation order parameter,[52] and then calculated the angle, θ, between the crystal orientation and the bacterial velocity. Contributions from bacteria in defective regions of the crystal were excluded by excluding from the analysis bacteria on regions where the local phase angle ψ_6 departed from the mean for the image by more than 10º. Figure 3-7a indicates that the averaged probability distribution for three different experiments on highly ordered 4 μm textures all peaked at 0º. In other words,

the bacteria have a tendency to move in the direction of the crystal axes. We then hypothesized that bacteria would move at a greater speed when moving in the direction of the crystal axes on the 4 μm texture. To test this hypothesis, we calculated the average displacement over 1 min. as a function of θ (Figure 3-7b). We found that when bacteria do move in the direction of a crystal axis, they travel at a greater speed (Figure 3-7b). Although the speed is greatest along the axis for the 4 μm texture, recall that the MSD is lower than on the flat and 1 μm texture.

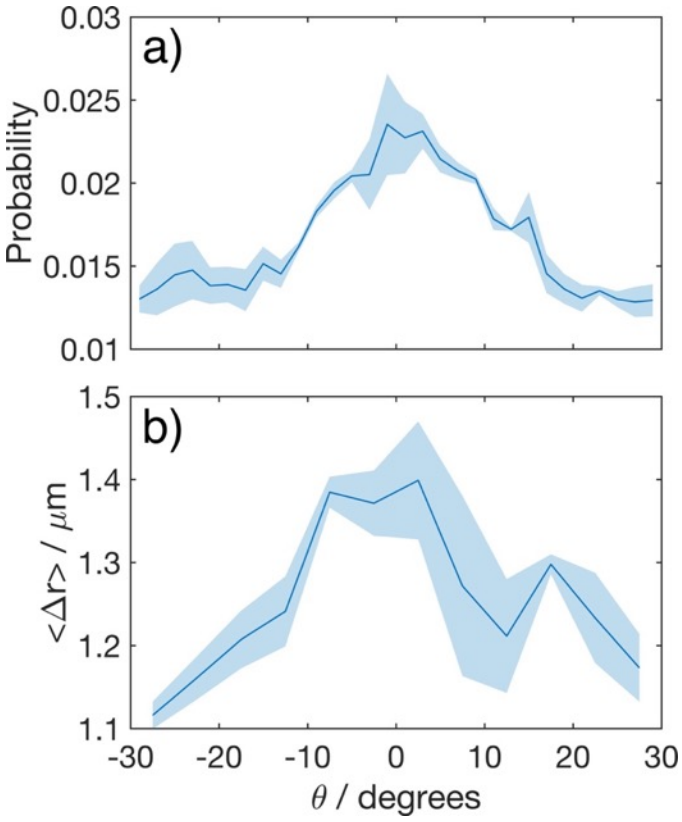

Figure 3-7. Bacteria are more likely to travel in the direction of the crystal lattice. Distribution of the angle of bacterial displacement *relative to the local lattice* on a 4 μm texture. Each displacement was measured over one minute. **(b)** Mean displacements over 1 min. *P. aeruginosa* is more likely to travel along a crystal axis and when it does so, travels at a greater speed. Data shown are for 2 h of measurements of three independent samples. The line shows the average and the shaded region is the standard error of three measurements. Both datasets in Figure 3-7 must be symmetric about $\theta = 0^{\circ}$ due to the symmetry in the

topography. But to robustly test whether or not the bacteria do have a preferred direction and if they do travel at a greater speed, we preformed statistical fits to determine 1) if there is a peak in both the datasets in Figure 3-7and 2) where the peak is located. For Figure 3-7a, the data were fit to a truncated normal distribution and the fit was found to be significant (ANOVA, p value < 0.001 compared no model) indicating that the distribution is not flat. The peak of the data is simply the mean of fitted normal distribution, which was $0.5^\circ \pm 0.7^\circ$. For Figure 3-7b, the data were fitted to a parabola and the fit was significant (ANOVA, p-value < 0.001 compared to no model), also indicating that there is a peak. The fitted peak was found to be $2^\circ \pm 2^\circ$.

In addition to a tendency to follow the crystal lattice, we also expected that bacteria would be more likely to change direction when they encounter a high obstacle. So, we examined the tendency of the bacteria to turn, i.e. to vary the angular component of velocity. The displacement was measured for each two minute interval, and the angle between each two consecutive displacement vectors, $\Delta\theta$, was determined. To exclude small errors in tracking and small-scale oscillation of the bacterium, we only included cases where the bacterium displacement was 2 μm or more in consecutive intervals. Figure 3-8 shows the net change in angle of motion, $\Delta\theta$. The inset to Figure 3-8 shows more detail for angles near 180º, i.e. when the bacterium reverses direction. The figure suggests that the bacteria are more likely to turn by more than 170º on the 2 and 8 μm topographies than on a flat surface, and a Tukey multiple comparison test confirms this (p<0.05). Clearly an increase in reversals decreases the net displacement and these reversals are part of the reason for the smaller displacements on the larger-scale topography

The bacteria on the 8 μm texture have a greater probability of turning by 30–40º on 8 μm texture than on the flat (Tukey test, p = 0.01) (see Figure 3-8). Visual inspection of Figure 3-5 suggested that the bacteria on the 8 μm texture appear to move on

hexagonal lattice defined by the particles. If the bacteria followed a hexagonal lattice, we would expect to see a high probability of 60º turns. The increased probability at slightly lower angles indicates that the angular changes are affected by the lattice, but that it typically takes longer than 2 min. to turn or that the bacteria cut corners, i.e. the bacteria execute a gradual turn to negotiate the topography. In summary, the bacteria are more likely to make gradual turns from one lattice direction to another on the highest topography, and more likely to make reversals on the 2 and 8 μm topography; both turns will reduce the distance travelled.

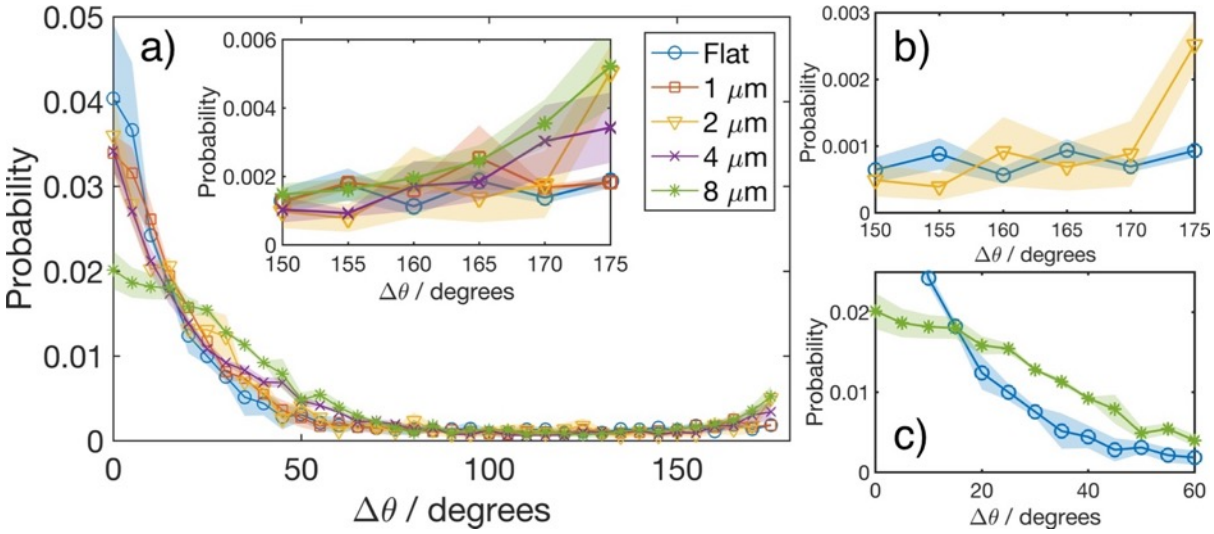

Figure 3-8. Bacteria turn more often on textured surfaces. Distribution of angular changes in velocity over 2 min. for *P. aeruginosa* for a series of textures surfaces. The total data set of 120 min long. (b)There is a larger probability of >170º turns on the 2 μm topography than on the flat. (c) On the 8 μm topography there is a lesser probability of maintaining direction than on the other topographies and a greater probability of turning by 30-40º.

3.4.4. Colloidal crystals can be used to hinder bacterial motion

If topography is to be used to hinder the motility of bacteria in a practical application such as a catheter coating, then the ease and cost of fabrication would be an important consideration. Colloidal crystals are much easier to prepare than polymer replicates: the colloidal crystal can be created in minutes, they can also be created on curved surfaces, and they are easy to stabilize.[53] Therefore, it is of interest to know whether the slowing of *P. aeruginosa* that we observed on replicates of colloidal crystals also occurs on colloidal crystals. Our experiments showed that the probability – displacement graph for the 1 μm colloidal crystal is very similar to the 1 μm template and likewise that the 2 μm colloidal crystal data is similar to the 2 μm template structure (see Figure 3-9). In common with the replicate samples, there is a distinct slowing of the bacteria on the 2 μm colloid crystal compared to the 1 μm colloidal crystal. This suggests that colloidal crystals may offer a simple, inexpensive coating to slow bacterial motion. It also suggests that the bottom half of the sphere on the colloidal crystal does not play a large role in affecting motility for the 1–2 μm particle size range.

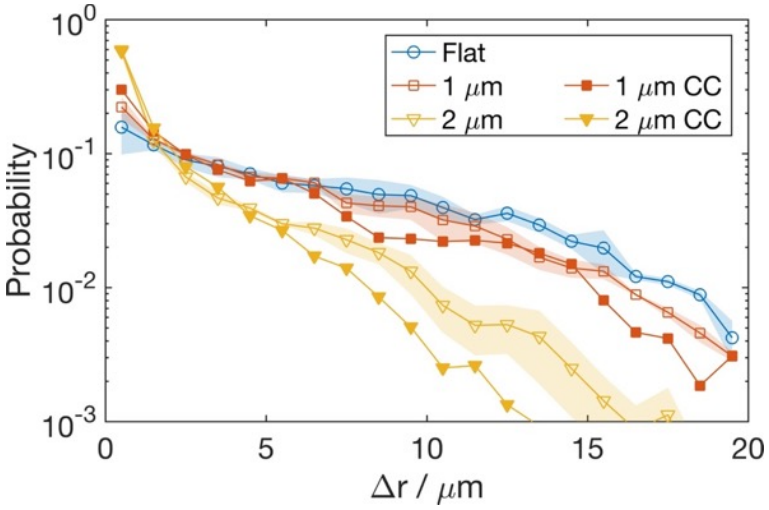

Figure 3-9. Comparison of probability/μm of displacement of *P. aeruginosa* for colloidal crystal and template polymer. For the same radius, the colloidal crystal and template have similar probability distributions.

3.5. Discussion

Previous studies by our lab demonstrated that colloidal crystals could inhibit the adhesion[30] and early biofilm formation of *P. aeruginosa.*[31] To form a biofilm, bacteria must first adhere to a surface, divide, organize into a micro-colony, and secrete an extracellular matrix. We hypothesize that surface topography may hinder bacteria in a number of ways: during the initial adhesion, growth, communication, or motility of bacteria. In this work, we studied how the *surface motility* of *P. aeruginosa* was impacted by surface micro-topography. We showed that, above a threshold features size, about 1–2 μm, the displacement was significantly reduced and that a smaller amount of the surface was explored. One way for a bacterium to form microcolonies is to search over a surface to find other bacteria, so it is possible that this reduced motility hinders that ability of the bacteria to reach other bacteria and therefore to organize into microcolonies or larger structures. Previous work by Meel et al. found a similar threshold that affected the ability of *Neisseria gonorrhoeae* and *Myxococcus xanthus* to migrate over barriers.[35]

A reduction in average net displacement will also affect net migration of bacteria. One route for infection of catheter patients is adsorption onto a catheter outside the body, and migration into the body along the catheter. By reducing the speed of that migration, one may be able to reduce the incidence of catheter infections.

We are not yet in a position to determine how the topography affected motility but here we will briefly speculate on the effect. The textures for which we see reduced mobility are the 2 μm, 4 μm, and 8 μm textures with feature heights 2 μm, 4 μm, and 2.4 μm

respectively. We find that the critical topographic height for obstruction is slightly larger than the diameter of the organism. *P. aeruginosa* (among other organisms) achieve surface motility using type IV pili[36-37] (~ 5 μm in length[54]) which adhere to the solid in advance of a bacterium and then the pilus is retracted and pulls the bacterium towards the point of adhesion.[51] Results of our Δ*pilA* mutant studies show that the absence of the pilus greatly reduces the displacement on three topographies (Figure 3-5), and therefore that the pili are agents of motion. We suggest that there are two requirements for the bacterium to advance across topography: (a) The end of pilus distant from the bacterium must be able to attach to a position on the solid from which it can apply a force. Attachment of the pilus requires a flight path for the pilus. (b) Once attached to the solid, the pilus must be able to apply a force to the pole of the bacterium with a component parallel to the direction of motion, or be able to apply a torque to rotate the body into a favorable position for future motion. Now considering the effect of topography, one can imagine that topography in front of the bacterium can block certain flight paths of the pili, and the topography under the bacterium can tilt the bacterial body such that the pilus is more or less likely to contact the solid in front of the pole. Convex surface topography, such as the hemispheres examined here may tilt the body away from attachment points for the pili. In contrast, in the grooves between hemispheres, there are features ahead of the pole that provide attachment points for the pili. When encountering a step, the pilus might not be able to reach over the step to strike an adhesion point that allows it to pull the bacterium forward. On a simplistic level, “retraction” of the pilus may bring the body up against a topographic feature such that the direction of force is being opposed by the riser of the solid. The force from the pilus acts on the pole of the bacterium at a point

which must be no higher than the maximum height of the bacterium. So when approaching a step, if the pilus is attached to the pole below the height of the step, the pilus may pull the bacterium toward the riser, and not over the step, thus hindering motion over the step. We intend to explore these mechanisms in future work.

3.6. Conclusions

P. aeruginosa surface motility is hindered by micrometer-scale surface topographical features. Specifically, we found that the mean displacement of *P. aeruginosa* is significantly reduced by 2 μm diameter and larger hemispheres whereas smaller diameter features (1 μm) did not hinder motion. Furthermore, we found that, on 2 μm and 8 μm features, *P. aeruginosa* was more likely to reverse direction. On the 4 μm texture, the bacteria have greater displacement when traveling in approximately straight lines in the groove along the crystal axis than in other directions. On the 8 μm texture, the bacteria were more likely to turn to follow an approximately hexagonal lattice of groves between features. Overall, our data indicates that surface micro-topography acts as a physical barrier that impedes surface motility of *P. aeruginosa*. The reduced motility was also observed on monolayer coatings of particles. Hindering motility may be a route for hindering biofilm formation which suggests a possible application of topographic coatings for medical devices.

3.7. Acknowledgements

The authors thank the Institute for Critical Technology and Applied Science (ICTAS) at Virginia Tech and the Virginia Commonwealth Commercialization Fund (CRFC) (MF15-

010-LS) for funding and support. We also thank the Nanoscale Characterization and Fabrication Laboratory (NCFL) at Virginia Tech for the use of their facilities. The authors also thank Dr. Joe Harrison at the University of Calgary for kindly providing all strains of *Pseudomonas aeruginosa* used in these experiments and for useful suggestions and Trevor E. Randall for technical assistance. The work of E.R.W. was supported by the National Science Foundation (DMR-1609763). E.R.W. thanks W.C.K.Poon for helpful discussions.

3.8. Supporting Information

Supporting Information can be found in Appendix B. Effect of fluorescence imaging on cell behavior compared to brightfield; comparison of the motion of the wild-type strain *P. aeruginosa* and a constitutively fluorescent strain; comparison of the displacement metric calculated from automated tracking to manual tracking; demonstration of the effect of different time intervals used to calculate displacement; validation that the complemented pilA strain recovers the motion of the wild-type.

References

1. Hall-Stoodley, L.; Costerton, J. W.; Stoodley, P., Bacterial biofilms: from the natural environment to infectious diseases. *Nature Reviews Microbiology* **2004,** *2* (2), 95-108.

2. Percival, S. L.; Malic, S.; Cruz, H.; Williams, D. W., Introduction to biofilms. In *Biofilms and Veterinary Medicine*, Springer: 2011; pp 41-68.

3. Monds, R. D.; O'Toole, G. A., The developmental model of microbial biofilms: ten years of a paradigm up for review. *Trends in microbiology* **2009,** *17* (2), 73-87.

4. Percival, S.; Walker, J., Potable water and biofilms: a review of the public health implications. *Biofouling* **1999,** *14* (2), 99-115.

5. Townsin, R., The ship hull fouling penalty. *Biofouling* **2003,** *19* (S1), 9-15.

6. Schultz, M.; Bendick, J.; Holm, E.; Hertel, W., Economic impact of biofouling on a naval surface ship. *Biofouling* **2011,** *27* (1), 87-98.

7. Costerton, J. W.; Stewart, P. S.; Greenberg, E., Bacterial biofilms: a common cause of persistent infections. *Science* **1999,** *284* (5418), 1318-1322.

8. Donlan, R. M., Biofilms and device-associated infections. *Emerging infectious diseases* **2001,** *7* (2), 277-281.

9. Klevens, R. M.; Edwards, J. R.; Richards, C. L.; Horan, T. C.; Gaynes, R. P.; Pollock, D. A.; Cardo, D. M., Estimating Health Care-Associated Infections and Deaths in U.S. Hospitals, 2002. *Public Health Reports* **2007,** *122* (2), 160-166.

10. Hassan, M.; Tuckman, H. P.; Patrick, R. H.; Kountz, D. S.; Kohn, J. L., Cost of hospital-acquired infection. *Hospital topics* **2010,** *88* (3), 82-89.

11. Mah, T.-F.; Pitts, B.; Pellock, B.; Walker, G. C.; Stewart, P. S.; O'Toole, G. A., A genetic basis for Pseudomonas aeruginosa biofilm antibiotic resistance. *Nature* **2003,** *426* (6964), 306-310.

12. Mah, T.-F. C.; O'Toole, G. A., Mechanisms of biofilm resistance to antimicrobial agents. *Trends in Microbiology* **2001,** *9* (1), 34-39.

13. Stewart, P. S.; Costerton, J. W., Antibiotic resistance of bacteria in biofilms. *The lancet* **2001,** *358* (9276), 135-138.

14. Epstein, A. K.; Wong, T.-S.; Belisle, R. A.; Boggs, E. M.; Aizenberg, J., Liquid-infused structured surfaces with exceptional anti-biofouling performance. *Proceedings of the National Academy of Sciences* **2012,** *109* (33), 13182-13187.

15. Iarikov, D. D.; Kargar, M.; Sahari, A.; Russel, L.; Gause, K. T.; Behkam, B.; Ducker, W. A., Antimicrobial surfaces using covalently bound polyallylamine. *Biomacromolecules* **2014,** *15* (1), 169-176.

16. Gu, H.; Lee, S. W.; Buffington, S. L.; Henderson, J. H.; Ren, D., On-Demand Removal of Bacterial Biofilms via Shape Memory Activation. *ACS Applied Materials & Interfaces* **2016,** *8* (33), 21140-21144.

17. Díaz, C.; Schilardi, P. L.; dos Santos Claro, P. C.; Salvarezza, R. C.; Fernández Lorenzo de Mele, M. A., Submicron Trenches Reduce the Pseudomonas fluorescens Colonization Rate on Solid Surfaces. *ACS Applied Materials & Interfaces* **2009,** *1* (1), 136-143.

18. Epstein, A. K.; Hong, D.; Kim, P.; Aizenberg, J., Biofilm attachment reduction on bioinspired, dynamic, micro-wrinkling surfaces. *New Journal of Physics* **2013,** *15* (9), 095018.

19. Ma, J.; Sun, Y.; Gleichauf, K.; Lou, J.; Li, Q., Nanostructure on taro leaves resists fouling by colloids and bacteria under submerged conditions. *Langmuir : the ACS journal of surfaces and colloids* **2011,** *27* (16), 10035-10040.

20. Perni, S.; Prokopovich, P., Micropatterning with conical features can control bacterial adhesion on silicone. *Soft Matter* **2013,** *9* (6), 1844-1851.

21. Xu, L.-C.; Siedlecki, C. A., Submicron-textured biomaterial surface reduces staphylococcal bacterial adhesion and biofilm formation. *Acta Biomaterialia* **2012,** *8* (1), 72-81.

22. Lin, J.; Wen, G.; Peihong, X.; Hainan, G.; Ming, Z.; Chen, Z.; Yali, Z.; Dong, H., Quantitative assay for the colonization ability of heterogeneous bacteria on controlled nanopillar structures. *Nanotechnology* **2015,** *26* (5), 055702.

23. Ling, G. C.; Low, M. H.; Erken, M.; Longford, S.; Nielsen, S.; Poole, A. J.; Steinberg, P.; McDougald, D.; Kjelleberg, S., Micro-fabricated polydimethyl siloxane (PDMS) surfaces regulate the development of marine microbial biofilm communities. *Biofouling* **2014,** *30* (3), 323-335.

24. Ling III, J. F.; Graham, M. V.; Cady, N. C., Effect of topographically patterned poly (dimethylsiloxane) surfaces on pseudomonas aeruginosa adhesion and biofilm formation. *Nano LIFE* **2012,** *2* (04), 1242004.

25. Bhattacharjee, A.; Khan, M.; Kleiman, M.; Hochbaum, A. I., Effects of Growth Surface Topography on Bacterial Signaling in

Coculture Biofilms. **2017,** *9*, 18531−18539.

26. Chung, K. K.; Schumacher, J. F.; Sampson, E. M.; Burne, R. A.; Antonelli, P. J.; Brennan, A. B., Impact of engineered surface microtopography on biofilm formation of Staphylococcus aureus. *Biointerphases* **2007,** *2* (2), 89-94.

27. Reddy, S. T.; Chung, K. K.; McDaniel, C. J.; Darouiche, R. O.; Landman, J.; Brennan, A. B., Micropatterned surfaces for reducing the risk of catheter-associated urinary tract infection: an in vitro study on the effect of sharklet micropatterned surfaces to inhibit bacterial colonization and migration of uropathogenic Escherichia coli. *Journal of endourology / Endourological Society* **2011,** *25* (9), 1547-1552.

28. May, R. M.; Hoffman, M. G.; Sogo, M. J.; Parker, A. E.; O'Toole, G. A.; Brennan, A. B.; Reddy, S. T., Micro-patterned surfaces reduce bacterial colonization and biofilm formation in vitro: Potential for enhancing endotracheal tube designs. *Clinical and translational medicine* **2014,** *3*, 8.

29. Mann, E. E.; Manna, D.; Mettetal, M. R.; May, R. M.; Dannemiller, E. M.; Chung, K. K.; Brennan, A. B.; Reddy, S. T., Surface micropattern limits bacterial contamination. *Antimicrobial resistance and infection control* **2014,** *3*, 28.

30. Kargar, M.; Pruden, A.; Ducker, W. A., Preventing bacterial colonization using colloidal crystals. *Journal of Materials Chemistry B* **2014,** *2* (36), 5962-5971.

31. Kargar, M.; Chang, Y. R.; Hoseinabad, H. K.; Pruden, A.; Ducker, W. A., Colloidal Crystals Delay Formation of Early Stage Bacterial Biofilms. *ACS Biomater Sci Eng* **2016,** *2* (6), 1039-1048.

32. Renner, L. D.; Weibel, D. B., Physicochemical regulation of biofilm formation. *MRS Bull.* **2011,** *36* (5), 347-355.

33. Hochbaum, A. I.; Aizenberg, J., Bacteria pattern spontaneously on periodic nanostructure arrays. *Nano Lett.* **2010,** *10* (9), 3717-3721.

34. Decker, J. T.; Kirschner, C. M.; Long, C. J.; Finlay, J. A.; Callow, M. E.; Callow, J. A.; Brennan, A. B., Engineered antifouling microtopographies: an energetic model that predicts cell attachment. *Langmuir : the ACS journal of surfaces and colloids* **2013,** *29* (42), 13023-13030.

35. Meel, C.; Kouzel, N.; Oldewurtel, E. R.; Maier, B., Three-Dimensional Obstacles for Bacterial Surface Motility. *Small* **2012,** *8* (4), 530-534.

36. Brill-Karniely, Y.; Jin, F.; Wong, G. C.; Frenkel, D.; Dobnikar, J., Emergence of complex behavior in pili-based motility in early stages of P. aeruginosa surface adaptation. *Scientific Reports* **2017,** *7*.

37. Mattick, J. S., Type IV pili and twitching motility. *Annual Reviews in Microbiology* **2002,** *56* (1), 289-314.

38. O'Toole, G. A.; Kolter, R., Flagellar and twitching motility are necessary for Pseudomonas aeruginosa biofilm development. *Mol. Microbiol.* **1998,** *30* (2), 295-304.

39. Klausen, M.; Aaes-Jorgensen, A.; Molin, S.; Tolker-Nielsen, T., Involvement of bacterial migration in the development of complex multicellular structures in Pseudomonas aeruginosa biofilms. *Mol. Microbiol.* **2003,** *50* (1), 61-68.

40. Conrad, Jacinta C.; Gibiansky, Maxsim L.; Jin, F.; Gordon, Vernita D.; Motto, Dominick A.; Mathewson, Margie A.; Stopka, Wiktor G.; Zelasko, Daria C.; Shrout, Joshua D.; Wong, Gerard C. L., Flagella and Pili-Mediated Near-Surface Single-Cell Motility Mechanisms in P. aeruginosa. *Biophys. J.* **2011,** *100* (7), 1608-1616.

41. Jin, F.; Conrad, J. C.; Gibiansky, M. L.; Wong, G. C., Bacteria use type-IV pili to slingshot on surfaces. *Proceedings of the National Academy of Sciences* **2011,** *108* (31), 12617-12622.

42. Chang, Y.-R.; Taylor, S.; Duncan, S.; Mazilu, D. A.; Ritter, A. L.; Ducker, W. A., Fabrication of stabilized colloidal crystal monolayers. *Colloids and Surfaces A: Physicochemical and Engineering Aspects* **2017,** *514*, 185-191.

43. Utech, S.; Bley, K.; Aizenberg, J.; Vogel, N., Tailoring re-entrant geometry in inverse colloidal monolayers to control surface wettability. *Journal of Materials Chemistry A* **2016,** *4* (18), 6853-6859.

44. Park, C.; Lee, T.; Xia, Y.; Shin, T. J.; Myoung, J.; Jeong, U., Quick, Large-Area Assembly of a Single-Crystal Monolayer of Spherical Particles by Unidirectional Rubbing. *Adv. Mater.* **2014,** *26* (27), 4633-4638.

45. Morgan, J. T.; Wood, J. A.; Shah, N. M.; Hughbanks, M. L.; Russell, P.; Barakat, A. I.; Murphy, C. J., Integration of basal topographic cues and apical shear stress in vascular endothelial cells. *Biomaterials* **2012,** *33* (16), 4126-4135.

46. Tolker-Nielsen, T.; Sternberg, C., Growing and Analyzing Biofilms in Flow Chambers. In *Current Protocols in Microbiology*, John Wiley & Sons, Inc.: 2005.

47. Shaner, N. C.; Steinbach, P. A.; Tsien, R. Y., A guide to choosing fluorescent proteins. *Nat Methods* **2005,** *2* (12), 905-909.

48. Weiss Nielsen, M.; Sternberg, C.; Molin, S.; ren; Regenberg, B., Pseudomonas aeruginosa and Saccharomyces cerevisiae Biofilm in Flow Cells. **2011,** (47), e2383.

49. Tinevez, J.-Y.; Perry, N.; Schindelin, J.; Hoopes, G. M.; Reynolds, G. D.; Laplantine, E.; Bednarek, S. Y.; Shorte, S. L.; Eliceiri, K. W., TrackMate: An open and extensible platform for single-particle tracking. *Methods* **2017,** *115* (Supplement C), 80-90.

50. Oliveira, N. M.; Foster, K. R.; Durham, W. M., Single-cell twitching chemotaxis in developing biofilms. *Proceedings of the National Academy of Sciences* **2016,** *113* (23), 6532-6537.

51. Burrows, L. L., Pseudomonas aeruginosa Twitching Motility: Type IV Pili in Action. In *Annual Review of Microbiology, Vol 66*, Gottesman, S.; Harwood, C. S.; Schneewind, O., Eds. 2012; Vol. 66, pp 493-520.

52. Bernard, E. P.; Krauth, W., Two-Step Melting in Two Dimensions: First-Order Liquid-Hexatic Transition. *Physical Review Letters* **2011,** *107* (15).

53. Chang, Y. R.; Taylor, S.; Duncan, S.; Mazilu, D. A.; Ritter, A. L.; Ducker, W. A., Fabrication of stabilized colloidal crystal monolayers. *Colloids and Surfaces a-Physicochemical and Engineering Aspects* **2017,** *514*, 185-191.

54. Skerker, J. M.; Berg, H. C., Direct observation of extension and retraction of type IV pili. *Proc Natl Acad Sci U S A* **2001,** *98* (12), 6901-6904.

Chapter 4 Effect of Topographical Steps on the Surface Motility of the Bacterium *Pseudomonas aeruginosa*

Yow-Ren Chang[1], Eric R. Weeks[2], Daniel Barton[3], Jure Dobnikar[3,4,5], and William A. Ducker[1]

[1]Department of Chemical Engineering and Center for Soft Matter and Biological Physics, Virginia Tech, Blacksburg, VA 24061, USA

[2]Department of Physics, Emory University, Atlanta, GA 30322, USA

[3]Institute of Physics, Chinese Academy of Sciences, Beijing 100190, P. R. China

[4]Songshan Lake Materials Laboratory, Dongguan, Guangdong 523808, China

[5]Department of Chemistry, University of Cambridge, Lensfield Road, CB21EW Cambridge, UK

4.1. Abstract

We demonstrate that topographical steps hinder the ability of the bacterium, *Pseudomonas aeruginosa* PAO1 (*P. aeruginosa*), to traverse a solid–liquid interface. Using time-lapse fluorescence microscopy and image analysis, we analyzed the motion of *P. aeruginosa* that were challenged with steps ranging in height from 0.4 μm to 9 μm. We found a threshold topographical step height between 0.4 μm and 0.9 μm, above which there was a large reduction in the probability of a bacterium crossing over a step. There is a higher frequency of finding bacteria near steps that are above this threshold height. The average speed of bacteria near the step is reduced in the direction perpendicular to the step. Interestingly, we find for 0.9–9 μm tall steps, there is a preference to go down a step, which is against gravity in our system. When a bacterium crosses a step, there is an extra distance required to traverse the riser of the step. The measured time taken for a bacterium to cross a step increases with the height of the step, as expected from the increase in distance travelled. When the height of the step is similar to the length of the bacterium, there is an extra time penalty to cross the step. When traversing the riser, the long axis of the rod-shaped bacterium is more likely than on the flat to be in an up-down direction, indicating reorientation. We also show that bacteria tend to cross steps where the step is concave on the fluid side, which we suggest is due to an increased target area for pili attachment. Our findings provide insights into how the surface motile organism *P. aeruginosa* navigates a topography, and how surface topography may be utilized to hinder the formation or spread of biofilms.

4.2. Introduction

Pseudomonas aeruginosa (*P. aeruginosa*) is an opportunisitic human pathogen known to form biofilms, which are communities of bacteria encased in an extracellular matrix at an interface.[1-2] Biofilms are particularly devastating in a hospital setting as bacteria can colonize medical devices, and cause infections in patients that are difficult to treat.[3] Therefore, researchers have been motivated to develop methods of preventing bacterial biofilm growth on surfaces. Several methods have been proposed in the literature such as the use of liquid-infused surfaces,[4-5] contact killing surfaces,[6-7] dynamic substrates,[8-10] and the use of micro-topographical features.[11-12] Our group has recently demonstrated that micro-particle arrays known as colloidal crystals with particle diameters on the μm scale can hinder biofilm growth, and that the effect of topography is additive to the effect of an antimicrobial surface film or a solution antibiotic treatment.[13-15]

While the effects of surface topography on bacterial biofilm formation have been studied, the mechanism(s) of action remains poorly understood and limits our ability to design better anti-biofilm topographical surfaces. There are several stages in the biofilm formation process[16] and the behavior of bacteria in each stage could be impacted by surface topography. Recent work has examined how the probability of attachment is affected by topography.[17-18] Here we focus on how the topography impacts the surface motility of a particular bacterium, *P. aeruginosa*. *P. aeruginosa* is a rod-shaped bacterium, for which surface twitching motility is important for biofilm formation.[19-20] Twitching motility is achieved by the extension and retraction of several μm long polymeric appendages known as type IV pili.[21-22] The dynamics of type IV pili leads to a wealth of motility behaviors[23-27] that may assist *P. aeruginosa* with the navigation of a surface, and the pili

may even act as sensors for biofilm formation.[28] As we demonstrate, the motion of surface motile bacteria is impacted by surface topography, therefore it is possible that the topography will also impact biofilm formation.

Meel et al. first investigated the effect of micrometer scale grooves of 0.6 and 1 μm height on the motility of *Neisseria gonorrhoeae* and *Myxococcus xanthus*, both of which exhibit surface motility via type IV pili.[29] They found that both organisms appeared to preferentially move within the grooves and that it was more difficult for them to cross taller (1 μm) grooves than shorter (0.6 μm) grooves.[29] We previously investigated the effect of periodic, close-packed, half-sphere arrays on the surface motility of *P. aeruginosa* and found that there was a threshold diameter between 1 and 2 μm where the motion was hindered.[30] We also found that the bacteria preferentially moved in the grooves between particle caps and that bacteria were rarely found on top of the spherical caps.[30] Importantly, the half-sphere texture reduces the average displacement of the bacteria, thereby demonstrating that topography can inhibit motility. Other recent work has also demonstrated that nanopillars also hinders motion of bacteria.[31] In the current work, we study bacterial interactions with widely-spaced, vertical steps in order to understand in more detail how a motile bacterium copes with a single topographic feature. We envision that in order to cross over that step, a bacterium must be able to attach a pilus over a step and pull its body in a direction that contributes to overall motion.

We hypothesize that there is a minimum step height required to measurably hinder motion of *P. aeruginosa*. To test this, we fabricated topographical steps (see Figure 4-1A-C) of various heights between 0.4 to 9 μm, which spans the dimensions of the bacteria and the pili. We placed the stepped topography in a flow chamber (Figure 4-1D) and

recorded the motion of constitutively fluorescent *P. aeruginosa* cells on the interface between the stepped topography and the liquid environment at 37˚C using time-lapse fluorescence microscopy. With image analysis and particle tracking methods, we analyzed the trajectories of single *P. aeruginosa* cells in relation to the topographical step. We also tested the hypothesis that bacteria will travel up and travel down a topographical step (Figure 4-1E) with the same probability. Neglecting the weak force of gravity, these paths are the same, except in the opposite order. Furthermore, we analyzed the modes of motion of single *P. aeruginosa* while crossing a step.

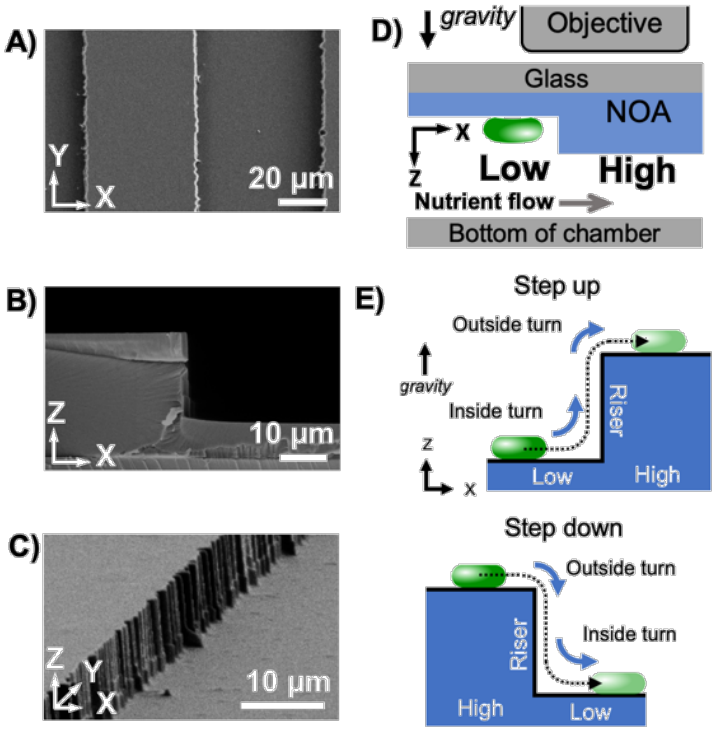

Figure 4-1. Schematic of experimental setup and topographic surfaces. Top-down scanning electron microscope (SEM) image of a fabricated topographical step. B) SEM cross-sectional view of a step. C) Angled SEM view of the face of the step. D) Schematic of the experimental setup. Note the direction of gravity. Because we use an upright microscope and view the solid–liquid interface through the sample, we think of the sample as being 'upside-down'. We refer to the plane that is physically closer to the microscope objective as "low" and the other surface as "high". E) Schematic to describe terms used to refer to motion

of a bacterium crossing a step. Gravity acts in the direction of positive Z. We refer to the face of the step as the riser. The motion of a bacterium traveling from the low plane of the step to the high plane (motion with the direction of gravity) is referred to as a step up and consists of an “inside turn” followed by an “outside turn.” Motion of a bacterium from high to low (against gravity) is referred to as a step down and consists of the same turns as a step up but in reverse order.

4.3. Materials and Methods

4.3.1. Bacterial growth

A constitutively fluorescent strain of *Pseudomonas aeruginosa* PAO1 that produces the fluorescence protein *tdTomato* was used for all studies (gift from Prof. Joe Harrison, Univ. of Calgary). All growth mediums were supplemented with 30 µg/mL gentamycin. Tryptic soy agar plates were streaked with frozen stock and incubated at 37˚C overnight. A 250 mL baffled flask with foam stopper and 50 mL of Tryptic Soy Broth (TSB) was inoculated with a single colony from the agar plate. This culture was grown overnight at 300 rpm and 37˚C. A subculture was started by inoculating 50 mL of TSB with 50 µL of the overnight culture and incubated in a baffled flask at 300 rpm and 37˚C for 4 hours to reach the early exponential growth phase. The suspension was diluted to OD_{600} 0.01 and then immediately used for flow chamber experiments.

4.3.2. Fabrication of topographical step features

Silicon wafer masters of topographical steps were fabricated using a standard deep-reactive ion etching process (DRIE) at the UNC CHANL microfabrication laboratory. Patterns were developed using photolithography on an Si wafer (<100> N-type 100 mm diameter wafer purchased from University Wafer). The wafer was initially coated with a

primer using spin-coating (MicroChem MCC Primer 80/20) at 3000 rpm for 30 seconds to improve adhesion between the photoresist and the wafer during the etching process. A positive photoresist (MicroChem S1813) was then spin-coated onto the surface at 3000 rpm for 30 seconds and subsequently baked for 1 minute at 95˚C. The wafer was then selectively exposed via the photomask to UV radiation using a dose of ~10 mW/cm^2 for 8 seconds and then developed in MF1319 for 60 seconds to expose the pattern for the steps on Si. Etching of the patterned Si wafer was performed using DRIE at 20˚C with alternating pulses of SF_6 at 200 cm^3/min for 3 seconds (etching) and C_4F_8 at 100 cm^3/min for 1.5 seconds (passivation) for a total etch rate of 1 μm/min. Finally, the remaining photoresist was stripped from the Si wafer using O_2 plasma in the DRIE to expose the etched steps in silicon.

The test samples for the bacteria experiments were Norland Optical Adhesive replicates of the silicon masters. To fabricate these replicates, we made a silicone mold that was a negative of the silicon pattern. The silicon wafers with the step topography were first oxygen plasma treated (Harrick Plasma) and then coated with nonafluorohexyltricholorsilane (Gelest) via vapor deposition to act as an anti-adhesion layer. Polydimethylsiloxane (PDMS) negative molds were fabricated by pouring mixed and degassed Sylgard 184 (Dow Corning, 10:1 base to curing agent) onto of the wafers and curing the PDMS at 60˚C overnight. Positive replicates were then fabricated in Norland Optical Adhesive 81 (NOA, Norland Products) by spin-coating NOA onto cleaned cover glass slides at 3000 rpm for 10 seconds, pressing the PDMS mold, and then UV curving the NOA. The curing process took place in two stages, an initial cure at 400 mW from 6 inches away for 120 seconds (Omnicure Series 1000, Excelitas Technologies) and

a final cure in a UV/ozone cleaner (Bioforce Nanosciences) for 10 min. We refer to the final step structure as the “sample”. Figure 4-1A-C shows scanning electron microscopy (SEM) images of the positive NOA steps along with the coordinate system we use in this work. The top-down view of the steps is the X-Y plane (Figure 4-1A) and a cross-sectional view of the step (Figure 4-1B) shows the X-Z plane. Note that riser of the step is not perfectly planar, it has curvature in the Y direction but not the Z direction (Figure 4-1C). We examine the effect of this later. We made two different sample types: one with steps that were 200 μm apart, and the other with steps 50 μm apart. Motility experiments were performed using both spacings and, unless otherwise specified, the results of both experiments were combined. Table 1 shows the measured step heights of both sample types determined from cross-section SEM images. In the remainder of the text, we refer to the step heights by their nominal values: 0.4, 0.9, 1.8, 3, 5, and 9 μm. The flow chamber was finally created by gluing with PDMS a topographic sample on its glass coverslip to a flow chamber and curing at 60˚C. Steps were always arranged such that the edge ran perpendicular to the direction of flow.

Table 1. Measured step heights from cross-section SEM images.

Nominal height / μm	Measured height (50 μm spacing) / μm	Measured height (200 μm spacing) / μm
0.4	0.4	0.4
0.9	0.9	0.9
1.8	1.8	1.8
3	3.1	2.7
5	5.1	5.0
9	9.1	9.4

The measurement uncertainty in step height is about $\pm$ 0.2 μm.

4.3.3. Motility experiments

Flow chamber experiments were performed as previously described.[30] The flow setup consisted of a medium bottle, a peristaltic pump, a bubble trap, the flow chamber, and a waste bottle. The flow setup was autoclaved prior to use and then placed in a custom-built microscope enclosure held at 37˚C. The medium used in flow experiments was 100% TSB and was pumped at ~4 mL/hr. The Reynolds number (*Re*) at this flow rate was calculated to be ~0.004. Prior to imaging, flow was stopped and 150 μL of bacterial suspension (see Section 4.3.1) was injected into each channel of the flow chamber to inoculate the surface. Bacteria were allowed to attach to the surface for 10 min under no flow conditions. The flow of medium was resumed to flush out non-attached bacteria for 10 min; at the flow rate used, this exchanged the volume of the flow chamber approximately 3 times. After flushing, the flow of medium continued to provide nutrients and remove waste, and the motion of bacteria on at the solid-liquid interface was recorded.

We imaged the surface motility of *P. aeruginosa* using a motorized Zeiss Imager.M2 upright fluorescent microscope equipped with a 63x, 1.4 numerical aperture, oil immersion lens. Brightfield images were collected to visualize the topographical step and fluorescence images (excitation: 545/25 nm, beam splitter: 570 nm, emission: 605/70 nm) were collected to visualize the bacteria. Time-lapse movies were collected at a rate of one image every 30 seconds for 2 hours, starting ~20 minutes after the inoculum period (10 min for attachment then 10 min to flush). Lamp intensities and exposures were optimized to prevent phototoxicity; we previously demonstrated that the surface motility of *P. aeruginosa* under these imaging conditions is not affected by fluorescence imaging nor does the motility of the fluorescent strain differ from the wild-type.[30] Since bacteria could be located at different focal planes, low steps (0.4 – 3 μm) were imaged twice, with one *z*-slice focused on the low plane and one on the high plane. The high steps, 5 and 9 μm, were imaged with 3 and 4 *z*-slices respectively.

4.3.4. Image and data analysis

Tracking

All image and data analysis were performed using MATLAB (MathWorks). For image analysis, fluorescence images were used to identify and track bacteria and brightfield images were used to detect the steps. Fluorescence images were collapsed in the *z*-direction to yield a 2-D image that showed bacteria on both the high and low side of the step. Bacteria were tracked using standard particle tracking methods.[32] The length of bacteria was measured by binarizing fluorescent images and measuring the long axis of an ellipse with the equivalent second moment using built-in MATLAB functions.

Step edge detection

To analyze the trajectories of single cells in relation to the step, the step edge needed to be determined in brightfield images. Initial inspection of SEM and brightfield images (Figure 4-1A-C) of the step showed that a) the step riser was not planar on a micrometer scale i.e. the edge has curvature in the Y-direction, and b) the location of the step edge is ambiguous in brightfield images due to bright and dark pixel bands at the edge. To address these points and in order to assess when a bacterium has crossed a topographical step, we took two approaches to defining the step edge:

1) A step zone (Figure 5-18A) was defined so that there is a finite distance that a bacterium must cross to be counted as a step crossing. Since a crossing event must take finite time, it would be difficult to ascribe a single time point in a bacterium's trajectory as the point of crossing the step. So, we defined a rectangular "step zone" in each image where the midline of the rectangle was a straight line fitted to the entire step edge within a field of view (Figure 5-18A). The midline was obtained from brightfield images from an entire movie using a built-in MATLAB edge detection function. These edge pixels were then fit with a line. The step zone was a rectangle in the image with 3.6 μm width, centered on the fitted line. We considered a crossing event to be when a bacterium entered one side of the step zone and exited the other side. Varying the width of the step zone did not qualitatively alter our results.

2) To enable analysis of the effect of topographic curvature in the X-Y plane, we fitted a curved line to the step edge obtained from the brightfield image, and calculated

the radius of X-Y curvature for points on this line (Figure 5-18B). See Supporting Information for details of this calculation.

4.3.5. Statistics

For the purposes of statistical analyses, we consider an experimental replicate to be all the results obtained from a fresh culture of bacteria with a fresh solid sample on a new day. The individual bacteria were not considered to be replicates. Thus, error bars indicating the standard error are derived from the number of replicate movies. We repeated experiments with each step height at least 3 times. Across all step heights and replicates, we identified ~700 crossing events over ~10,000 frames (45 movies total). Statistical testing was performed with *t*-tests or analysis of variance (ANOVA) followed by a multiple comparison test when appropriate. In general, we considered differences with *p*-values less than 0.05 to be significant.

4.4. Results

All results are for cells that were allowed to adsorb for approximately 20 minutes before imaging was commenced, when most of the cells are still actively moving and there are no clusters of cells at the interface. The total time of an experiment was 120 min. We used the concept of a step zone (see Figure 5-18A) to determine when a bacterium had crossed the edge or how far the bacterium is from the edge, except in the final section on the effect of curvature. The presence of fluid flow in our conditions does not influence the motion of bacteria (see Supporting Information).

4.4.1. Bacteria are more likely to be found near a step edge

We hypothesized that topographical steps of 1–2 μm in height would hinder the ability of a bacterium to move across a solid–liquid interface. If steps frustrate the passage of a bacterium across a surface we would expect to find a higher probability density of bacteria at or near the step edge, so we used the distribution of bacteria as the first test of the influence of steps. Figure 4-2 indicates the probability of a bacterium being a particular perpendicular distance from a step. The average probability at a certain distance is drawn as a solid line and the standard error is shown as a shaded region around the average. Flat surfaces with fictional step edges were used as zero step-height controls, for which we would expect no dependence on the distance from the non-existent "step."

On a flat surface, the probability distribution of distance to a fictional linear step was independent of distance (dashed gray line in Figure 4-2), which demonstrates that time-averaged position was spatially homogenous. Likewise, the probability distribution on 0.4 μm steps was also independent of distance. In contrast, for all steps of greater height, there was an increased probability of finding bacteria at or near the step edge (<5 μm away). At distances greater than ≈5 μm from the step edge, the probability distribution was constant, indicating that the distribution of bacteria far away from the step is uniform.

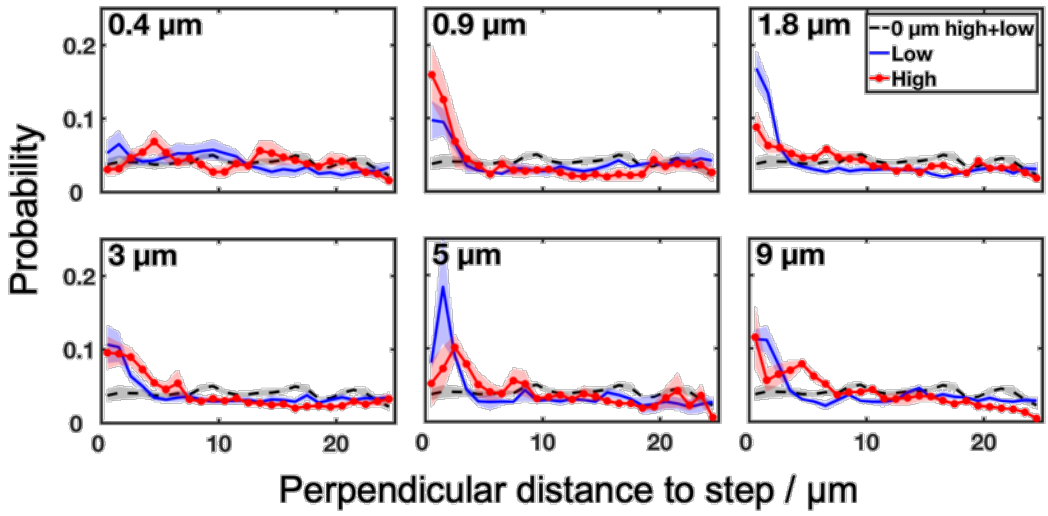

Figure 4-2. Probability distribution of perpendicular distance to a step. Locations on the high and low plane near the step are considered separately. The distance is measured to the midline of the step zone. Bacteria are more likely to be found near steps when the step height is greater than 1 μm. Only data from samples with 50 μm spacing between steps were used in this analysis.

4.4.2. Motion towards a topographical step is reduced near the step

Since Figure 4-2 suggests that there is a higher probability density of bacteria near a step edge for step heights taller than 1 μm, we investigated how the bacteria move near the step edge. We calculated the displacement vector of each bacteria over a 5 min. time interval, Δr, as a function of perpendicular distance to a step edge at the start of the time period. We decomposed Δr into components that were parallel ($\Delta r_{\parallel}$) and perpendicular ($\Delta r_{\perp}$) to the step (see Figure 5-20 for diagram). $|\Delta r_{\parallel}|$ is independent of step height and proximity and is shown in Figure 5-21. Thus, motion of bacteria parallel to the plane of step riser is unaffected by the presence of the step. For perpendicular motion, we only recorded displacements towards a step edge. Figure 4-3 plots the magnitudes of the vector, $|\Delta r_{\perp}|$ as a function of starting distance to the step for different step heights. Data

for motion towards a step down (blue) are plotted separately to data for motion towards a step up (red dotted line). $|\Delta r_{\perp}|$ near the 0.4 μm step is similar to similar to $|\Delta r_{\perp}|$ and to $|\Delta r_{\parallel}|$ on the flat steps, that is, 0.4 μm tall steps do not slow down bacteria near the step. This is consistent with our findings in Fig. 2 for the 0.4 μm tall steps. For 0.9-9 μm steps, $|\Delta r_{\perp}|$ decreases from ≈4 μm for those bacteria starting more than 10 μm away from the step down to ≈2 μm for those starting near the step edge. Since type IV pili are several μm in length, this could be the range in which type IV pili are sensing the topographical step. Overall, this data suggests that motion of bacteria towards a topographical step is hindered if the step is of sufficient height (>0.4 μm).

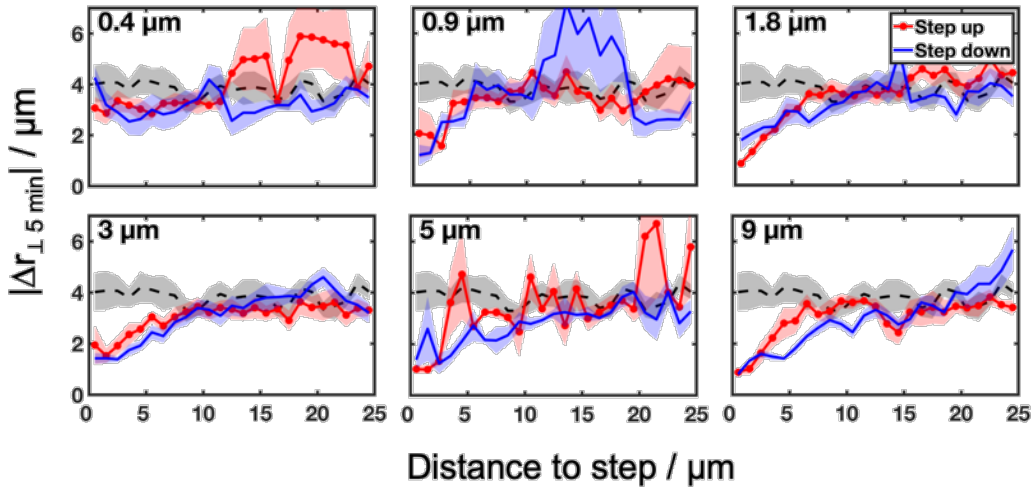

Figure 4-3. Average displacement of cells moving perpendicularly to a step as a function of the starting distance to the midline of the step. For example, a bacterium starting 5 μm to the left of the step and ending at 5 μm to the right has $\Delta r_{\perp}$= 10 and contributes to the average at a distance of 5 μm. $\Delta r_{\perp}$ is plotted for a flat surface (dashed black), motion towards a step up (solid red line), and motion towards a step down (solid blue line). Only data from samples with 50 μm spacing between steps was used in this analysis.

4.4.3. Steps reduce the crossing probability of bacteria

We next determined the probability of a bacterium crossing over a step barrier. For this metric, we defined a step zone that extended 1.8 μm on each side of the step (see Figure 5-18A). We defined the probability as the ratio between (a) the number of bacteria that traversed the entire width of the strike zone and (b) the number of bacteria that were ever in the strike zone (see Figure 4-4A inset). Figure 4-4A plots the crossing probability for individual experimental replicates (dotted markers) as well as the average (square markers) for each step height. We find that the crossing probability is less than 1 for bacteria on a flat surface with an imaginary step, which is reasonable because the bacterial motion is not ballistic in one direction. Thus, bacteria that are sufficiently close to the imaginary step may not cross even though there is no physical barrier. We find that the crossing probability is dramatically reduced from 0.68 ± 0.03 on a flat surface down to ≈ 0.2 on steps taller than 0.9 μm. We confirmed this observation by performing an ANOVA followed by a Tukey-Kramer multiple comparison test. We found that the crossing probability of bacteria on a surface with 0.4 μm steps was not different than on a flat ($p = 0.20$), and that both 0 and 0.4 μm were different than all steps taller than 0.9 μm ($p << 0.001$ for each pair-wise comparison between 0 μm and 0.9-9 μm and between 0.4 μm and 0.9-9 μm). We hypothesized that there might be an intermediate step height, of order of the length of the bacteria (≈3 μm), that was more difficult to cross, however, we did not find a statistically significant difference between step heights 0.9-9 μm ($p >> 0.1$ for each pair-wise comparison between step heights 0.9-9 μm).

We also tested our hypothesis on the rectification of crossings, i.e., is there a difference between going up and down? We defined rectification as the quantity number

of crossings up minus the number of steps down divided by the total number of crossings. Thus, a positive rectification would indicate a preference for the bacteria to step up. In Figure 4-4B, we compared the average rectification of 0-0.4 μm steps to 0.9-9 μm tall steps. The average rectification for 0-0.4 μm steps was –0.08 ± 0.05 indicating that bacterial crossings up and down were almost equal. The average rectification of step heights in the range 0.9-9 μm steps was –0.27 ± 0.07 and a *t*-test comparing the rectification to zero rectification yielded a *p*-value of 0.003. Thus, we have resolved a preference for travel *against* gravity. (see Figure 4-1D for direction of gravity).

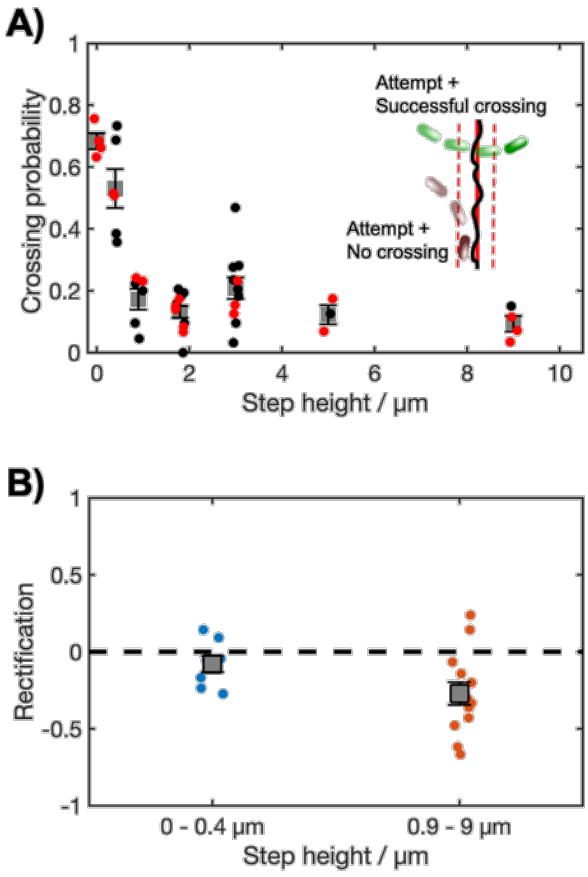

Figure 4-4. Probability of crossing steps and rectification. A) Probability of *P. aeruginosa* crossing a step. Black dots indicate experiments performed with a single topographical step in a field of view. Red dots indicate experiments with multiple steps in a field of view. Circles represent individual experimental

replicates and artificial spread has been applied to the x-axis for so that overlapping data points can be viewed. The average for each step height is shown in square markers. We identified 736 crossing events across all experiments. Inset: schematic of how attempts to cross is defined. B) Rectification of motion of *P. aeruginosa* crossing a topographical step. Rectification is defined as the number of steps up minus the number of steps down all divided by the total number of crossings. Thus, negative rectification is bias for motion opposing gravity. We did not include data from steps where the total number of crossings was less than 10. Replicate data points are plotted with circular markers, the average with square markers, and the standard error with error bars. The step heights are grouped into two groups: 0–0.4 μm and 0.9–9 μm heights.

4.4.4. Steps are not simply extra distance for a bacterium to travel

When a bacterium crosses a step, it must also travel over an extra distance of at least the height of the step. In the simplest model, the extra distance would be modeled as an extra section of flat terrain, and turning the corners (Figure 4-1E) would not require any extra time or otherwise affect the trajectory (see Figure 5-22). In this section we examine the model that the effects of the step are entirely due to the extra distance of the step riser. Because motion is not ballistic, the extra distance would not simply add a proportional amount of time; in fact, we have shown previously that the mean squared displacement is proportional to $(\Delta t)^{1.5}$, where t is time.[30] We examined this simple model by measuring the time it takes for a bacterium to cross a step, t. Figure 4-5 plots the arithmetic averages of individual replicates (dots) along with the grand averages (square markers). We see that the average t increases with step height. We then compared the average t from bacteria crossing real steps (black square markers, Figure 4-5) to the time taken by bacteria to cross a section of a flat surface of the equivalent distance as a step, t_{eq} (blue square markers, see Figure 4-5 and Figure 5-22).

To see how the t compares to t_{eq}, we performed a two-factor ANOVA where factor 1 was the step height (p = 0.003) and factor 2 was a real step or a flat surface of the equivalent distance. Importantly, we found a significant influence of factor 2 (p = 0.008) indicating that the overall average t was different to the overall average t_{eq}. We found that the average t across all steps was greater than the average t_{eq}, thus demonstrating that steps have an effect in addition to merely requiring an extra distance to travel. In other words, there is an excess time penalty to cross certain step heights.

We then calculated the difference, Δt_{cross}, between the times t and t_{eq} for different step heights and performed a multiple comparison test to investigate which step heights had an extra time penalty to cross. We expected that Δt_{cross} will be small for the flat and 0.4 μm step heights. Interestingly, we find that Δt_{cross} was greater than Δt_{cross} on a flat for only for 1.8 and 3 μm steps (p = 0.04 for 0 vs 1.8 μm and p = 0.006 for 0 vs 3 μm) and not for the higher steps. Since the p-value for the comparison between 0 μm and 1.8 μm was close to the value that we set for significance, we performed three additional entirely independent experiments on only the 1.8 μm steps. The p-value for new experiments yielded p = 0.15, so we are not in a position to make a conclusion that the 1.8 μm step in particular requires additional time beyond the time to traverse the distance of the riser. However, we do conclude that the bacteria took extra time, about 2.5 × as long, to cross the 3 μm step. We explore the implications of this finding further in the Discussion. On higher steps (5 μm and 9 μm) the main effect of the step appears to be the extra distance required for travel; the extra time to turn the corners was small.

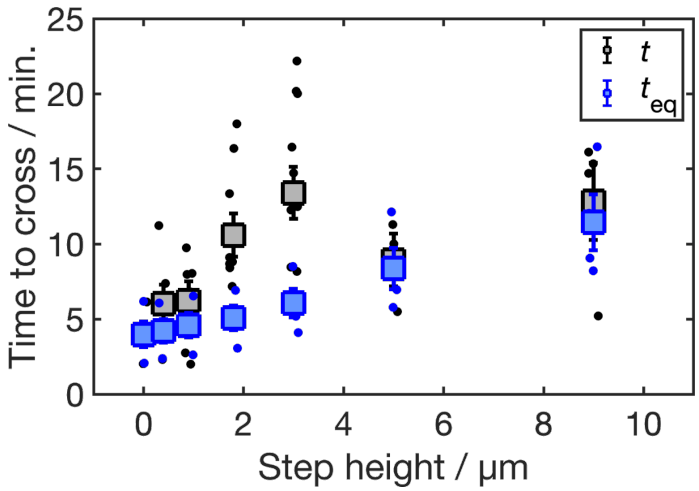

Figure 4-5. Time for *P. aeruginosa* to traverse a topographical step as a function of step height. The arithmetic mean time to cross of individual replicates is plotted as circular markers and the grand average is plotted as square markers. The error bars indicate standard error. The time to cross a real step, t, is compared to the time to cross a flat surface of the equivalent pathlength, t_{eq}. Note that markers for the grand average t and t_{eq} for the flat (0 μm) surface overlap each other and that the x-axis is on a log scale.

4.4.5. Bacteria crossing tall steps predominately do so in the crawling mode

For tall steps, we investigated the mode in which bacteria crawled up a step. It is well known that on a flat surface, *P. aeruginosa* can adopt different modes of surface motility. Specifically, they can "crawl" where the long axis of the body is parallel to a surface or "walk", where the long axis is perpendicular or angled to the surface.[33] In an X-Y image, crawlers appear as rods and walkers appear as circles, when perpendicular to the interface (Figure 4-6A). We measured the lengths of bacteria in the X-Y plane on a flat surface and find two peaks: one at ~3 μm corresponding to the crawlers and another at ~1 μm, corresponding to the walkers (Figure 4-6B). To check whether there is a predominate motility mode while *P. aeruginosa* crawls up a tall step, we measured the X-Y lengths of individual bacteria as they cross steps.

Figure 4-6C is a fluorescence image of a bacterium (dashed white circle) traversing a 9 μm step overlaid with a brightfield image of the step in the X-Y plane (top-down view). Since images are Z-stacks, we can project the fluorescence image onto the X-Z or Y-Z planes (side panels) to visualize the profile of the bacterium as it moves up the face of the step. We define the mode relative to the local surface plane, so on the riser of the step, a bacterium with a short X-Y length corresponds to the crawling mode (see Figure 5-23). So, the bacterium in Figure 4-6C is traversing the step in a crawling mode (circular in X-Y plane) but is actually elongated as shown in the X-Z or Y-Z planes. Figure 4-6D is a time-course plot of the X-Y length of the bacterium shown in Figure 4-6C as it crosses a step. The projected length diminished when it started on the step and then increased as it leaves the step, clearly showing the bacterium crawled up the vertical face of the step. In other words, a crawler on the riser of a step looks in our images like a walker on a flat and vis-versa.

Figure 4-6D showed one example; we are interested in typical behavior, so we compared probability distributions of X-Y lengths of bacteria crossing steps. Figure 4-6E and Figure 4-6F compare a histogram of X-Y lengths of bacteria on steps to those on a flat surface (dashed black line). The distribution of X-Y lengths of bacteria traversing a (low) 0.4 μm step is not drastically altered from the distribution on the flat. This is expected as the 0.4 μm is shorter than the height of a bacterium and may not alter the bacterium's mode of motility. In contrast, the distribution of X-Y lengths of bacteria traversing high (3-9 μm) steps shows a single peak at ~1 μm suggesting that bacteria traversing tall topographical steps predominately adopt the crawling mode while on the riser of the step.

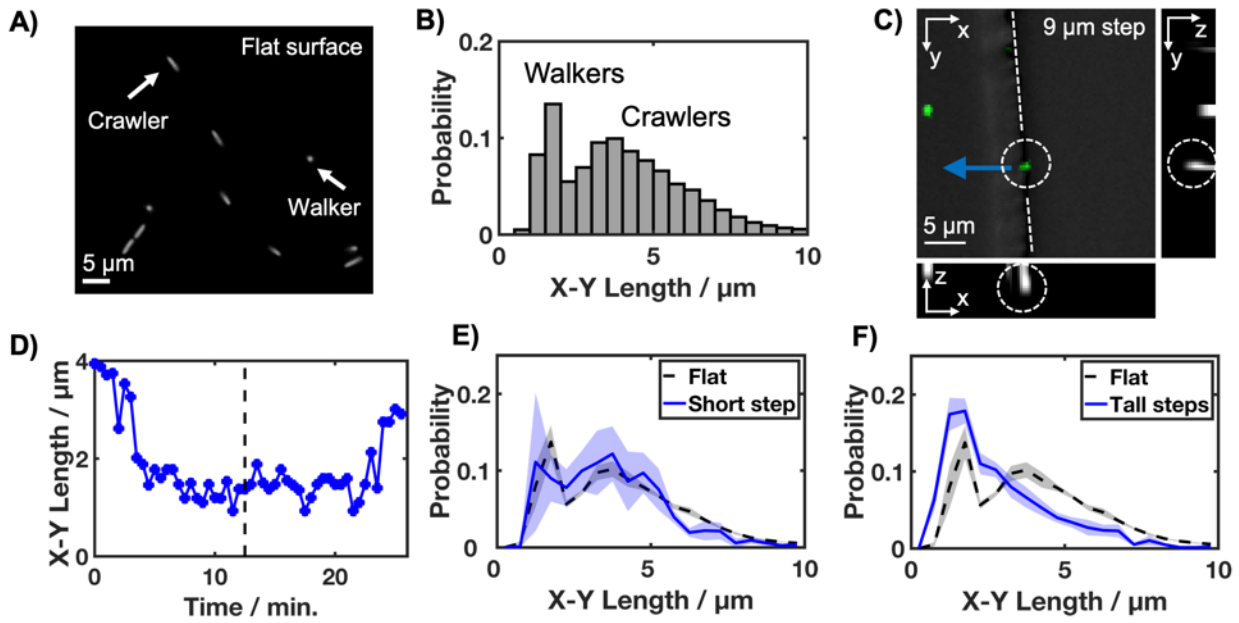

Figure 4-6. Orientation of bacteria while crossing a step. A) Fluorescence image of several *P. aeruginosa* cells of different aspect ratios on a flat surface. The image shows the cross section in the X-Y plane. The long aspect ratio is the crawling mode and the low aspect ratio is the walking mode. B) Distribution of X-Y length on a flat sample. There is a peak at ~1-2 μm associated with walking and a peak at ~3 μm associated with crawling. C) Fluorescence image (green) of *P. aeruginosa* on a 9 μm topographical step (gray) shown for the X-Y, X-Z, and Y-Z planes. A dashed line is drawn to show the step edge. The same bacterium is circled in white to show that while the X-Y length is small while crossing the step, the long axis of the bacterium is parallel to the step face (X-Z image). A dashed white line shows the position of the step edge. The Z scale has been rescaled in the X-Z and Y-Z images. D) Example time course of measured X-Y length of the bacterium shown in C. The length of the bacterium decreases as it approaches and climbs the riser and increased again when it departs. The dashed line in D indicates the time of the image shown in C. E) Probability distribution of X-Y length while crossing short topographical steps (step height 0.4 μm). The data for a flat surface is reproduced from B for comparison. The distributions on the short step is similar to that on the flat step. F) Probability distribution of measured X-Y lengths of *P. aeruginosa* while crossing tall topographical steps (3-9 μm).

4.4.6. The local X–Y step curvature influences bacterial motion

In the analysis so far, we have ignored the fact that the risers in our samples have curvature in the X-Y plane with radius of the same order as the bacteria (~1 μm). We hypothesize here that crossing bacteria may be more likely to cross from low to high in the immediate vicinity of regions of step where the curvature is concave relative to the fluid (assigned negative, see Figure 5-18) rather than at points where the radius is positive. Regions of negative curvature would give a greater cone angle where the pili could strike the riser (see Figure 5-24). This hypothesis was inspired by the author's experience that we find it is easier to climb rock faces that have negative curvature on our human scale than to climb rock faces with positive curvature.

To test this hypothesis, we first fit a (curved) line in the X-Y plane to the image of the step edge and then characterized the local curvature at each point on this curve (see Supporting Information for details, Figure 5-18 and Figure 5-19). Since the step is now defined by a mathematically thin line, we do not use the step zone concept to define a crossing. Instead, we determine if a bacterium has crossed the step by searching for intersections between the trajectory of the bacterium and the line fitted to the step. Next, we recorded the local curvature at points where an ellipse fitting the body of the bacterium overlaps with the step edge. Figure 4-7 compares the histograms for all points on the step line (white bars) to curvatures that bacteria sampled while crossing up (gray bars). The values of R are binned into small (0-2 μm), medium (2-5 μm), and large (>5 μm) R values. The data for all points (white bars) shows that there are approximately equal fractions of positive and negative curvature in each bin, yet the bacteria are more likely to cross at small negative curvatures (gray bars), thus supporting the hypothesis.

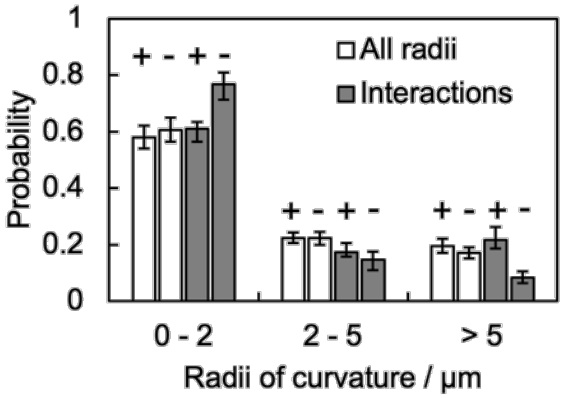

Figure 4-7. Bacteria interact with local curvature. Radius of curvature for 9 µm step edge. The curvature of the entire step ("All radii") is compared to the points where the body of the bacterium overlaps with the step edge ("Interactions"). The sign of the radii is indicated above the column. The probability of a bacterium crossing at small negative curvature (R < 2 µm) is greater than the probability of there being negative curvature on the step line, demonstrating that bacteria tend to more frequently cross at negative curvature sites.

4.5. Discussion

4.5.1. Increasing the impediment to motility

We investigated how the opportunistic human pathogen *P. aeruginosa* navigates topographical steps of heights 0.4-9 µm. Our data demonstrate that steps of 0.9 µm or taller significantly hinder the ability of bacteria to traverse a solid–liquid interface. Since surface topography has been shown to be important for bacterial biofilm formation, our results could have implications for the design of topographical surfaces for biofilm prevention or help elucidate the mechanisms of topography in slowing down biofilm growth. First, the demonstrated reduction in movement by the steps may hinder bacteria from finding each other and therefore hinder biofilm growth. Second, the reduction in

movement may slow the spread of bacteria from one point to another. For example, it might potentially slow the progression of bacteria up catheters and into patients.

To increase the impediment to bacteria, we fabricated samples with a greater density of steps, and steps running in both X and Y directions: a 50 x 50 μm raised square patterns (checkerboard) of 2 μm height. Figure 4-8A shows a maximum intensity image from a 2-hour time-lapse movie of *P. aeruginosa* on this checkboard. The image indicates that trails of *P. aeruginosa* interact with the walls of the checkerboard pattern. We tracked the bacteria and quantified the average speed on a 2 μm checkerboard pattern, and compared that to the average speed of bacteria on a flat surface. We found that on the 2 μm checkerboard pattern, the average displacement in 5 min. was 4.7 ± 0.1 μm versus 6.1 ± 0.6 μm on a flat surface. Figure 4-8B shows a probability distribution of displacement in 5 min. of bacteria on a flat surface (solid blue) and a 2 μm tall checkerboard pattern (dashed black). Compared to a flat surface, bacteria on a 2 μm tall checkerboard pattern have more short displacement events and fewer long displacement events. It is reasonable that if the steps were placed even more closely, then a greater fraction of short paths would have been affected.

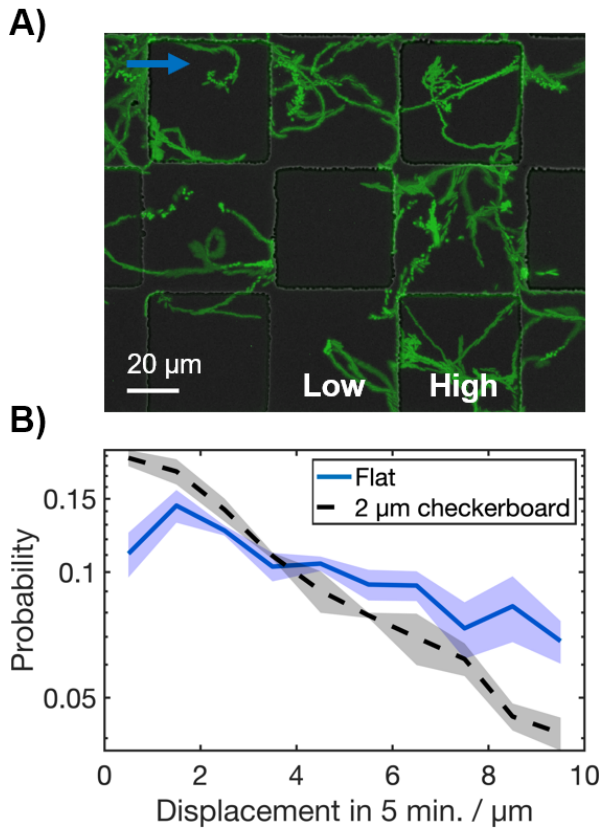

Figure 4-8. Checkerboard pattern slows down bacterial motility. Maximum intensity image of a *P. aeruginosa* time-lapse motility experiment on 2 µm tall checkerboard patterns over the course of 2 hours. The fluorescence image of bacteria (green) is overlaid with a brightfield image of the checkerboard (gray). The direction of flow is indicated by the blue arrow. The steps are spaced by 50 µm on the checkerboard. Some *P. aeruginosa* trajectories are hindered by the walls and others run alongside the walls. B) Probability distribution of displacement of bacteria in 5 min. on a flat (solid blue) and a 2 µm tall checkerboard pattern (dashed black). The shaded regions indicate standard error.

4.5.2. The mechanism for motility inhibition on steps

There are to date only a few studies of bacterial motility on micrometer-scale topography, so we are not yet in a position to prove how topography affects motility, but our results provide some insight. Both the work of Meel et al. (*Neisseria gonorrhoeae* and *Myxococcus xanthus*) on grooves[29] and our work (*P. aeruginosa*) find a threshold where

topographical barriers of ~1 μm in height are more difficult to cross. Thus, the critical length-scale is similar to the dimensions of the bacterium and the length of pili. Recent work has also shown that nanopillar arrays influence the surface motility (*P. aeruginosa*) and the authors hypothesize that the available area for attachment for type IV pili may be important.[31]

Meel et al. state "that grooves provide a larger adhesive area for the bacteria than the ridges, explaining why bacteria remain preferentially within the groove..."[29] In prior work we showed that the motion of *P. aeruginosa* in our systems was lost when for mutants lacking pili.[30] Here we hypothesize that an important factor is the availability of attachment sites for the pili. This may include the area available for pili attachment and a path for the pili to reach an attachment site.[30] If the topography in a particular direction is not favorable for pili attachment, then that direction of motion may be disfavored. Since our microscopy cannot resolve the type IV pili interactions, we cannot provide direct evidence of how the pili attach on various topographies; we can only discuss consistency with the observed motion of the bacterial body. We envision that there may be a conformational space in which type IV pili may explore while trying to attach to a surface. We hypothesize that a bacterium's ability to navigate topography is related to the intersection of this conformational space with the surface (Figure 4-9).

We propose that when a bacterium crosses a simple step, it must navigate three sections: an outside turn, the riser, and an inside turn (see Figure 4-1E). These are the same three components whether the bacterium is going up or down the step. In the limit of a long riser, we assume the interaction with these three components to be independent. Given that the extra time to cross a step is largely explained by the extra distance from

the riser, this leads us to conclude that the turns are very important on the high steps. This is surprising. A bacterium approaching an inside turn may have a greater area of attachment points for pili due to the presence of the riser (see Figure 4-9, left diagram). In contrast, when a bacterium approaches an outside turn, it increasingly faces a void ahead, and thus diminishing areas for pilus attachment (see Figure 4-9, right diagram). Thus, we would have expected that the outside turn would be the rate limiting step when a bacterium is navigating a step due to extra time required for pili to sample its conformational space and find a solid surface for attachment. Therefore, our results suggest that the exploration of the conformational space by the pili is rapid compared to other processes (such as the movement of the body).

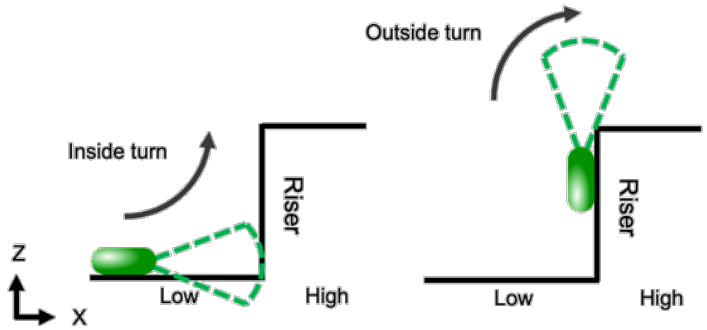

Figure 4-9. Schematic of possible available attachment points as *P. aeruginosa* navigates a step. We envision that there is a region of possible conformations that a type IV pili may have as it extends (dashed green cone). We hypothesize that attachment to a surface is more likely when there is maximum intersection of the pilus conformational space with a solid surface, such as an inside turn (left image). When the bacterium approaches an outside turn (right), the pilus may need more time to find a suitable attachment point on the step.

For a riser of length similar to the bacterium and pili, different parts of a bacterium may encounter all three components simultaneously. For the 3 μm steps, the time to cross

was much larger (2–3x) than for the equivalent distance on the flat surface, demonstrating that crossing the combination of the two turns was more difficult.

Furthermore, we observed some mild rectification. The bacteria are more likely to cross a high step in the direction *against* gravity. Rectification requires both asymmetry in the Z direction and some active motion. The active motion is clearly driven by type IV pili. There are several possible sources of asymmetry in our system: the fluid flow, the topography, and gravity. We have shown that the effect of fluid flow is negligible (see Supporting Information) in our system. The steps were originally etched from top to bottom in silicon, so in principle the steps could be asymmetric in this direction, but we could not detect asymmetry in the SEM images. Finally, it is possible that the asymmetry arises from gravity. We explored whether gravity was significant by observing Δ*fliC* mutants which lack flagella and therefore are unable to actively swim against gravity. These bacteria do settle, so although the force of gravity is insignificant compared to the force of the pilus, the gravitational energy is significant compared to thermal energy (*kT*). This gravitational force could bias the body to be below the pili on the riser. Because pili mediated motion is in the direction from the body towards the pili, this gravitation bias would bias motion against gravity rather than with gravity, which is the observed direction or rectification.

4.6. Conclusions

There is a critical step height in the range 0.4–0.9 μm where the ability of *P. aeruginosa* to navigate a surface is affected. Specifically, we find (a) a reduced magnitude of speed perpendicular to the step when the bacteria are very near the step, (b) the

probability of crossing the step is drastically reduced compared to crossing a point on a flat surface, and (c) that bacteria are more frequently found near steps. For bacteria that do cross a step, we find a mild rectification of motion against the direction of gravity. Furthermore, there is a time penalty to cross step heights that are similar to the length of the bacterium; but, we do not resolve a time penalty to cross tall steps (5 and 9 μm) in excess of the additional time expected to cross the riser of the step. Images show that *P. aeruginosa* predominantly crawl on the step riser, which means that some bacteria rotate on encountering a step such that the orientation relative to the local topographic plane is similar on the step riser and a flat plane. The bacteria more commonly cross a step where the step is concave relative to the fluid. Overall, these findings show that steps with heights similar to the dimensions of the bacteria affect motility. The observed retardation of motion across a plane may be useful for inhibiting colonization and biofilm formation.

4.7. Acknowledgements

We thank Prof. Joe Harrison (Univ. of Calgary) for providing the fluorescent strain of P. aeruginosa. The authors also thank Prudvi Gaddam (Virginia Tech) and Bob Geil (UNC CHANL) for assistance with the fabrication of the silicon masters used to generate topography, the Fralin Imaging Center (Virginia Tech), the Nanoscale Characterization and Fabrication Laboratory (Virginia Tech), and Chang Lu (Virginia Tech) for the use of equipment and facilities. We also thank Prof. Daan Frenkel (Univ. of Cambridge) for useful discussions and for setting up the collaboration. We acknowledge financial support from Virginia's 4-VA program and the Institute for Critical Technology and Applied

Science (ICTAS) at Virginia Tech for funding and support, and from CAS-TWAS Presidential Scholarship and from the National Science Foundation of China (NSFC, Grant 1874398).

References

1. Hall-Stoodley, L.; Costerton, J. W.; Stoodley, P., Bacterial biofilms: from the natural environment to infectious diseases. *Nature Reviews Microbiology* **2004,** *2* (2), 95-108.

2. Donlan, R. M., Biofilms: microbial life on surfaces. *Emerg Infect Dis* **2002,** *8* (9).

3. Donlan, R. M., Biofilms and device-associated infections. *Emerging infectious diseases* **2001,** *7* (2), 277-281.

4. Howell, C.; Grinthal, A.; Sunny, S.; Aizenberg, M.; Aizenberg, J., Designing Liquid-Infused Surfaces for Medical Applications: A Review. *Adv. Mater.* **2018,** *30* (50), 1802724.

5. Epstein, A. K.; Wong, T.-S.; Belisle, R. A.; Boggs, E. M.; Aizenberg, J., Liquid-infused structured surfaces with exceptional anti-biofouling performance. *Proceedings of the National Academy of Sciences* **2012,** *109* (33), 13182-13187.

6. Ivanova, E. P.; Hasan, J.; Webb, H. K.; Truong, V. K.; Watson, G. S.; Watson, J. A.; Baulin, V. A.; Pogodin, S.; Wang, J. Y.; Tobin, M. J., Natural bactericidal surfaces: mechanical rupture of Pseudomonas aeruginosa cells by cicada wings. *Small* **2012,** *8* (16), 2489-2494.

7. Ivanova, E. P.; Hasan, J.; Webb, H. K.; Gervinskas, G.; Juodkazis, S.; Truong, V. K.; Wu, A. H. F.; Lamb, R. N.; Baulin, V. A.; Watson, G. S.; Watson, J. A.; Mainwaring, D. E.; Crawford, R. J., Bactericidal activity of black silicon. *Nat Commun* **2013,** *4*.

8. Gu, H.; Lee, S. W.; Buffington, S. L.; Henderson, J. H.; Ren, D., On-Demand Removal of Bacterial Biofilms via Shape Memory Activation. *ACS Applied Materials & Interfaces* **2016,** *8* (33), 21140-21144.

9. Lee, S. W.; Gu, H.; Kilberg, J. B.; Ren, D., Sensitizing bacterial cells to antibiotics by shape recovery triggered biofilm dispersion. *Acta Biomaterialia* **2018,** *81*, 93-102.

10. Levering, V.; Wang, Q.; Shivapooja, P.; Zhao, X.; López, G. P., Soft Robotic Concepts in Catheter Design: an On-Demand Fouling-Release Urinary Catheter. *Advanced Healthcare Materials* **2014,** *3* (10), 1588-1596.

11. Chung, K. K.; Schumacher, J. F.; Sampson, E. M.; Burne, R. A.; Antonelli, P. J.; Brennan, A. B., Impact of engineered surface microtopography on biofilm formation of Staphylococcus aureus. *Biointerphases* **2007,** *2* (2), 89-94.

12. Hasan, J.; Chatterjee, K., Recent advances in engineering topography mediated antibacterial surfaces. *Nanoscale* **2015,** *7* (38), 15568-15575.

13. Kargar, M.; Pruden, A.; Ducker, W. A., Preventing bacterial colonization using colloidal crystals. *Journal of Materials Chemistry B* **2014,** *2* (36), 5962-5971.

14. Kargar, M.; Chang, Y. R.; Hoseinabad, H. K.; Pruden, A.; Ducker, W. A., Colloidal Crystals Delay Formation of Early Stage Bacterial Biofilms. *ACS Biomater Sci Eng* **2016,** *2* (6), 1039-1048.

15. Mon, H.; Chang, Y.-R.; Ritter, A. L.; Falkinham, J. O.; Ducker, W. A., Effects of Colloidal Crystals, Antibiotics, and Surface-Bound Antimicrobials on Pseudomonas aeruginosa Surface Density. *ACS Biomater Sci Eng* **2018,** *4* (1), 257-265.

16. Monds, R. D.; O'Toole, G. A., The developmental model of microbial biofilms: ten years of a paradigm up for review. *Trends in microbiology* **2009,** *17* (2), 73-87.

17. Decker, J. T.; Kirschner, C. M.; Long, C. J.; Finlay, J. A.; Callow, M. E.; Callow, J. A.; Brennan, A. B., Engineered antifouling microtopographies: an energetic model that predicts cell attachment. *Langmuir : the ACS journal of surfaces and colloids* **2013,** *29* (42), 13023-13030.

18. Ye, Z.; Kim, A.; Mottley, C. Y.; Ellis, M. W.; Wall, C.; Esker, A. R.; Nain, A. S.; Behkam, B., Design of Nanofiber Coatings for Mitigation of Microbial Adhesion: Modeling and Application to Medical Catheters. *ACS Applied Materials & Interfaces* **2018,** *10* (18), 15477-15486.

19. O'Toole, G. A.; Kolter, R., Flagellar and twitching motility are necessary for Pseudomonas aeruginosa biofilm development. *Mol. Microbiol.* **1998,** *30* (2), 295-304.

20. Klausen, M.; Aaes-Jorgensen, A.; Molin, S.; Tolker-Nielsen, T., Involvement of bacterial migration in the development of complex multicellular structures in Pseudomonas aeruginosa biofilms. *Mol. Microbiol.* **2003,** *50* (1), 61-68.

21. Skerker, J. M.; Berg, H. C., Direct observation of extension and retraction of type IV pili. *Proc Natl Acad Sci U S A* **2001,** *98* (12), 6901-6904.

22. Merz, A. J.; So, M.; Sheetz, M. P., Pilus retraction powers bacterial twitching motility. *Nature* **2000,** *407* (6800), 98.

23. Brill-Karniely, Y.; Jin, F.; Wong, G. C.; Frenkel, D.; Dobnikar, J., Emergence of complex behavior in pili-based motility in early stages of P. aeruginosa surface adaptation. *Scientific Reports* **2017,** *7*.

24. Jin, F.; Conrad, J. C.; Gibiansky, M. L.; Wong, G. C., Bacteria use type-IV pili to slingshot on surfaces. *Proceedings of the National Academy of Sciences* **2011,** *108* (31), 12617-12622.

25. Conrad, Jacinta C.; Gibiansky, Maxsim L.; Jin, F.; Gordon, Vernita D.; Motto, Dominick A.; Mathewson, Margie A.; Stopka, Wiktor G.; Zelasko, Daria C.; Shrout, Joshua D.; Wong, Gerard C. L., Flagella and Pili-Mediated Near-Surface Single-Cell Motility Mechanisms in P. aeruginosa. *Biophys. J.* **2011,** *100* (7), 1608-1616.

26. Shen, Y.; Siryaporn, A.; Lecuyer, S.; Gitai, Z.; Stone, H. A., Flow directs surface-attached bacteria to twitch upstream. *Biophys. J.* **2012,** *103* (1), 146-151.

27. Lecuyer, S.; Rusconi, R.; Shen, Y.; Forsyth, A.; Vlamakis, H.; Kolter, R.; Stone, H. A., Shear stress increases the residence time of adhesion of Pseudomonas aeruginosa. *Biophys. J.* **2011,** *100* (2), 341-350.

28. Persat, A.; Inclan, Y. F.; Engel, J. N.; Stone, H. A.; Gitai, Z., Type IV pili mechanochemically regulate virulence factors in Pseudomonas aeruginosa. *Proceedings of the National Academy of Sciences* **2015,** *112* (24), 7563-7568.

29. Meel, C.; Kouzel, N.; Oldewurtel, E. R.; Maier, B., Three-Dimensional Obstacles for Bacterial Surface Motility. *Small* **2012,** *8* (4), 530-534.

30. Chang, Y.-R.; Weeks, E. R.; Ducker, W. A., Surface Topography Hinders Bacterial Surface Motility. *ACS Applied Materials & Interfaces* **2018,** *10* (11), 9225-9234.

31. Rosenzweig, R.; Perinbam, K.; Ly, V. K.; Ahrar, S.; Siryaporn, A.; Yee, A. F., Nanopillared Surfaces Disrupt Pseudomonas aeruginosa Mechanoresponsive Upstream Motility. *ACS Applied Materials & Interfaces* **2019,** *11* (11), 10532-10539.

32. Crocker, J. C.; Grier, D. G., Methods of digital video microscopy for colloidal studies. *J. Colloid Interface Sci.* **1996,** *179* (1), 298-310.

33. Conrad, J. C., Physics of bacterial near-surface motility using flagella and type IV pili: implications for biofilm formation. *Res. Microbiol.* **2012,** *163* (9–10), 619-629.

Chapter 5 Future work

5.1. Effect of negative curvature on surface motility

Our work has demonstrated the different types of surface geometries can have different effects on bacterial motion. Indeed, studies presented in Chapter 4 suggest that bacteria may more favorably interact with negative curvature (features that curve towards the bacterium). Thus, the surface motility of bacteria should also be investigated on negatively curved surfaces. Using similar soft lithography techniques used in Chapter 3 and 4, we can fabricate arrays of negatively curved features (termed negative colloidal crystal, see Figure 5-1). In brief, a colloidal crystal stabilized with TEOS treatment (see Chapter 2) is stamped into a photo-curable polymer (Norland Optical Adhesive, see Chapter 4 and 5 Methods) to form the negative of a colloidal crystal.

We anticipate two effects of negative curvature on motility: 1) bacteria will more favorably interact with more negatively curved features and will thus be more likely found in the center of a negatively curved feature and 2) the boundaries between wells will act like barriers that bacteria need to frequently cross in order to progress across a surface. Therefore the hypothesis would be that the mean squared displacement would be much lower on these negative curvature surfaces. Figure 5-1B shows a maximum intensity image of *P. aeruginosa* motility on a negative 2 μm colloidal crystal surface. The trails appear more jagged and jerky, suggesting that bacteria have a difficult time traversing the surface.

Current challenges with the fabrication of these topographies include optimizing the procedure to obtain a deeper cross-section of the negative well and to reduce the number of adhered particles to the surface after removing the positive stamp. The TEOS

treatment presented in Chapter 2 can be modified to tune the size and strength of silica bridges and anti-adhesive layers such as polyvinyl alcohol can be used to reduce the adhesion between particles and the surface.

The trajectories of bacteria can be analyzed for mean square displacement. We expect a lower mean square displacement if bacteria are trapped in the negative wells. One can also quantify a probability of hopping out of the negative wells and how long bacteria may dwell inside. The radius of curvature can be varied by changing the diameter of the positive colloidal crystal used to make the negative surface. The data from these experiments can be compared to prior work on bacterial motility on positively curved surfaces (see Chapter 3). The analysis of this data could address if negative or positive curvature has a more substantial effect of bacterial surface motility and whether there is an optimal radius of curvature. These data may be used to help inform the design of a hybrid topographical surface pattern that could be used to reduce the rate of infections.

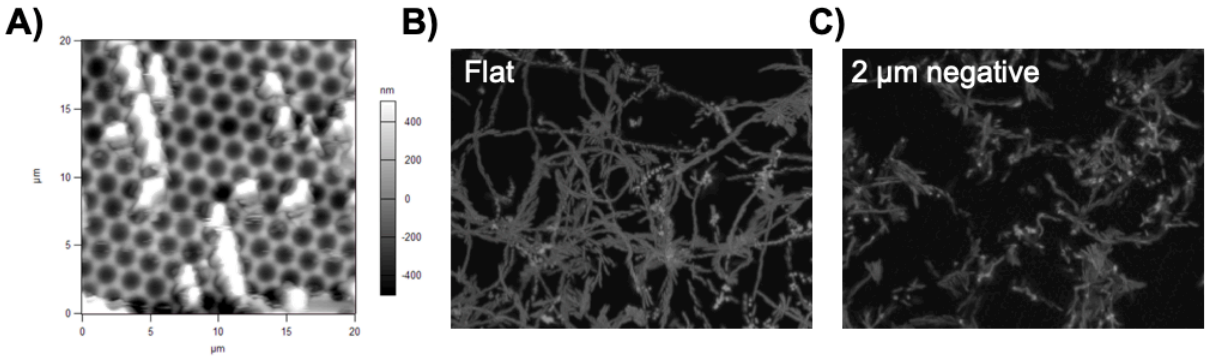

Figure 5-1. *P. aeruginosa* motility of negative curvature. AFM height image of a 2 µm negative colloidal crystal surface. Note that the fabrication method can be optimized to reduce the retention of particles adhered to the surface. B and C) Maximum intensity image of *P. aeruginosa* motility over the course of 2 hr on a flat and 2 µm negative colloidal crystal surface. The direction of flow is from left to right. The motion of *P. aeruginosa* is more jerky and sporadic-like on the topography when compared to a flat surface.

5.2. Simulations of motility and design of optimal surface topography

In the Discussion sections of Chapter 3 and 4, some outstanding questions remain. How do type IV pili interact with micro-scale topography? Why is the optimum topographic length scale between 1-2 μm? How are bacteria able to navigate over sharp corners? These questions are difficult to answer since the pili are not easily visualized. Current methods in the literature to visualize type IV pili *in vitro* are fluorescent labeling,[1] traction force microscopy,[2] or very recently with interferometric scattering microscopy.[3] The visualization of type IV pili is further complicated by the presence of topography, which may scatter light making direct pili visualization more difficult. Thus, simulations of type IV pili driven motility may offer insights into answering some of these outstanding questions. Simulations could be rule-based statistical methods such as Cellular Automata[4] or Monte Carlo type simulations where the microscopic details of exerted forces are described.[5]

5.3. Investigation of other mechanisms of action

Biofilm formation consists of many different steps as reviewed in Section 1. The work presented so far has focused solely on bacterial surface motility and how surface topography impacts motion. It is likely that surface topography may impact other processes and thus, in this section we briefly discuss other possible mechanisms of action.

5.3.1. Attachment

The first step in biofilm formation is the initial attachment of bacteria onto a solid surface. We hypothesize that surface topography may influence the rate of attachment of

bacteria; furthermore, there may be preferential sites on a surface for attachment. To investigate this, two types of experiments are proposed: 1) time-lapse experiments to count the number of attached bacteria on a surface with time and 2) record high-frame rate movies of bacteria swimming a bulk liquid and transitioning to attachment to a surface. In both experiments, suspensions of bacteria are flowed into a flow chamber and attachment events are recorded using fluorescence microscopy. Bacteria are then tracked and analyzed. Initial experiments of type 1 have been performed; the cumulative number of attachment events was counted plotted on **Figure 5-2** for a flat surface (0 μm) compared to 1 and 2 μm colloidal crystal replicas.

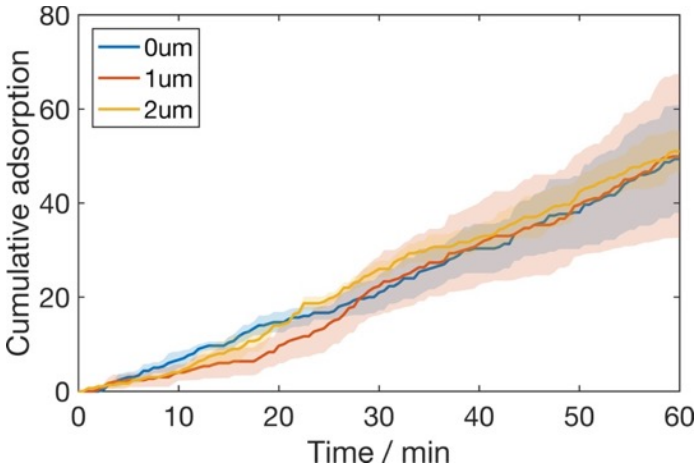

Figure 5-2. Cumulative adsorption of single *P. aeruginosa* cells onto topographical surfaces.

Adsorption events were counted using particle tracking algorithms and monitored for 1 hour on a flat (0 μm), 1 and 2 μm replica colloidal crystal (see Methods in Section 3 for fabrication of topographical surfaces). Shaded regions indicate standard error from replicate experiments.

These experiments suggest that the cumulative adsorption rate of *P. aeruginosa* is unaltered by the presence of micron-scale surface topography. It should be noted that these initial experiments were performed with topographical replicas (see Section 3) and not the original colloidal crystals where there are deeper gaps between particles. It is possible that the attachment rate is different on the original colloidal crystal compared to the replicas. Furthermore, the mechanism by which topography hinders bacterial biofilms may not be through a reduction in the number of attachments. Additional experiments could be performed to confirm this observation. Colony forming unit count experiments could be done to quantify the number of attached bacteria in a separate and independent experimental procedure. High speed data that show the actual attachment event could also be performed to investigate the mechanisms by which bacteria attach. For example, there may be short-lived attachment events that time-lapse data could not capture. Bacteria may also have preferential sites for attachment on a topographical surface.

5.3.2. Cell division and colony growth

Recent studies on micro-colony formation suggests that local mechanical instabilities cause dividing bacteria to tilt up in a third dimension, thus causing growing colonies to extend out from a surface (see Figure 5-3).[6] Here we hypothesize that surface topography may alter the angles at which a bacterium sits at a solid-liquid interface; thus, dividing bacteria on the surface may lack the external pressure of a neighboring cell to induce verticalization. Future work could use fluorescence and confocal microscopy to measure the vertical growth rate of microcolonies of *P. aeruginosa* on flat surfaces and

compare that to bacteria grown on topographical surfaces. Furthermore, we hypothesize that the rate of cell division may be impacted by surface topography.

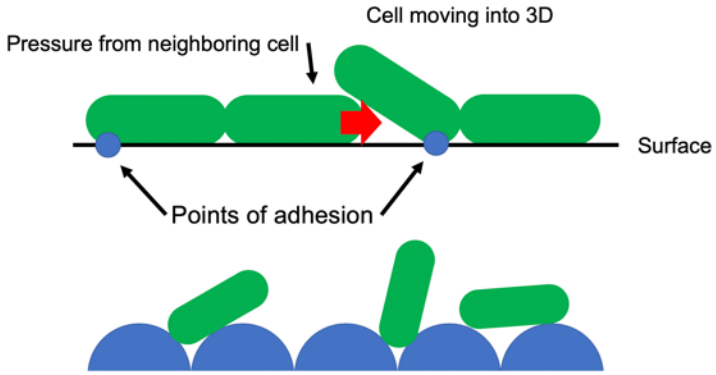

Figure 5-3. Schematic of vertical growth of bacterial colonies. (Top) Schematic of a growing colony of bacteria interpreted from Yan et al.[6] Mechanical instabilities cause adjacent bacteria to be pushed up into the third dimension, thus driving vertical growth of the colony. (Bottom) Schematic of bacteria on a topographical surface. There may be a variety of tilt angles of bacteria which may disrupt the colony vertical growth mechanism.

Furthermore, we analyzed the time for a bacterium to divided on different topographical surfaces. By monitoring the length of a bacterium, we see that a bacterium elongates as it grows in length and when the daughter cell detaches, there is a sudden drop in length (see Figure 5-4). We can then measure the time it takes a bacterium to divide. From initial studies, we found that on a flat surface, the division time was 35 $\pm$ 2 min. whereas on a 2 μm surface, the time was 36 $\pm$ 2 min. These results suggest that the division rate of bacteria is unaltered by surface topography. This result may be reasonable if bacteria tend to align to the topography and therefore divisions occur in-between particles where there is no physical obstruction of cell growth.

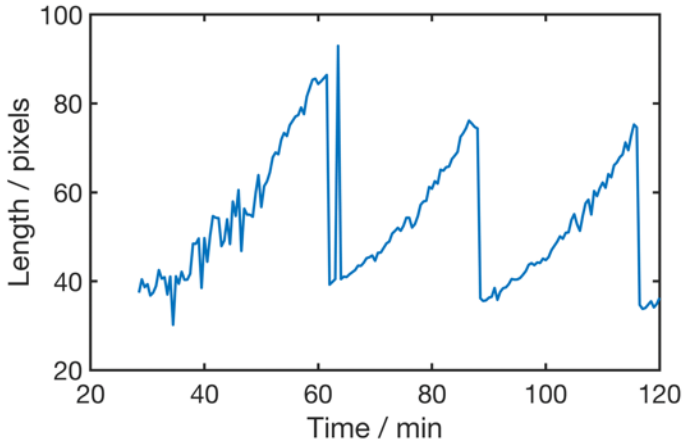

Figure 5-4. Plot of the length of a bacterium with time. The length of a bacterium is measured and monitored with time. Periodic drops in length indicate that a bacterium has divided. The time to divide is approximately 30 min.

References

1. Skerker, J. M.; Berg, H. C., Direct observation of extension and retraction of type IV pili. *Proc Natl Acad Sci U S A* **2001,** *98* (12), 6901-6904.

2. Sabass, B.; Koch, M. D.; Liu, G.; Stone, H. A.; Shaevitz, J. W., Force generation by groups of migrating bacteria. *Proceedings of the National Academy of Sciences* **2017,** *114* (28), 7266-7271.

3. Talà, L.; Fineberg, A.; Kukura, P.; Persat, A., Pseudomonas aeruginosa orchestrates twitching motility by sequential control of type IV pili movements. *Nature Microbiology* **2019,** *4* (5), 774-780.

4. Wolfram, S., Statistical mechanics of cellular automata. *Rev. Mod. Phys.* **1983,** *55* (3), 601-644.

5. Brill-Karniely, Y.; Jin, F.; Wong, G. C.; Frenkel, D.; Dobnikar, J., Emergence of complex behavior in pili-based motility in early stages of P. aeruginosa surface adaptation. *Scientific Reports* **2017,** *7*.

6. Yan, J.; Sharo, A. G.; Stone, H. A.; Wingreen, N. S.; Bassler, B. L., Vibrio cholerae biofilm growth program and architecture revealed by single-cell live imaging. *Proceedings of the National Academy of Sciences* **2016,** *113* (36), E5337-E5343.

CONCLUSIONS

The effects of different surface geometries on the type IV pili mediated motility of the opportunistic human pathogen *P. aeruginosa* was investigated under flow conditions at 37˚C using time-lapse fluorescence microscopy. Utilizing particle tracking techniques and image analysis, we found that surface motility is altered by micron-scale curvature and recti-linear features when compared to a flat surface. Specifically, on positively curved, hexagonally packed hemi-spheres, the average displacement in 5 min. is reduced when compared to a flat surface. Bacteria are frequently found in-between hemi-spheres and rarely on top of a topographic feature. When challenged with a recti-linear feature, *P. aeruginosa* has immense difficulty traversing a step height greater than 1 μm, despite having motility appendages that are 5-10 μm long. Overall, our data offer new insights into how surface topography impacts bacterial surface motility, which in turn may impact bacterial biofilm formation. Thus, these results indicate that the reduction in surface motility may be one mechanism by which topography hinders the growth of bacterial biofilm formation.

Appendix

Appendix A - Supporting Information for Chapter 2

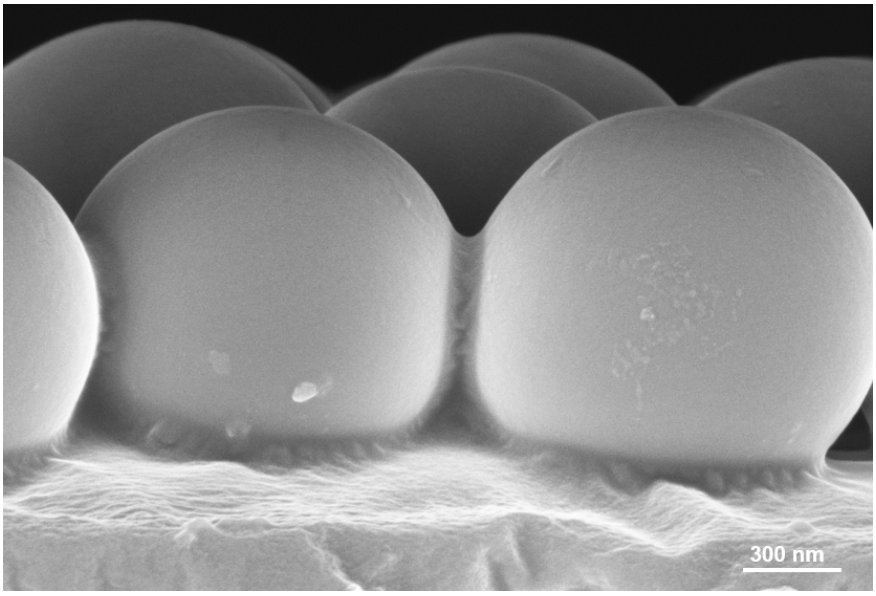

Figure 5-5. SEM image of 2 μm silica colloidal crystal monolayer on PDMS with no TEOS treatment. Necks are clearly present.

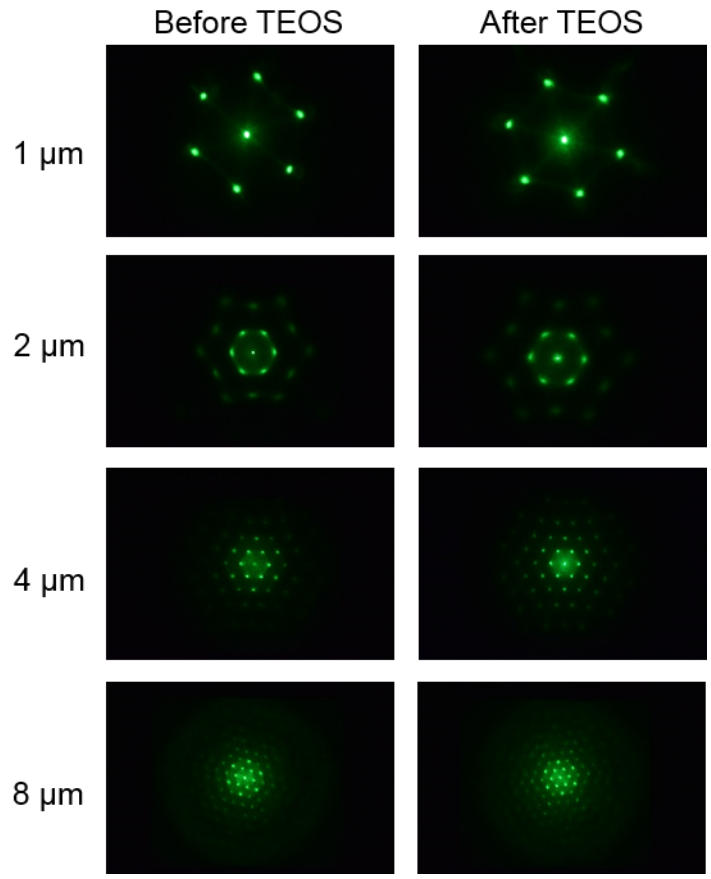

Figure 5-6. 532 nm laser scattering patterns produced by colloidal crystal monolayers before and after TEOS treatment.

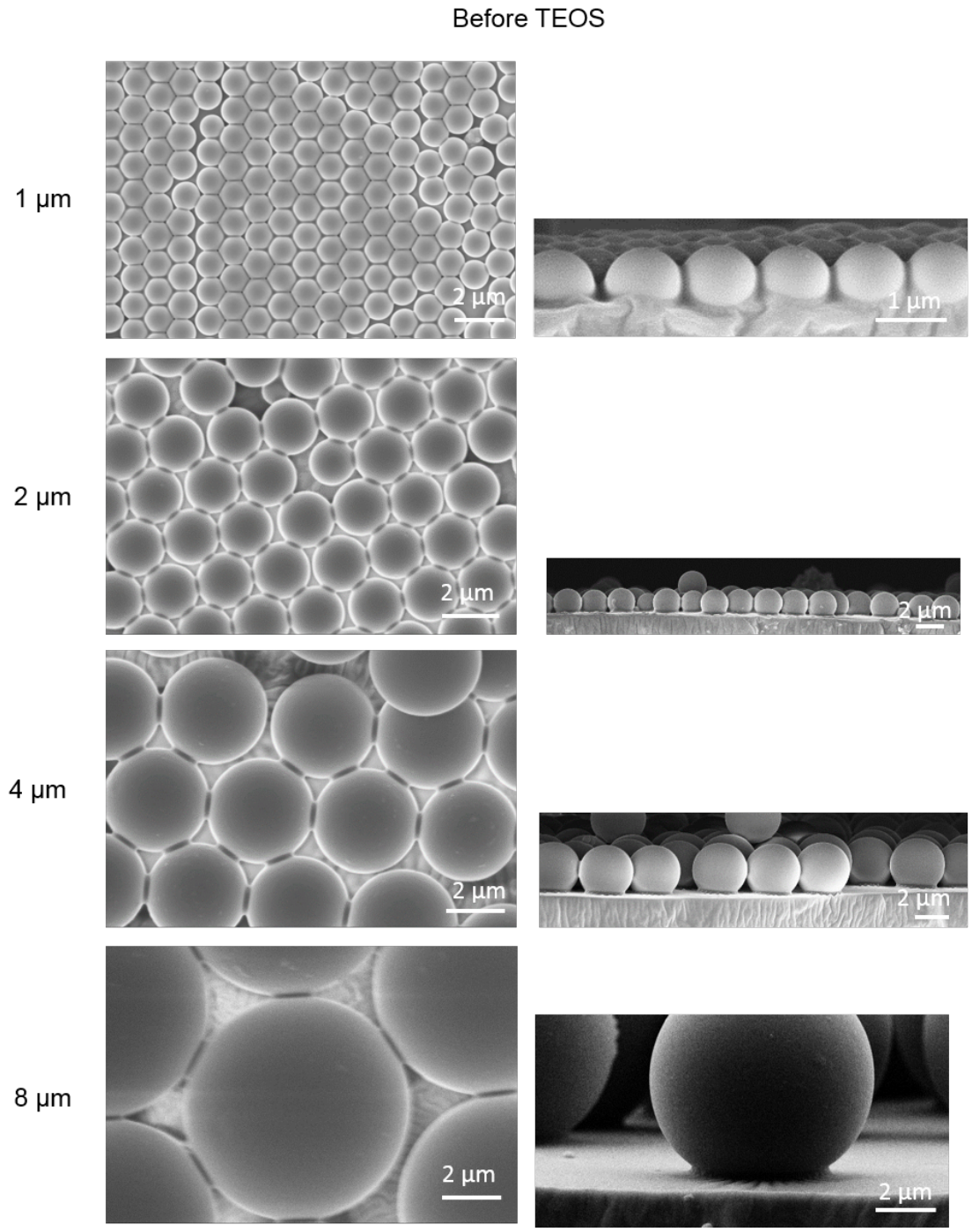

Figure 5-7. SEM images of colloidal crystal monolayers before TEOS treatment

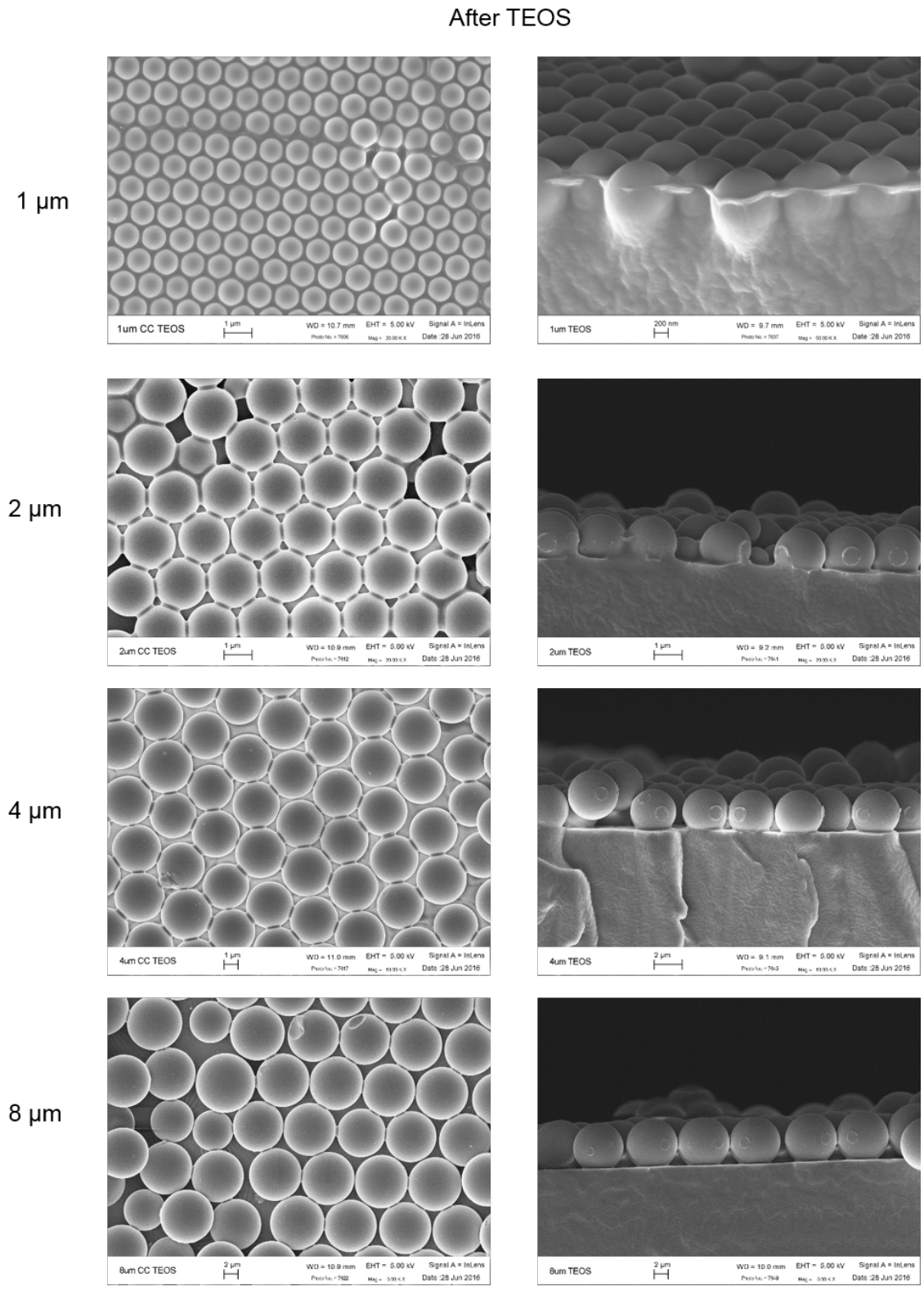

Figure 5-8. SEM images of colloidal crystal monolayers after TEOS treatment.

Scaling analysis of robustness of CCMs

We wish to consider how particle radius may impact the strength of a colloidal crystal monolayer (CCM) against a peel test. In an actual peel test, the mechanism of detachment may be quite complex; the particle is adhered to the substrate but as part of the film lifts off, there may be bends and additional vertical force components such that particle-particle interactions are important (see Fig. S5). Here we consider a simplified case of the peel test (Fig S5). We assume that in a given area, the particles in a CCM are simultaneously lifted off vertically.

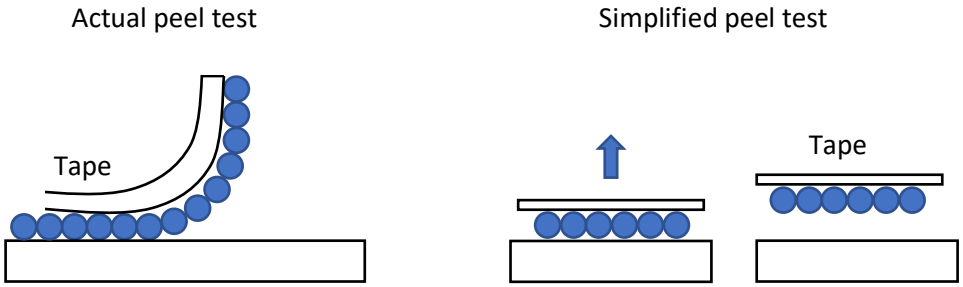

Figure 5-9. Schematic of two peel test scenarios.

The question is now how the energy required to remove the particles scales with the particle radius. Assuming that all the contacts are independent and separated, the total energy (A_T with dimensions of energy) to do this is a product of the number of particles in a given area (N with dimensions of 1), the contact area of a single particle to the substrate (A with dimensions of length^2), and the work of adhesion between the particle and substrate (W_{12} with dimensions of energy/length^2):

$$A_T = N \times A \times W_{12}. \qquad \text{S1}$$

We assume that W_{12} is independent of particle size. The number of particles in a given area is

$$N = b \times A_{test}/A_{particle} \quad \text{S2}$$

$$= b \times A_{test}/\pi R^2 \quad \text{S3}$$

where b is the packing factor, A_{test} is a macroscopic peel test area, $A_{particle}$ is the area of a single particle, and R is the particle radius. Therefore, N scales with $1/R^2$. The contact area of a spherical particle with the polymer is a spherical cap:

$$A = 2\pi Rh \quad \text{S4}$$

where h is the height of the bridge between the particle and the substrate (See Fig. S6). We now require $h(R)$ to determine how the total adhesion energy depends on R. From the geometry, we can express h as a function of R:

$$(R - h)^2 + a^2 = R^2, \quad \text{S5}$$

where a is the contact radius of the bridge between the particle and the substrate. For particles that are immersed only below the equator:

$$h = R - \sqrt{R^2 - a^2}, \quad \text{S6}$$

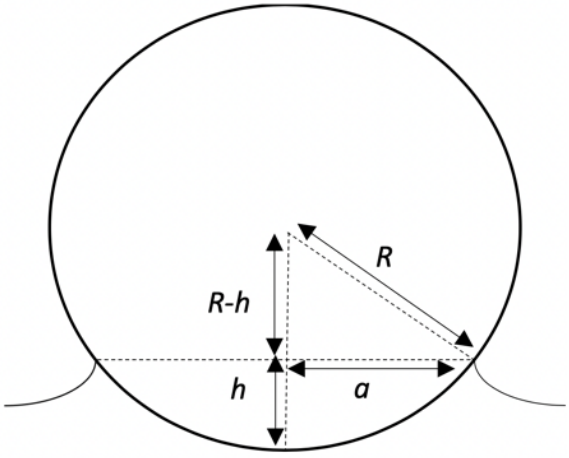

Figure 5-10. Schematic of the contact of a particle with the substrate. Here R is the particle radius, h is the height of the contact between the particle and the substrate and a is the radius of the contact between the particle and the substrate.

But to proceed, we need a as a function of R for the TEOS-treated samples. We assume that

$$a = cR^n \qquad \text{S7}$$

where c is some proportionality constant and n is a real number. We plot ln(a) vs. ln(R) (Fig. S7) and obtain the slope of the best fit line to determine n and the intercept to determine c (Table S1).

	Before TEOS	After TEOS
Slope, n	0.75 ± 0.03	0.74 ± 0.06
Intercept, ln(c)	-0.18 ± 0.03	-0.17 ± 0.05
c	0.84 ± 0.02	0.84 ± 0.04

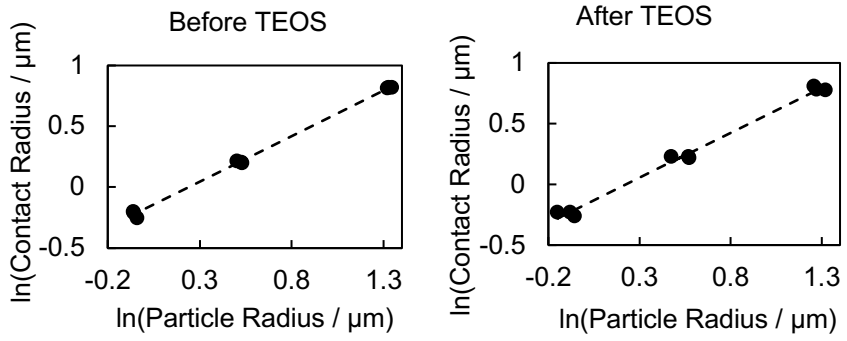

Figure 5-11. Effect of particle radius on contact radius.

Table S1. Slope and intercept of best fit lines through plots in Fig. S7 with 95% confidence intervals.

	Before TEOS	**After TEOS**
Slope, n	0.75 ± 0.03	0.74 ± 0.06
Intercept, ln(c)	-0.18 ± 0.03	-0.17 ± 0.05
c	0.84 ± 0.02	0.84 ± 0.04

Fig. S7 and Table S1 suggest that the power law of Eq. S5 is a reasonable description. Substituting S7 into Eq. S6, we obtain:

$$h = R - \sqrt{R^2 - c^2R^{2n}} \quad \text{S8}$$

$$= R - R\sqrt{1 - c^2R^n}. \quad \text{S9}$$

Performing a series expansion of the radical, we obtain

$$h = R - R(1 - \tfrac{1}{2}c^2R^{2(n-1)} + \tfrac{1}{8}c^4R^{4(n-1)} - \tfrac{1}{64}c^6R^{6(n-1)} + \ldots). \quad \text{S10}$$

For our particles (R ~ 1 μm), the third term in the series is approximately 18% of the previous term. Continuing, we retain only the first two terms of the series expansion. We obtain:

$$h = R - R(1 - \tfrac{1}{2}c^2R^{2(n-1)}) \quad \text{S11}$$

$$= \tfrac{1}{2}c^2R^{2n-1}. \quad \text{S12}$$

The contact area can now be obtained from Eq. S4:

$$A = 2\pi R\left(\tfrac{1}{2}c^2R^{2n-1}\right) \quad \text{S13}$$

$$= \pi c^2R^{2n}. \quad \text{S14}$$

The total adhesion (Eq. S1) is then:

$$A_T = b\frac{A_{test}}{\pi R^2} \times \pi c^2 R^{2n} \times W_{12} \qquad \text{S15}$$

$$= bc^2 A_{test} W_{12} \times R^{2n-2}. \qquad \text{S16}$$

For our experiments, n ≈ 0.75 and A_T scales as $R^{-0.5}$ and so the total adhesion of the CCM in a given area decreases weakly with increasing particle radius. We note that the uncertainty in determining *n* in Eq. S7 propagates through to the exponent of *R*, which has an uncertainty of 2Δ*n* where Δ*n* is the uncertainty in *n*.

From Fig. 5 we know that the TEOS reaction did not affect the contact radius. So we also consider whether *a = f(R)* can be determined from a model of the elastic contact that occurred *prior* to the TEOS treatment. For a single particle adhered to an elastic solid, Style *et al.* have shown that JKR theory applies in the limit of:

$$a \gg \frac{Y}{E}, \qquad \text{S14}$$

where *Y* is the solid surface tension and *E* is the elastic modulus. This limit is applicable to the current situation and allows calculation of the contact radius as a function of *R*:

$$a = \left(\frac{9\pi W(1 - v^2)}{2E}\right)^{1/3} R^{2/3}, \qquad \text{S15}$$

where *W* is work of adhesion, *v* is Poisson's ratio, *E* is the elastic modulus, and *R* is the particle radius. The 2/3 power dependence (Eq. S15) is similar to the ¾ power dependence observed by experiment (Table S15). While the discrepancy is outside the 95% confidence interval of the experimental value, the statistical testing does not include any systematic errors that may have been made.

In summary, we expect that the adhesion energy of a set of spherical particles in the JKR limit will diminish weakly with radius of the particle (power law of about –2/3), if

the work of adhesion and packing are held constant. A slightly more negative power law might be expected for our system based on measurements of contact area.

Appendix B - Supporting Information for Chapter 3

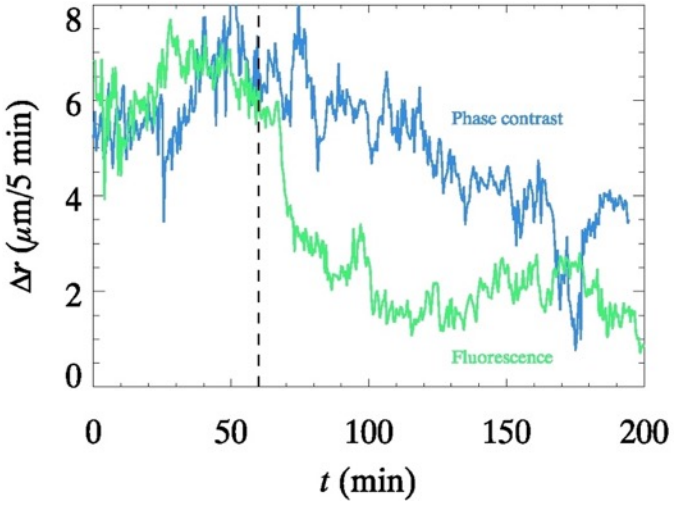

Figure 5-12. Effect of fluorescence-imaging on cell behavior. Our conditions for fluorescence imaging had much higher light intensity than for phase contrast imaging, so we checked for phototoxicity. After about 1 h of imaging at 30 s intervals (120 exposures), the average displacement (Δr) began to decrease. Data described in Chapter 3 are for bacteria that were tracked for less than 60 min. since we identified them. Identification occurs very soon after the bacteria enter the high intensity light, so this is effectively 60 min. after exposure.

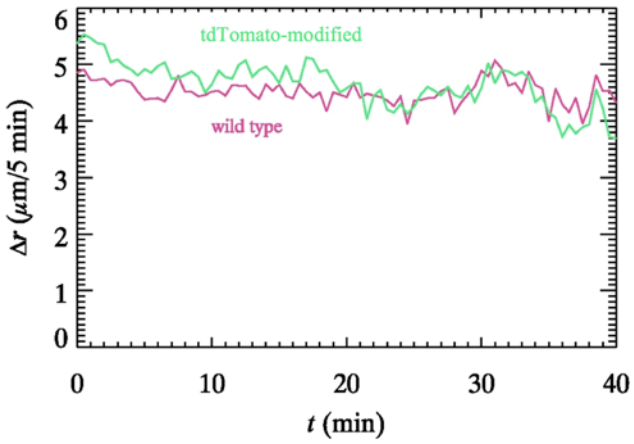

Figure 5-13. Comparison of results for wild-type and fluorescent *P. aeruginosa* on flat sample. High resolution phase contrast imaging of bacteria is possible on the flat samples because they scatter much less light than the textured samples, so we are able to directly compare results for the fluorescent mutant and the wild-type. We find that there is no difference between the behavior of the wild-type and the fluorescent bacteria.

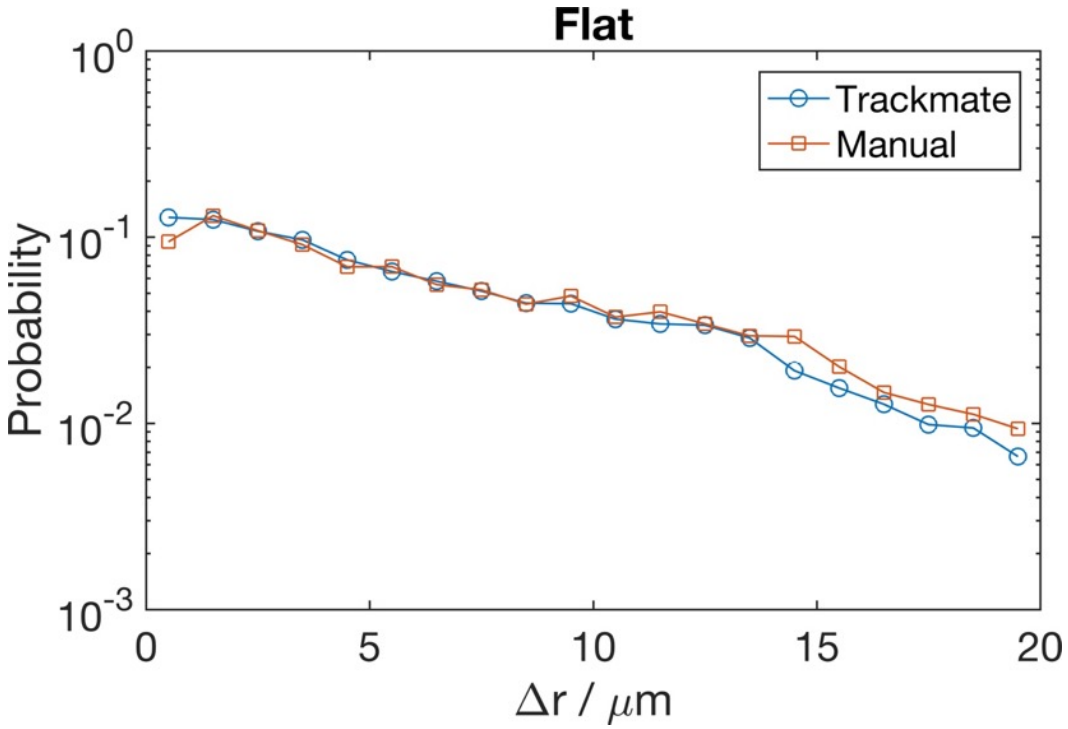

Figure 5-14. Comparing manual and automated tracking. Comparison of probability distribution functions on the flat surface generated from manual tracking and TrackMate tracking. The distribution is for one replicate.

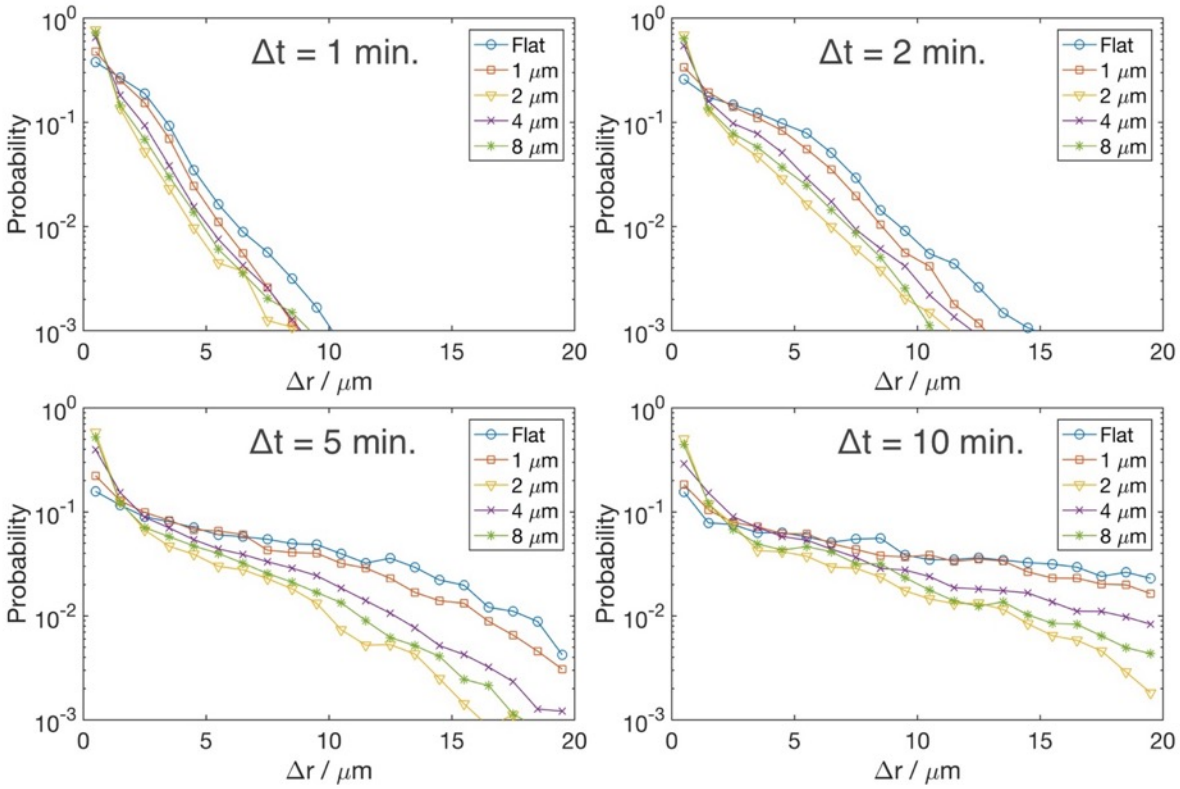

Figure 5-15. Probability distribution of displacements in various time intervals. The same data that was used for Figure 3-5 was analyzed with a variety of time intervals. For shorter time intervals, the probability distribution is shifted to smaller displacements, as expected. However, the flat and 1 μm topographies always have the greatest displacements and the 2 and 8 the smallest, with the 4 μm in between.

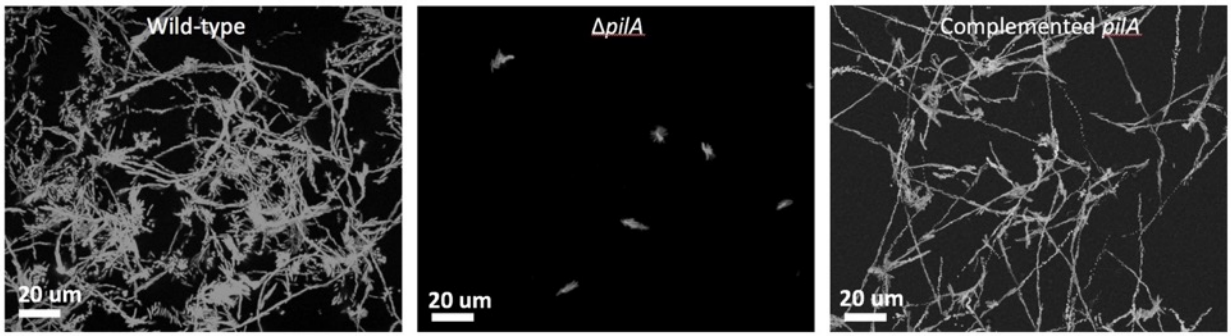

Figure 5-16. Maximum intensity image of wild-type, Δ*pilA* mutant, and the complemented *pilA* strains of *P. aeruginosa*. The images are made from 2 hour time lapse movies. The complemented *pilA* strain recovers the motion of the wild-type bacteria.

Appendix C - Supporting Information for Chapter 4

Characterization of local radii of curvature of step edge

To characterize the local curvature, we first identified pixels in brightfield images that are associated with the step edge. Since there is ambiguity in the location of the step edge in the brightfield image due to the presence of a dark and bright band, we identified which of the bright and dark band is the edge through the use of confocal microscopy. We first coated NOA step samples with fluorescein, submerged the sample in water and took Z-stack images using a confocal microscope (Zeiss LSM 880). A cross-section of the fluorescence and brightfield intensities (Figure 5-17) shows that the step edge, as determined by the high fluorescence intensity, corresponds to the dark band in a brightfield image.

We calculated the local curvature of the dark band in a brightfield image as follows. A threshold to brightfield images was applied to obtain the dark pixels associated with the step edge and then rotated such that a straight line fitting all edge pixels was parallel to a transformed X-coordinate, x^*. A third order polynomial, $f(x^*)$ was fitted to points on the line and the radius of an osculating circle was calculated according to

$$R = \frac{\left(1+(f\prime)^2\right)^{1.5}}{f\prime\prime},$$

where the prime denotes differentiation with respect x^*. The sign of *R* was defined as positive if the center of the osculating circle is in the solid (Figure 5-18). We performed a similar analysis on SEM images of the step edge to verify our methodology (Figure 5-19). The probability distribution of radii of curvatures obtained in high resolution SEM images was similar to that for brightfield images, which suggested that the optical images did resolve the curvature.

No effects of flow on bacterial motility on a flat surface

We argue that the low *Re* in our system suggests that flow should not affect the motion of bacteria. To verify this, we calculated the mean displacement of bacteria in a given time interval on a flat surface in the X and Y directions, $\langle d_x \rangle$ and $\langle d_y \rangle$. The X-direction corresponds to the direction of flow. For ~600 individually tracked bacteria from three independent experiments $\langle d_x \rangle$ = -0.06 $\pm$ 0.07 μm in 5 min and $\langle d_y \rangle$ = -0.16 $\pm$ 0.12 μm in 5 min, each of which were not statistically different to zero and not different to each other, suggesting that the presence of flow does not bias the motion of bacteria. Furthermore, we find that the mean absolute displacement in X and Y, $\langle |d_x| \rangle$ and $\langle |d_y| \rangle$, are not statistically different to each other (*t*-test, *p*-value = 0.67) indicating that bacterial motion is isotropic.

Direction of flow does not bias crossings up and down a step

Figure 4-4B shows that we resolved a preference for *P. aerugionsa* to go down a topographical step, i.e. there was rectification of motion down a step. We acknowledge that the presence of flow across a step could be a factor in causing the observed rectification. The steps were always arranged such that the edge ran perpendicular to the direction of flow. In our system, the Reynolds number was estimated to be 0.004, indicating laminar flow. Thus, we envision that there are two types of stream-lines across a step: 1) flow from high to low and 2) flow from low to high. For each case, it is possible for a bacterium to either travel (up or down a step) *with* or *against* the flow. To investigate if the direction of flow over a step influenced motion, we counted the number of crossings either with or against the direction of fluid flow (see Table S1). We then performed a two

factor ANOVA (see Table S2) with Factor 1 as the direction of motion (either up or down the step) and Factor 2 as motion relative to the flow (either with or against flow). We find that the crossing direction (either up or down) was significant (p = 0.017), which is consistent with our rectification findings. Importantly, we find that motion relative to flow (either with or against flow) was *not* an important factor (p = 0.59) nor was the interaction term between factors (p = 0.34). This analysis demonstrates that the direction of flow did not bias the motion of bacteria up or down a step.

Table S1. Measured number of crossings up and down a step under different flow conditions. The motion over a step can be either with or against the direction of flow. The total count is the total number of bacterial crossings measured and the average count is the number of crossings averaged across experimental replications. Error bars for averages are standard error.

	Total count	Average count
Step up – against flow	71	4.2 ± 1
Step up – with flow	87	5.1 ± 0.9
Step down – against flow	123	7.2 ± 1
Step down – with flow	105	6.2 ± 1

Table S2. Two-factor ANOVA test on the number of bacterial crossings over a step. Factor 1 was whether a crossing was up or down a step. Factor 2 was whether motion was with or against the flow direction. Importantly, the *p*-value for Factor 2 is much greater than 0.05, indicating that the direction of flow is not an important factor that influences the direction of motion.

Source	Sum Sq.	DF	Mean Sq.	F	Prob>F
Factor 1	86.4	1	86.4	6	0.0174
Factor 2	4.267	1	4.2667	0.3	0.5883
Factor 1*Factor 2	13.067	1	13.0667	0.91	0.3448
Error	806	56	14.3929		
Total	909.733	59			

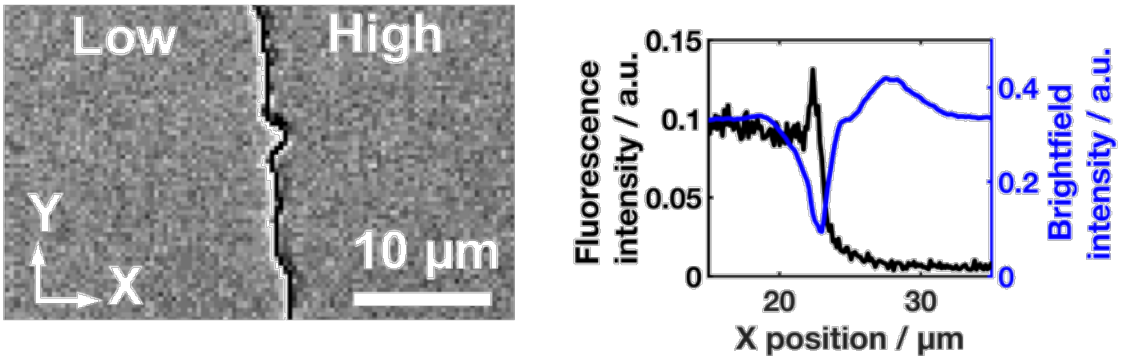

Figure 5-17. Magnified image of the step edge. Left) Brightfield image of a step edge. The edge appears as a bright and dark band in the image. Right) Steps coated with fluorescein then submerged in water were imaged with a confocal microscope to obtain an image of the step profile. A cross-section of the intensity shows that the step edge, defined by the maximum in fluorescence intensity, is coincident with the minimum (dark line) in a brightfield image.

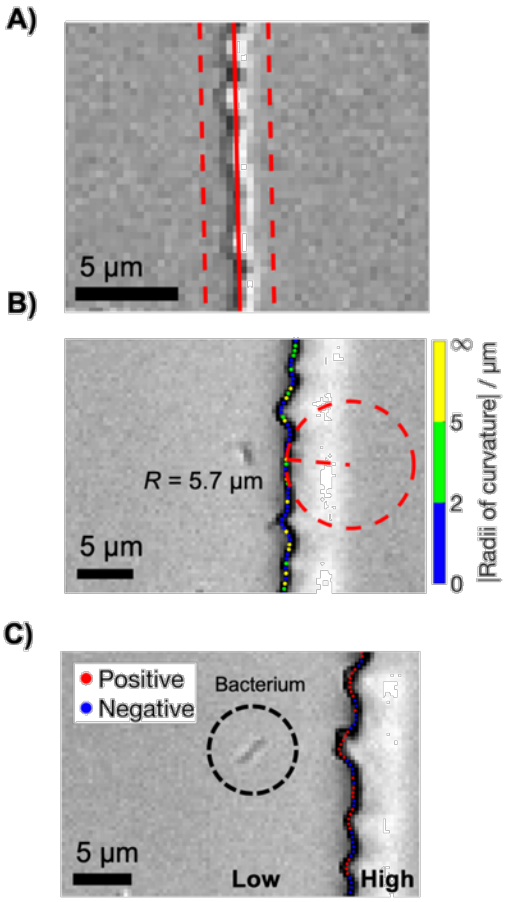

Figure 5-18. Detecting the step edge. A) Definition of a step zone. The entire step in the field of view is fitted with a line that we define to be the midline of a rectangular step zone. A step crossing was defined by a bacterium entering one side and exiting the other side of the step zone. B) An example of the calculated linear edge (black pixels), an osculating circle of R = 5.7 µm for one point, and the calculated X-Y curvature, which is indicated by colored bins. C) Brightfield image of a step edge color-coded to show positive and negative curvature. The sign of the radius of curvature was defined relative to the position of the high step: positive curvature is concave to the fluid. A bacterium (circled) illustrates that both the radius of local curvature and the scale change in curvature is similar to the length scale of a bacterium.

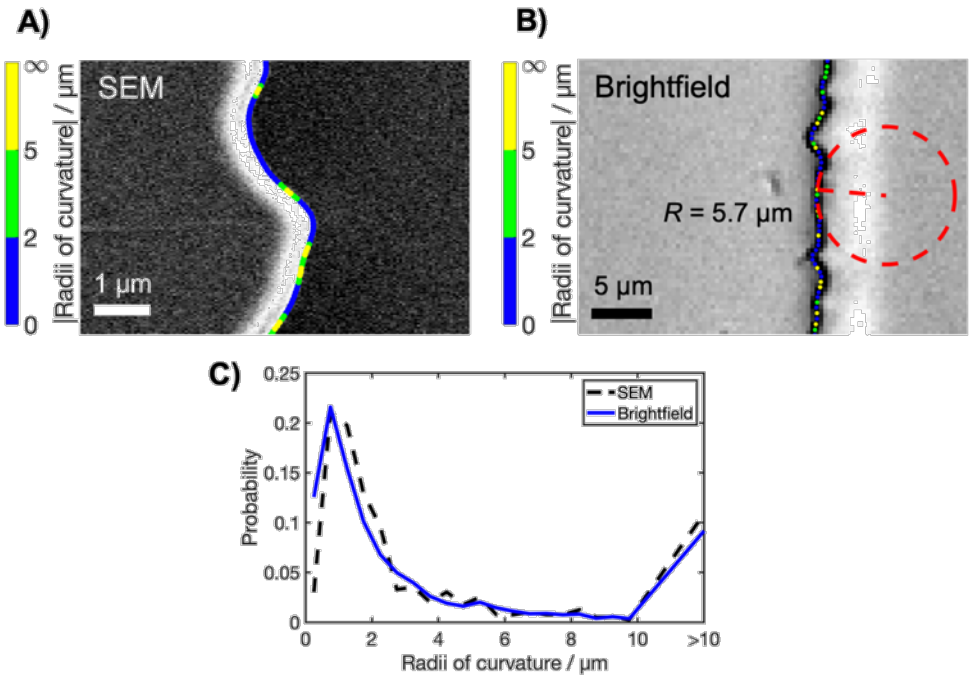

Figure 5-19. Characterization of the curvature in steps. A) Characterization of the local radii of curvature of a step edge from an SEM image. The step edge is clearly visualized in an SEM image as a sharp gradient in pixel intensity. The detected step edge is plotted in color on-top of a grey-scale SEM image. The magnitude of the local radii of curvature, *R,* is binned and color-coded to visualize highly curved sections and less curved sections of the step edge. B) Reproduced from Figure 5-18 for comparison. C) Histogram of magnitude of *R* from SEM and brightfield images. There is good agreement between the two measurements.

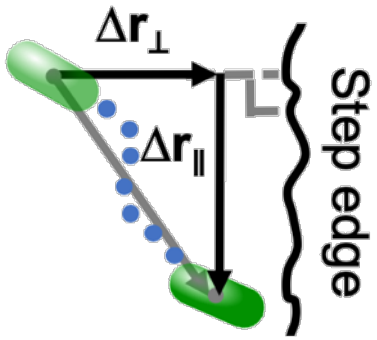

Figure 5-20. Schematic of a bacterium's displacement vector near a step. The displacement vector is resolved into components that are perpendicular or parallel to the step edge.

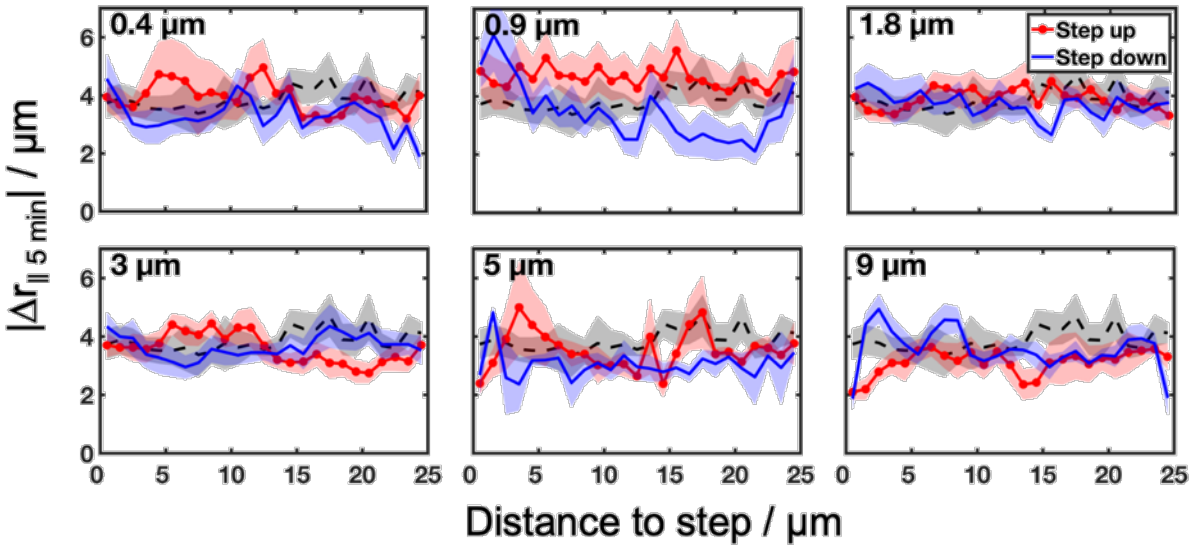

Figure 5-21. Average displacement of cells moving parallel to a step as a function of the starting distance to the step.

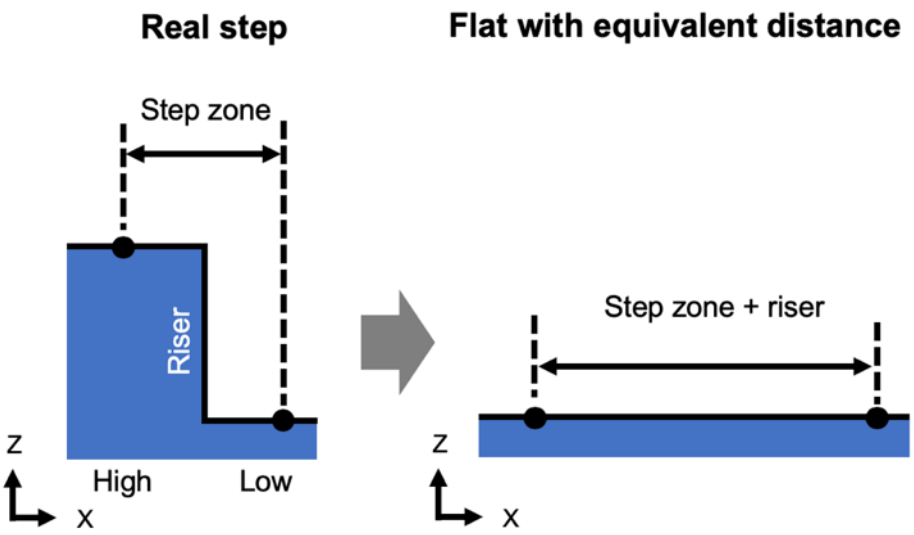

Figure 5-22. Model of extra distance travelled on a step. Left) Schematic of the distance a bacterium travels while crossing a step. Right) A flat surface with the equivalent distance as the real step.

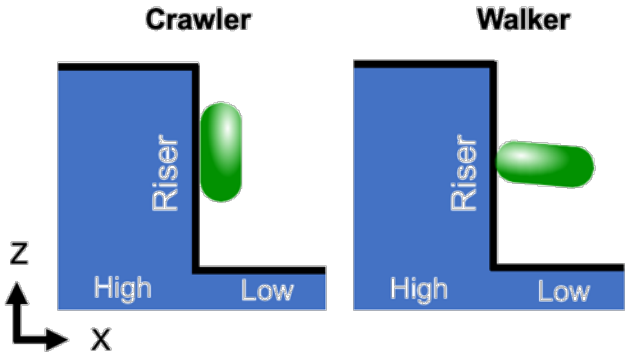

Figure 5-23. Schematic of a crawler vs a walker traversing a step. The long axis of the body is parallel to the riser of the step for a crawler.

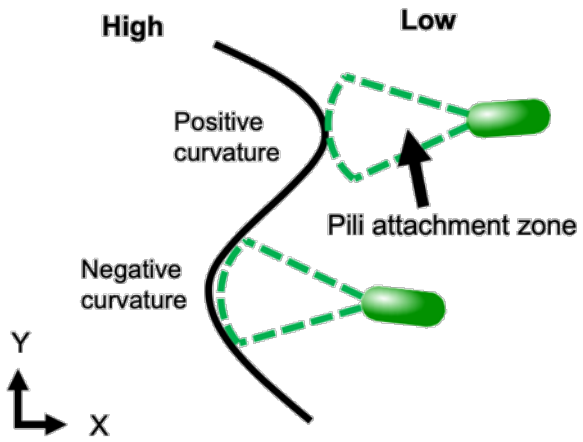

Figure 5-24. Schematic of possible bacterial interactions with the local curvature of a step edge. A hypothetical region of possible pilus attachment points ahead of the bacterium (dotted cone region). As a bacterium approaches a step with negative curvature, there is a greater area of attachment points for pili.

Appendix D MATLAB code

Particle tracking

The main particle tracking code can be found here: http://www.physics.emory.edu/faculty/weeks//idl/. An example script utilizing this code is provided below.

```
path = uigetdir;
stack = make_stack(path);
[~,~,p] = size(stack);

% find ellipses
ellipse = zeros(1,6);
for i = 1:p
    image = stack(:,:,i);
    fits = ellipse_fit(image,2,0);
    ellipse = vertcat(ellipse,[fits ones(size(fits,1),1)*i]);
end
ellipse = ellipse(2:end,:);

% try tracking with the ellipse centers
% Define parameters for track function
% change these values to "capture" the bacteria better
f1 = 'mem'; v1 = 2; % this is how many frames track can "remember" a
% bacteria e.g. if identification looses the bacteria for # frames
f2 = 'dim'; v2 = 2;
f3 = 'good'; v3 = 2; % This is how many frames to reject "short" runs
% For attachment experiments, this number should be small to "capture"
% attachment attempts.
f4 = 'quiet'; v4 = 0;

para = struct(f1,v1,f2,v2,f3,v3,f4,v4);

tr = track([ellipse(:,1:2) ellipse(:,6)],10,para);

% tack on the ellipse data to tr
new_tr = zeros(size(tr,1),7);
for i = 1:size(tr,1)
    loc = find(ellipse(:,1)==tr(i,1));
    new_tr(i,:) = [tr(i,1:2) ellipse(loc(1,1),3:5) tr(i,3) tr(i,4)];
end

tr = new_tr;
```

Calculating displacements

```
function out = dr(tr,t_step,scale,time,time2,xyz)

% out = dr(tr,t_step,[x y z],time,time2,xyz)
% generate motion over "time" min graph from tr matrix
% inputs are tr, t_step, pix, time
% tr - track matrix with positions, time and ID number
% t_stp - interval at which images were taken in seconds
% scale - pixel scaling in um per pixel for x, y, and z. input as a
1x3
% vector
% time - time interval over which to calculate dr in minutes
% time2 - how long to track for in min
% xyz – flag to do 2d displacements or 3d


% get the ID numbers
ids = unique(tr(:,end));

% initialized dr
out = zeros(1,6);

for i = 1:length(ids)
    if ids(i) == 0
    else
        data = tr(tr(:,end)==ids(i),:);
        t = data(end,end-1);
        if t > (1/t_step)*60*time2
            t = (1/t_step)*60*time2;
        end
        for j = 1:t
            try
                test = data(j+time*60/t_step,1);
            catch
                break
            end
            x = [data(j,1) data(j+time*60/t_step,1)].*scale(1);
            y = [data(j,2) data(j+time*60/t_step,2)].*scale(2);
            z = [data(j,3) data(j+time*60/t_step,3)].*scale(3);
            if xyz == 1
                out = vertcat(out,[((y(2)-y(1))^2+(x(2)-x(1))^2+(z(2)-
z(1))^2)^0.5 data(j,4) data(j,5)]);
            elseif xyz == 0
                out = vertcat(out,[((y(2)-y(1))^2+(x(2)-x(1))^2)^0.5
data(j,1) data(j,2) 0 data(j,end-1) data(j,end)]);
            end
        end
    end
end

out = out(2:end,:);
end
```

Calculating mean squared displacement

```
function [all_msd,kmsd] = msd(tr,time,pix)


% function for calculating the mean squared displacement
% [all_msd,kmsd] = msd(tr,time,pix)
% inputs:
%   tr - track matrix
%   time - time interval for frame
%   pix - pixel scaling
% outputs:
%   all_msd - 2 column matrix with time in the first column and MSD in
%   second column. units are t = seconds and MSD = μm^2
%   kmsd - 1xn matrix list of slope of MSD vs time on log-log scale
for
%   every individual bacterium

% get all ids
ids = unique(tr(:,end));
% get size of this matrix
n = size(ids,1);

% get the number of frames
% frame number starts at 0
f = max(tr(:,end-1))+1;

% convert frames to time
t = (0:f-1)'*(time);

% for each id number, calculate msd and record it with time
% create holder for msd of each cell
msd_holder = cell(n,1);
kmsd = [0 0];
for i = 1:n
    % grab all data for that id number
    data = tr(tr(:,end) == ids(i),:);
    % proceed to calculate msd for each frame
    % get the size of this dataset
    foo1 = size(data,1);
    % create temp holder. this will have msd in 1 column and the time
    % in the other
    temp_msd = zeros(foo1-1,2);
    x1 = data(1,1)*pix;
    y1 = data(1,2)*pix;
    t1 = data(1,end-1);
    for j = 1:foo1-1
        tpoint = (data(j+1,end-1)-t1)*time;  % time in seconds
        x2 = data(j+1,1)*pix;
        y2 = data(j+1,2)*pix;
        d = (x2-x1)^2+(y2-y1)^2;    % distance squared in um
        temp_msd(j,:) = [tpoint d];
```

```
    end
    msd_holder{i} = temp_msd;
    % get slope of msd curve on a log-log scale
    % only take the slope if there is sufficient data
    if size(temp_msd,1) > 5
        [~,ii] = min(abs(temp_msd(:,1) - 1000));
        fitdata = log(temp_msd(1:ii,:));
        [a] = polyfit(fitdata(:,1),fitdata(:,2),1);
        dt = linspace(1,1000,100);
        g = (dt.^a(1)).*exp(a(2));
        if isnan(a(1,1)) == 1
            continue
        end

        kmsd = vertcat(kmsd,[a(1,1) ids(i)]);
    end
end
% vertically concatnate the msd holder cells
msd = vertcat(msd_holder{:,1});
kmsd = kmsd(2:end,:);

% now loop back through each time. average msd for each time point
% create holder for all msd data with time
all_msd = zeros(f-1,2);
for i = 1:f-1
    % get the time point in seconds
    tpoint = t(i+1);
    % find all data at this time point
    data = msd(ismember(msd(:,1),tpoint),2);
    % if there is data, calculate the average
    if isempty(data) == 0
        avg_msd = mean(data);
        all_msd(i,:) = [tpoint avg_msd];
    end
end


end
```

Detecting step edges and tracking code used in Chapter 4

```
% manually combine images and do tracking. This is the preprocessing
section
clear all
close all
clc

%%%%%%%%%%% select a movie to process. select the low fluorescence
movie first
pathL = uigetdir('~/Desktop/Step project/Multiple steps');

% do some text parsing to find the date and the surface
location = find(pathL=='/');
folderName = pathL(location(end)+1:end);
umLocation = strfind(folderName,'um');
ucLocation = strfind(folderName,'_');
% find the closest underscore but whose index is less the um location
nearestUnderscore = ucLocation(ucLocation<umLocation);
surface = folderName(nearestUnderscore(end)+1:umLocation-1);
% the date is always 6 numbers in a row. The first 6 characters is
always
% BTPA97 so cut this out
truncFolderName = folderName(umLocation:end);
% find numbers
numberIndices = regexp(truncFolderName,'[0-9]');
% get sequential numbers. this should be the date
dateIndices = numberIndices(diff(numberIndices) == 1);
% grab the indices of these sequential numbers
date = truncFolderName([dateIndices dateIndices(end)+1]);

% Handle the 5 and 10 um steps differently. 5 um steps have 3 z
positions
% and 10 um have 4 z positions
% getting the hight step and brightfield images is the same for all
steps
markers = find(pathL == '/');
t = strfind(folderName,'_L_');
HfolderName = folderName;
% find the high step and brightfield folders based on pathL
% modify folderName
HfolderName(t+1) = 'H';
pathH = [pathL(1:markers(end)) HfolderName];
pathB = [pathL(1:markers(end))
strrep(folderName,'fluorescence','brightfield')];
% make stacks and handle the 5 and 10 um steps
stackL = make_stack(pathL);
stackH = make_stack(pathH);
stackBg = make_stack(pathB);
lowSteps = {'0','0.5','1','2','3'};
% get size of stacks
[m,n,T] = size(stackL);
if any(strcmp(surface,lowSteps)==1) == 1
```

```
    % these are low steps (0-3 um)
    % we have already made stacks
    % combine into z stack
    zStack = uint8(zeros(m,n,2,T));
    zStack(:,:,1,:) = stackL;
    zStack(:,:,2,:) = stackH;
elseif any(strcmp(surface,'5')==1) == 1
    % 5 um step
    % find the M1 fluorescence path
    M1folderName = [folderName(1:t) 'M1' folderName(t+2:end)];
    pathM1 = [pathL(1:markers(end)) M1folderName];
    % make stacks
    stackM1 = make_stack(pathM1);
    % make z stack
    zStack = uint8(zeros(m,n,3,T));
    zStack(:,:,1,:) = stackL;
    zStack(:,:,2,:) = stackM1;
    zStack(:,:,3,:) = stackH;
elseif any(strcmp(surface,'10')==1) == 1
   % 10 um step, find M1 and M2 folders
   M1folderName = [folderName(1:t) 'M1' folderName(t+2:end)];
   pathM1 = [pathL(1:markers(end)) M1folderName];
   M2folderName = [folderName(1:t) 'M2' folderName(t+2:end)];
   pathM2 = [pathL(1:markers(end)) M2folderName];
   % make stacks
   stackM1 = make_stack(pathM1);
   stackM2 = make_stack(pathM2);
   % make z stack
   zStack = uint8(zeros(m,n,4,T));
   zStack(:,:,1,:) = stackL;
   zStack(:,:,2,:) = stackM1;
   zStack(:,:,3,:) = stackM2;
   zStack(:,:,4,:) = stackH;
end

% save z stacks
save(['~/Desktop/Step project/z stacks/' surface 'um_' date
'.mat'],'zStack')

% save brightfield images
save(['~/Desktop/Step project/multiple steps brightfield/' surface
'um_' date '.mat'],'stackBg')

% make max image of lowest z slice and overlay with brightfield. this
is
% only for checking "bowing" of low step in some experiments. this can
be
% commented out normally, only for troubleshooting
maxT = max(zStack,[],4);
imageB = addScaleBar(stackBg(:,:,1),20,0.36);
image = combine_image(imageB,maxT(:,:,1));
figure;
imshow(image)
```

```
text(20,20,[surface ' ' char(181) 'm - '
date],'color','w','fontsize',14)
export_fig(['~/Desktop/Step project/max image z 1/' surface 'um_' date
'.tif'],'-r300')
close all

% now make a max pixel image from the two slices at each time point
% stackB is the stack of images of bacteria
% handle this differently for 5 and 10 um steps
[m,n,p] = size(stackL);
stackB = im2uint8(zeros(m,n,p));
if any(strcmp(surface,lowSteps)==1) == 1
    % low steps (0-3 um)
    for i = 1:p
        mini_stack = im2uint8(zeros(m,n,2));
        mini_stack(:,:,1) = stackL(:,:,i);
        mini_stack(:,:,2) = stackH(:,:,i);
        maximage = max(mini_stack,[],3);
        stackB(:,:,i) = maximage;
    end
elseif any(strcmp(surface,'5')==1) == 1
    % 5 um step
    mini_stack = im2uint8(zeros(m,n,3,p));
    for i = 1:p
        mini_stack(:,:,1,i) = stackL(:,:,i);
        mini_stack(:,:,2,i) = stackM1(:,:,i);
        mini_stack(:,:,3,i) = stackH(:,:,i);
        maximage = max(mini_stack(:,:,:,i),[],3);
        stackB(:,:,i) = maximage;
    end
    save(['~/Desktop/Step project/z movies/' surface 'um_' date
'.mat'],'mini_stack')
elseif any(strcmp(surface,'10')==1) == 1
    % 10 um step
    mini_stack = im2uint8(zeros(m,n,4,p));
    for i = 1:p
        mini_stack(:,:,1,i) = stackL(:,:,i);
        mini_stack(:,:,2,i) = stackM1(:,:,i);
        mini_stack(:,:,3,i) = stackM2(:,:,i);
        mini_stack(:,:,4,i) = stackH(:,:,i);
        maximage = max(mini_stack(:,:,:,i),[],3);
        stackB(:,:,i) = maximage;
    end
    save(['~/Desktop/Step project/z movies/' surface 'um_' date
'.mat'],'mini_stack')
end

save(['~/Desktop/Step project/all movies/' surface 'um_' date
'.mat'],'stackB')
maxImage = max(stackB,[],3);
image = combine_image(addScaleBar(stackBg(:,:,1),20,0.36),maxImage);
figure;
imshow(image);
```

```
export_fig(['~/Desktop/Step project/Multiple steps max images/'
surface 'um_' date '.tif'],'-r300')
close all
%%%%%%%%%%%%%%%%%%%%


%%%%%%%%%%%%%%%%%%%% do tracking
% Set the parameters for the identification. Need to play around with
these
% numbers to get "good" tracking
bpass_a = 1;            % parameters that go into bpass. a is usually
1
bpass_b = 10;            % b is like the diameter of the object
pk_a = 12;               % parameters that go into pkfnd. a is like a
threshold
pk_b = 8;               % b is like diameter of the object
cnt_a = 10;              % parameter that goes into cntrd
how_fast = 0;        % this parameter will "slow down the loop so you
can watch the tracking

% Loop through files to identify the position of the bacteria
% Uses pkfnd macro to find center of object
% threshold and size can be changed to "capture" bacteria
cnt_total = [0 0 0];    % initialize
warning('off','all')
close all
for i = 1:p
    image = stackB(:,:,i);
    % run bpass function to filter image
    b = bpass(image,bpass_a,bpass_b);
    % run pkfnd to roughly find objects
    pk = pkfnd(b,pk_a,pk_b);
    % run cntrd to get better position estimate
    cnt = cntrd(b,pk,cnt_a);
    if i == 1
        figure;
        imshow(image);
        hold on
        data = plot(cnt(:,1),cnt(:,2),'rx');
        delete(data);
        a = get(gca,'children');
    else
        set(a,'cdata',image)
        hold on
        data = plot(cnt(:,1),cnt(:,2),'rx');
        pause(how_fast)
        delete(data);
    end
    cnt_time = [horzcat(cnt(:,1:2)) (i-1)*ones(length(cnt(:,1)),1)];
    cnt_total = vertcat(cnt_total,cnt_time);
end
close all
cnt_total = cnt_total(2:end,:);
```

```
% Define parameters for track function
% change these values to "capture" the bacteria better
f1 = 'mem'; v1 = 1; % this is how many frames track can "remember" a
% bacteria e.g. if identification looses the bacteria for # frames
f2 = 'dim'; v2 = 2;
f3 = 'good'; v3 = 5; % This is how many frames to reject "short" runs
% For attachment experiments, this number should be small to "capture"
% attachment attempts.
f4 = 'quiet'; v4 = 0;
size_c = 10;            % parameter that goes into track
                        % approximate distance bacteria can travel in
one frame in pixels
para = struct(f1,v1,f2,v2,f3,v3,f4,v4);

% Track the bacteria and save results
tr = track(cnt_total,size_c,para);

% check tracking
close all
for i = 1:p
    image = stackB(:,:,i);
    foo1 = tr(tr(:,end-1)==i-1,:);
    if i == 1
        figure;
        imshow(image)
        hold on
        txt = num2str(foo1(:,end));
        label =
text(foo1(:,1),foo1(:,2),txt,'color','g','fontsize',8);
        gif(['~/Desktop/step project/multiple steps tracking/'
num2str(surface) 'um_' num2str(date) '.gif'])
        delete(label)
        a = get(gca,'children');
    else
        set(a,'cdata',image);
        txt = num2str(foo1(:,end));
        label =
text(foo1(:,1),foo1(:,2),txt,'color','g','fontsize',8);
        gif
        delete(label)
    end
end
close all

save(['~/Desktop/Step project/multiple steps tracks/' num2str(surface)
'um_' num2str(date) '.mat'],'tr')
%%%%%%%%%%%%%%%%%%%%%%%% end of tracking section


%%% save checkerboard files
```

```
% save(['~/Desktop/Step project/Checkerboard tr/' num2str(surface)
'um_' date '.mat'],'tr')
% save(['~/Desktop/Step project/Checkerboard stack/' num2str(surface)
'um_' date '.mat'],'stackB')
% save(['~/Desktop/Step project/Checkerboard brightfield/'
num2str(surface) 'um_' date '.mat'],'stackBg')
%%%



%%%%%%%%%%%%%%%%%%%%%%% now find the step edges
% we already have a stack of brightfield images called stackBg
% begin looping through each frame
% find the edge of the step
for i = 1:p
    bw = edge(stackBg(:,:,i),'Sobel',0.04);
    bw = imfill(bw,'holes');
    bw2 = bwareaopen(bw,100);
    step = im2uint8(bw2);
    stack_b(:,:,i) = step;
end
% get pixels of the step
max_step_stack = max(stack_b,[],3);
% there are now multipe steps so we need to fit a line to each step
% individually. first find connected pixels
connectedPixels = bwconncomp(max_step_stack);

% this is the number of steps
numSteps = size(connectedPixels.PixelIdxList,2);

% we will fit a line through each step so create a holder for this fit
coeffsHolder = zeros(numSteps,2);

close all
figure;
imshow(~max_step_stack)
% imshow(stackB(:,:,1))
hold on
% go through each object
for i = 1:numSteps
    % get indexes of pixels
    [stepPixelsX,stepPixelsY] =
ind2sub([m,n],connectedPixels.PixelIdxList{1,i});
    fiteq = fittype('(x-b)./m');
    fitx = fit(stepPixelsX,stepPixelsY,fiteq,'startpoint',[1 1]);
    coeffs = coeffvalues(fitx);
    boundary_line = [coeffs(2) coeffs(1)];
    fit_x = 1:n;
    fit_y = polyval(boundary_line,fit_x);
    coeffsHolder(i,:) = coeffs;
    plot(fit_x,fit_y,'r-','linewidth',1.5)
end
```

```
% save the boundary lines. The boundary lines should be enough to
determine
% what step the bacterium is on. Another way to do this is to create a
mask
% with each section coded to a high or low step.
save(['~/Desktop/Step project/multiple step edge/' num2str(surface)
'um_' date '.mat'],'coeffsHolder')
% now we have fits for the step edges. for the new steps, there should
be 4
% in the field of view. the middle step, and two edges are high steps
and
% the rest of low steps. so from left to right, the steps are high,
low,
% high, low, high.


% create a mask based on the pixels or based on the fit?
% need to create 5 zones. each zone will then be assigned to a low or
high
% step

% get all step pixels
stepPixels = max_step_stack == 255;
% fill in pixels
stepPixels = imfill(stepPixels,'holes');
% get all black pixels
blackPixels = stepPixels == 0;

figure;
imshow(blackPixels);
hold on
% we now can grab each step region. there should be 5 areas.
stepAreas = bwconncomp(blackPixels);
numAreas = size(stepAreas.PixelIdxList,2);
counter = 1;
for i = 1:numAreas
    [stepAreaX,stepAreaY] =
ind2sub([m,n],stepAreas.PixelIdxList{1,i});
    if size(stepAreaX,1) > 100
        if mod(counter,2) == 0
            % even number

plot(stepAreaY,stepAreaX,'bo','markerfacecolor','b','markersize',0.4)
            counter = counter + 1;
        elseif mod(counter,2) == 1
            % odd number

plot(stepAreaY,stepAreaX,'ro','markerfacecolor','r','markersize',0.4)
            counter = counter + 1;
        end
    end
end
```

```
save(['~/Desktop/Step project/multiple steps mask/' num2str(surface)
'um_' date '.mat'],'stepAreas')
%%%%%%%%%%%%%%%%%%%%%%%%%% end of step edge detection
%%%%%%%%%%%%%%%%%%%%%%%%%% Preprocessing is done
```

Bacteria crossing steps code used in Chapter 4

```
% new analysis for multipe steps 181002
% still based off of prior analysis (see notes_180409) but generalized
to
% more steps in an image

% update 181002
% changing the format of some output files
% streamlining code to handle both single and multi-step data


%% Now do analysis. We will loop through multistep trajectories and do
analysis
clear all
close all
clc

pathMovies = '~/Desktop/Step project/all movies';
% path of trajectories
pathTrajectories = '~/Desktop/Step project/multiple steps tracks';
pathEdges = '~/Desktop/Step project/multiple step edge';
pathBrightfield = '~/Desktop/Step project/multiple steps brightfield';
list = dir([pathTrajectories '/*.mat']);
n = size(list,1);
doFlat = 1;
SS = 0;

%%%%% this part is a test for combining single step analysis with
multiple
%%%%% steps
% pathTrajectories = '~/Desktop/Step project/Matlab tracks';
% pathEdges = '~/Desktop/Step project/step edge';
% pathBrightfield = '~/Desktop/Step project/all movies brightfield';
% list = dir([pathTrajectories '/*.mat']);
% n = size(list,1);
% doFlat = 0;
% SS = 1;
%%%%%%%%%%

% create holder for ups, downs, and attempts for all topographies
allUp = nan(20,7);
allDown = nan(20,7);
allUpDownDates = cell(20,7);
attemptsUp = nan(20,7);
attemptsDown = nan(20,7);
crossTimes = cell(n,7);
maxExtent = cell(n,7);
travelAngle = cell(n,7);
allSurfaces = [0 0.5 1 2 3 5 10];

% we will need to create boundary lines away from the step edge
```

```
% define d here
d = 5;
% begin looping through each trajectory

% define some plotting flags for visualization and troubleshooting
plotting = 0;
troubleshootBorders = 0;

nStepUp_I = 0;
nStepUp_II = 0;
nStepDown_I = 0;
nStepDown_II = 0;

for i = 1:n
    % load trajectories and edges
    load([pathTrajectories '/' list(i).name])
    load([pathBrightfield '/' list(i).name])
    load([pathMovies '/' list(i).name]);
    % grab surface name
    filename = list(i).name;
    surface = filename(1:strfind(filename,'um')-1);
    trackName = filename(1:end-4);
    nearIDs = zeros(1,2);
    crossingIDs = zeros(1,2);
    date = filename(end-9:end-4);

    disp(filename)

    if doFlat ~= 1
        if strcmp(surface,'0') == 1
            continue
        end
    end

    load([pathEdges '/' list(i).name])

    % old edge data is named boundary_line, so here we change it to
the
    % most recent nomenclature.
    if exist('boundary_line') == 1
        coeffsHolder = [boundary_line(1,2), boundary_line(1,1)];
    end

    % check if this is a single or multiple step
    jEnd = size(coeffsHolder,1);

    if jEnd == 1 && strcmp(surface,'0') == 1
        break
    end

    % next need to create vectors to determine if a bacterium is
crossing a
```

```
    % step. this can handle single or multiple steps
    % create holders for the different steps
    minus_vectorHolder = zeros(jEnd,4);
    plus_vectorHolder = zeros(jEnd,4);
    x = 1:528;
    yHolder = zeros(4,size(x,2));
    y_minusHolder = zeros(4,size(x,2));
    y_plusHolder = zeros(4,size(x,2));
    slope = zeros(4,1);
    b_minus = zeros(4,1);
    b_plus = zeros(4,1);
    b = zeros(4,1);
    minus_line = cell(4,1);
    plus_line = cell(4,1);
    plus_side = zeros(4,1);
    minus_side = zeros(4,1);

    if exist('stackBg') == 1
        image = stackBg(:,:,1);
    elseif exist('stack_bg') == 1
        image = stack_bg(:,:,1);
    end
    if exist('stack') == 1
        maxImage = max(stack,[],3);
    elseif exist('stackB') == 1
        maxImage = max(stackB,[],3);
    end
    cimage = combine_image(addScaleBar(image,20,0.36),maxImage);

    figure;
    imshow(cimage)
    hold on

%     close all
%     image(289:290,283:283+14) = 0;
%             figure;
%         imshow(image)
%         hold on
    for j = 1:jEnd

        % calculate x and y of the boundary line
        x = 1:528;
        y = polyval([coeffsHolder(j,2) coeffsHolder(j,1)],x);
        % calculate angle of this line
        theta = atand(coeffsHolder(j,2));
        b(j,1) = coeffsHolder(j,1);
        slope(j,1) = coeffsHolder(j,2);

        % calculate the offset needed to make parallel lines that are
d pixels away
        bshift = abs(d/cosd(theta));
        b_minus(j,1) = b(j,1)-bshift;
```

```
        b_plus(j,1) = b(j,1)+bshift;
        boundary_line_minus = [slope(j,1) b_minus(j,1)];
        boundary_line_plus = [slope(j,1) b_plus(j,1)];
        y_minus = polyval(boundary_line_minus,x);
        y_plus = polyval(boundary_line_plus,x);

        % define which side is the high and low sides
        % There are 4 steps and the order should always be high, low,
high,
        % low, high. So for j = 1 (or odd numbers), we go from high to
low. for j = 2, we go
        % from low to high.
        if mod(j,2) == 1
            % j is odd, this is high to low step
            plus_side(j) = 1;
            minus_side(j) = 0;
        elseif mod(j,2) == 0
            % j is even, this is a low to high step
            plus_side(j) = 0;
            minus_side(j) = 1;
        end

        minus_line{j,1} = [x(1) y_minus(1); x(end) y_minus(end)];
        plus_line{j,1} = [x(1) y_plus(1); x(end) y_plus(end)];

        % create a inward normal vector for the minus and plus lines
        perp_theta = theta-90;
        perp_slope = tand(perp_theta);
        y1 = median(1:432);
        x1 = (y1-b(j,1))/slope(j,1);
        perp_b = y1-perp_slope*x1;
        perp_y = polyval([perp_slope perp_b],x);

        % find intersection of perp line with minus line, edge line
and plus line
        xi_minus = (perp_b-b_minus(j,1))/(slope(j,1)-perp_slope);
        xi_edge = (perp_b-b(j,1))/(slope(j,1)-perp_slope);
        xi_plus = (perp_b-b_plus(j,1))/(slope(j,1)-perp_slope);
        yi_minus = slope(j,1)*xi_minus + b_minus(j,1);
        yi_edge = slope(j,1)*xi_edge+b(j,1);
        yi_plus = slope(j,1)*xi_plus+b_plus(j,1);

        % create the vectors. we will use these to determine if a
bacterium enters
        % or leaves the plus and minus sides
        minus_vector = [xi_minus,yi_minus,xi_edge-xi_minus,yi_edge-
yi_minus];
        plus_vector = [xi_plus,yi_plus,xi_edge-xi_plus,yi_edge-
yi_plus];

        % write boundary lines to holder
        minus_vectorHolder(j,:) = minus_vector;
```

```
        plus_vectorHolder(j,:) = plus_vector;
        yHolder(j,:) = y;
        y_minusHolder(j,:) = y_minus;
        y_plusHolder(j,:) = y_plus;

%         plot(x,y,'r-','linewidth',6)
%         plot(x,y_minus,'r--','linewidth',6)
%         plot(x,y_plus,'r--','linewidth',6)

    end

    % initialize counter for steps up and down
    step_up = 0;
    step_down = 0;
    time_cross = 0;
    travel_angle = 0;
    max_dist = 0;
    attempts_minus = 0;
    attempts_plus = 0;
    crossingTr = zeros(1,6);

    % begin main looping through each bacterium
    id = unique(tr(:,4));
    for q = 1:size(id,1)
        foo1 = tr(tr(:,end) == id(q),:);
        % search this bacterium's trajectory frame by frame
        crossed = 0;
        for j = 1:size(foo1,1)
            % is this bacterium in the strike zone?
            % use the two parallel strike zone lines to test if the
point is
            % between them
            xy = foo1(j,1:2);
            test_zone = xy(2)-slope*xy(1);
            % this value must be between b_minus and b_plus
            % note with the multistep experiment, there are now 4
zones to
            % test.
            if any(min([b_minus b_plus],[],2) < test_zone & test_zone
< max([b_minus b_plus],[],2))
                % bacterium is in one of the zones. which edge is it?
                % edge will determine which edge step to test
                edge = find(min([b_minus b_plus],[],2) < test_zone &
test_zone < max([b_minus b_plus],[],2) == 1);
                % this bacteria is in the zone
                %
plot(xy(1),xy(2),'rx','markersize',10)
                % which side is it on?
                if min([b_minus(edge,1) b(edge,1)]) < test_zone(edge)
&& test_zone(edge) < max([b_minus(edge,1) b(edge,1)])
                    % on minus side
                    which_side = -1;
```

```
                    attempts_minus = attempts_minus + 1;
                elseif min([b(edge) b_plus(edge)]) < test_zone(edge)
&& test_zone(edge) < max([b(edge) b_plus(edge)])
                    % on plus side
                    which_side = +1;
                    attempts_plus = attempts_plus + 1;
                end
                % save this ID number. use this to make the near
                % trajectories
                nearIDs = vertcat(nearIDs,[foo1(j,end) which_side]);
                % create new set to search for crossings from this
point on
                foo2 = foo1(j:end,:);
                for k = 2:size(foo2,1)
                    if crossed == 1
                        break
                    end
                    % create its displacement line for frame 1 to j
                    bacteria_line = [foo2(1,1) foo2(1,2); foo2(k,1)
foo2(k,2)];
                    bacteria_vector = [foo2(1,1) foo2(1,2) foo2(k,1)-
foo2(1,1) foo2(k,2)-foo2(1,2)];
                    % does this line cross to the other side? if
bacteria
                    % starts on minus side, it must cross to plus side
and vice
                    % versa.
                    if which_side == -1
                        test_crossing =
isintersect(bacteria_line,plus_line{edge});
                        if test_crossing == 1
                            % this was a step from minus to plus
                            if minus_side(edge) == 0
                                step_up = step_up + 1;
                                last_dir = -1;

quiver(bacteria_vector(1),bacteria_vector(2),bacteria_vector(3),bacter
ia_vector(4),0,'color','r','linewidth',2,'maxheadsize',0.5)
                            elseif minus_side(edge) == 1
                                step_down = step_down + 1;
                                last_dir = +1;

quiver(bacteria_vector(1),bacteria_vector(2),bacteria_vector(3),bacter
ia_vector(4),0,'color','b','linewidth',2,'maxheadsize',0.5)
                            end
                            if minus_side(edge) == 0 && mod(edge,2) ==
0
                                % step up, even step number, type II
flow
                                nStepUp_II = nStepUp_II + 1;
                            elseif minus_side(edge) == 0 &&
mod(edge,2) == 1
```

```
                                % step up, odd step number, type I
flow
                                nStepUp_I = nStepUp_I + 1;
                            elseif minus_side(edge) == 1 &&
mod(edge,2) == 0
                                % step down, even step number, type II
flow
                                nStepDown_II = nStepDown_II + 1;
                            elseif minus_side(edge) == 1 &&
mod(edge,2) == 1
                                % step down, odd step number, type I
flow
                                nStepDown_I = nStepDown_I + 1;
                            end
                            % check how long it took to cross
                            time_cross = vertcat(time_cross,foo2(k,3)-
foo2(1,3));
                            % get indices of crossing
                            startCross = j; endCross = j+k-1;
                            % get angle between crossing with step
                            disp_vector = [foo2(k,1)-foo2(1,1)
foo2(k,2)-foo2(1,2)];
                            if last_dir == -1
                                travel_angle =
vertcat(travel_angle,angle_vector(minus_vector(1,3:4),disp_vector));
                            elseif last_dir == +1
                                travel_angle =
vertcat(travel_angle,angle_vector(plus_vector(1,3:4),disp_vector));
                            end
                            crossed = 1;
                            crossingIDs =
vertcat(crossingIDs,[foo2(k,end) foo2(k,end-1)]);
                            % what is the max distance travelled after
                            % crossing?
                            max_dist =
vertcat(max_dist,(((foo2(end,2)-foo2(k,2))^2+(foo2(end,1)-
foo2(k,1))^2)^0.5)*0.36);
                        end
                    elseif which_side == 1
                        test_crossing =
isintersect(bacteria_line,minus_line{edge});
                        if test_crossing == 1
                            % this was a step from plus to minus
                            if plus_side(edge) == 0
                                step_up = step_up + 1;
                                last_dir = -1;

quiver(bacteria_vector(1),bacteria_vector(2),bacteria_vector(3),bacter
ia_vector(4),0,'color','r','linewidth',2,'maxheadsize',0.5)
                            elseif plus_side(edge) == 1
                                step_down = step_down + 1;
                                last_dir = +1;
```

```
quiver(bacteria_vector(1),bacteria_vector(2),bacteria_vector(3),bacter
ia_vector(4),0,'color','b','linewidth',2,'maxheadsize',0.5)
                            end
                            if plus_side(edge) == 0 && mod(edge,2) ==
0
                                % step up, even step number, type II
flow
                                nStepUp_II = nStepUp_II + 1;
                            elseif plus_side(edge) == 0 && mod(edge,2)
== 1
                                % step up, odd step number, type I
flow
                                nStepUp_I = nStepUp_I + 1;
                            elseif plus_side(edge) == 1 && mod(edge,2)
== 0
                                % step down, even step number, type II
flow
                                nStepDown_II = nStepDown_II + 1;
                            elseif plus_side(edge) == 1 && mod(edge,2)
== 1
                                % step down, odd step number, type I
flow
                                nStepDown_I = nStepDown_I + 1;
                            end
                            % check how long it took to cross
                            time_cross = vertcat(time_cross,foo2(k,3)-
foo2(1,3));
                            % get indices of crossing
                            startCross = j; endCross = j+k-1;
                            % get angle between crossing with step
                            disp_vector = [foo2(k,1)-foo2(1,1)
foo2(k,2)-foo2(1,2)];
                            if last_dir == -1
                                travel_angle =
vertcat(travel_angle,angle_vector(minus_vector(1,3:4),disp_vector));
                            elseif last_dir == +1
                                travel_angle =
vertcat(travel_angle,angle_vector(plus_vector(1,3:4),disp_vector));
                            end
                            crossed = 1;
                            crossingIDs =
vertcat(crossingIDs,[foo2(k,end) foo2(k,end-1)]);
                            % what is the max distance travelled after
                            % crossing?
                            max_dist =
vertcat(max_dist,(((foo2(end,2)-foo2(k,2))^2+(foo2(end,1)-
foo2(k,1))^2)^0.5)*0.36);
                        end
                    end
                end

                break
```

```
            end

        end


        newTrtemp = zeros(size(foo1,1),6);
        newTrtemp(:,1:2) = foo1(:,1:2);
        newTrtemp(:,5:6) = foo1(:,3:4);
        crossingColumn = zeros(size(foo1,1),2);
        if crossed == 1
            crossingColumn(startCross:endCross,:) = [ones(endCross-
startCross+1,1) ones(endCross-startCross+1,1).*last_dir];
        end
        newTrtemp(:,3:4) = crossingColumn;
        crossingTr = vertcat(crossingTr,newTrtemp);
    end
    time_cross = time_cross(2:end).*30/60;      % this is now in
minutes
    % truncate these matrices
    nearIDs = nearIDs(2:end,:);
    crossingIDs = crossingIDs(2:end,:);
    travel_angle = travel_angle(2:end,:);
    crossingTr = crossingTr(2:end,:);

%     % check if crossingTr is same size as tr
%     if size(tr,1) == size(crossingTr,1)
%         disp('equal size')
%     else
%         disp('not equal size')
%     end

    timeAngle = [travel_angle, time_cross];

    % figure out which column to place data in
    index = find(allSurfaces==str2double(surface));
    % now save all the data
    allUp(sum(double(~isnan(allUp(:,index))))+1,index) = step_up;
    allDown(sum(double(~isnan(allDown(:,index))))+1,index) =
step_down;

allUpDownDates{sum(double(~cellfun(@isempty,allUpDownDates(:,index))))
+1,index} = date;
    attemptsUp(sum(double(~isnan(attemptsUp(:,index))))+1,index) =
attempts_minus;
    attemptsDown(sum(double(~isnan(attemptsDown(:,index))))+1,index) =
attempts_plus;
    crossTimes{q,index} = time_cross;
    maxExtent{q,index} = max_dist;
    travelAngle{q,index} = travel_angle;

    % look at MSD of near IDs bacteria
    % take all bacteria in tracks file and split MSD into x and y
```

```
    % directions
    [msdX,msdY,msd] =
msdXY(tr(ismember(tr(:,end),crossingIDs(:,1)),:),30,0.36);

    % look at dr left and right as function of distance away from step
    dt = 10; pixelScaling = 0.36;
    [drXUp,drXDown,drYUp,drYDown,allDist2Step] =
drDist2step(tr,dt,coeffsHolder,plus_vectorHolder,minus_vectorHolder,pi
xelScaling,image);

    % save metrics
    save(['~/Desktop/Step project/multiple steps drXUp/'
list(i).name(1:end-4) '.mat'],'drXUp')
    save(['~/Desktop/Step project/multiple steps drYUp/'
list(i).name(1:end-4) '.mat'],'drYUp')
    save(['~/Desktop/Step project/multiple steps drXDown/'
list(i).name(1:end-4) '.mat'],'drXDown')
    save(['~/Desktop/Step project/multiple steps drYDown/'
list(i).name(1:end-4) '.mat'],'drYDown')
    save(['~/Desktop/Step project/multiple steps dist2step/'
list(i).name(1:end-4) '.mat'],'allDist2Step')
    save(['~/Desktop/Step project/crossing angle/' list(i).name(1:end-
4) '.mat'],'travel_angle')
    save(['~/Desktop/Step project/crossing time/' list(i).name(1:end-
4) '.mat'],'time_cross')
    save(['~/Desktop/Step project/crossingTr/' list(i).name(1:end-4)
'.mat'],'crossingTr')
    save(['~/Desktop/Step project/timeAngle/' list(i).name(1:end-4)
'.mat'],'timeAngle')

    export_fig(['~/Desktop/Step project/crossing figures/'
list(i).name(1:end-4) '.tif'],'-r300')

    close all

     % reset some variables for next loop
    if exist('stack_bg') == 1
        clear stack_bg
    elseif exist('stackBg') == 1
        clear stackBg
    end
    clear boundary_line
    if exist('stack') == 1
        clear stack
    end
    if exist('stackB') == 1
        clear stackB
    end

end

% save final metrics
```

```
if SS == 0
    % these are multisteps
    save('~/Desktop/Step project/up down
dates/allUpDownDates.mat','allUpDownDates')
    save('~/Desktop/Step project/allUp/allUpMS.mat','allUp')
    save('~/Desktop/Step project/allDown/allDownMS.mat','allDown')
    save('~/Desktop/Step
project/attemptsUp/attemptsUpMS.mat','attemptsUp')
    save('~/Desktop/Step
project/attemptsDown/attemptsDownMS.mat','attemptsDown')
elseif SS == 1
    save('~/Desktop/Step project/up down
dates/allUpDownDates.mat','allUpDownDates')
    save('~/Desktop/Step project/allUp/allUpSS.mat','allUp')
    save('~/Desktop/Step project/allDown/allDownSS.mat','allDown')
    save('~/Desktop/Step
project/attemptsUp/attemptsUpSS.mat','attemptsUp')
    save('~/Desktop/Step
project/attemptsDown/attemptsDownSS.mat','attemptsDown')
end
```

Characterizing local curvature of steps in Chapter 4

```
% look at bacteria crossing the step edge and see if the local
curvature
% affects crossings
% to get local curvature, do cubic spline fit to a step edge

% version 2
% 181129
% changed which frame we use for cubic splines
% prior version did cubic spline for each image
% this uses the first frame or the max image frame i.e. we use one
frame
% for the cubic spline fit
% this prevents small changes in brightfield intensity to affect the
cubic
% spline and thus change the local curvature from spline fits

%% initialize script
close all
clear all
clc

% grab a crossingTr file, use it to grab associated brightfield and
% fluorescence stack images
[fn, fp] = uigetfile('~/Desktop/Step project 2/crossingTr/');
load([fp fn])
loc = find(fp == '/');
fileBrightfield = [fp(1:loc(end-1)) 'brightfield/' fn];
load(fileBrightfield);
fileStacks = [fp(1:loc(end-1)) 'stacks/' fn];
load(fileStacks)


%% load a brighfield stack
% define the first image and max images
image = stackBg(:,:,1);
maxImage = max(stackBg,[],3);
[m,n,p] = size(stackBg);

% do cubic spline fits for each image
% set default values for inputs
threshMethod = 0;
nKnots = 180;
pixScaling = 0.36;
plotFlag1 = 1;
plotFlag2 = 1;
knotFlag = 0;

% adjust the contrast
image2 = imadjust(image);
% do simple threshold
```

```
if threshMethod == 0
    bw = imbinarize(image2,graythresh(image2));
end
% invert the image
bw = ~bw;
% fill in any holes
bw = imfill(bw,'holes');
% remove large isolated objects
bw = bwareaopen(bw,100);
% the step is the bw image
step = bw;
% show it if plot flags are on
if plotFlag1 == 1
    h(1) = figure;
    set(gcf,'color','w')
    imshow(image2)
    hold on
end
if plotFlag2 == 1
    h(2) = figure;
    set(gcf,'color','w')
    ax1 = axes;
    imagesc(image2)
    xlim([1 n])
    ylim([1 m])
    colormap(ax1,'gray')
    ax1.Visible = 'off';
    ax2 = axes;
end
% grab the connected pixels in the bw image
connectedPixels = bwconncomp(step);
% this is the number of steps
numSteps = size(connectedPixels.PixelIdxList,2);
% there should be 4 step edges
if numSteps ~= 4
    disp('Number of steps does equal 4. Check thresholding')
    return
end
% create holder for step edges
radii = cell(numSteps,1);
rotspDataHolder = cell(numSteps,1);

% begin going through each step
% loop through the number of grouped objects
for i = 1:numSteps
    % grab the pixel of this object
    [stepPixelsX,stepPixelsY] =
ind2sub([m,n],connectedPixels.PixelIdxList{1,i});
    % first fit a trend line through the data to determine overall
tilt
    fiteq = fittype('(x-b)./m');
    fitx = fit(stepPixelsX,stepPixelsY,fiteq,'startpoint',[1 1]);
    coeffs = coeffvalues(fitx);
```

```
    boundary_line = [coeffs(2) coeffs(1)];
    fit_x = 1:n;
    fit_y = polyval(boundary_line,fit_x);
    coeffsHolder(i,:) = coeffs;
    % look for local curvature of edge by cubic splines
    % first transform edge pixels by rotation to a horizontal line
such
    % that waveyness is in the y direction
    % get current angle
    theta = atand(coeffsHolder(1,2));
    % calculate the rotation matrix
    R = [cosd(theta) sind(theta); -sind(theta) cosd(theta)];
    Rinv = [cosd(-theta) sind(-theta); -sind(-theta) cosd(-theta)];
    Rdata = R*[stepPixelsY' ;stepPixelsX'];
    Rx = Rdata(1,:);
    Ry = Rdata(2,:);
    % now do cubic spline
    xint = round(min(Rx),0):0.1:round(max(Rx),0);
    sp = spap2(nKnots,3,Rx,Ry);
    % grab the knots of the splines
    xKnot = sp.knots;
    yKnot = fnval(sp,xKnot);
    % take first derivative
    spD = fnder(sp,1);
    % take second derivative
    spDD = fnder(sp,2);
    % evaluate cubic spline at xint
    spEval = fnval(sp,xint);
    % evaluate first derivative at xint
    spDEval = fnval(spD,xint);
    % evaluate second derivative at xint
    spDDEval = fnval(spDD,xint);
    % calculate local curvature
    radii{i,1} = (((1+spDEval.^2).^(3/2))./spDDEval)';
    % re-assign the sign in reference to where the solid is
    % the order of the steps goes: high, low, high, low, high
    % so from left to right, the steps are solid-liquid, liquid-solid,
    % solid-liquid, liquid-solid. So if the step number is odd, the
    % interface goes solid-liquid and if the step number is even, the
    % interfaces goes liquid-solid
    % we will define the sign of curvature in reference to the solid
e.g.
    %%%% note radii is still in units of pixels %%%
    if mod(i,2) == 0
        % even number
        % the interface is liquid-solid
        % flip the sign
        % also correct the sign of radii
        radii{i,1} = -1.*radii{i,1};
    elseif mod(i,2) == 1
        % odd number
        % the interface is solid-liquid
        % no need to flip the sign
```

```
        % also correct the sign of radii
        radii{i,1} = 1.*radii{i,1};
    end
    % rotate data back and plot on original image to compare
    spData = [xint;spEval];
    rotspData = (Rinv*spData)';
    %%% rotspDataHolder contains the xy position of the fitted spline
along
    %%% with the local radii of curvature calculated at that point
    rotspDataHolder{i,1} = [rotspData radii{i,1}];
    xyKnot = [xKnot;yKnot];
    rotxyKnot = [Rinv*xyKnot]';
    % plot the sign of curvature onto the brightfield image
    if plotFlag1 == 1
        % plot1 is the brightfield image overlayed ontop of identified
positive and
        % negative curvature areas.
        figure(h(1))
        plot(rotspData(sign(radii{i,1}) ==
1,1),rotspData(sign(radii{i,1}) ==
1,2),'go','markersize',4,'markerfacecolor','g')
        plot(rotspData(sign(radii{i,1}) == -
1,1),rotspData(sign(radii{i,1}) == -
1,2),'ro','markersize',4,'markerfacecolor','r')
        set(gca,'fontsize',40)
        set(gcf,'color','w')
        [~,icons] = legend('Positive','Negative');
        icons = findobj(icons,'type','line');
        icons = findobj(icons,'marker','none','-xor');
        set(icons,'markersize',16)
    end
    if plotFlag2 == 1
        % plot2 is the brightfield image overlayed ontop of color
coded
        % radii of curvature magnitudes
        figure(h(2))
        colorMap = parula(10);
        xBins = linspace(0,10,11);
        temp = radii{i,1}*pixScaling;      % convert to length
        data = abs(temp);                   % take absolute value
        for j = 1:10
            if j < 10
                indx = data(:,1)<xBins(j+1) & data(:,1)>xBins(j);
            elseif j == 10
                indx = data(:,1)>xBins(j);
            end

plot(ax2,rotspData(indx,1),rotspData(indx,2),'o','color',colorMap(j,:)
,'markerfacecolor',colorMap(j,:));
            hold on
        end
        if knotFlag == 1
```

```
            hKnots =
plot(ax2,rotxyKnot(:,1),rotxyKnot(:,2),'r^','markerfacecolor','r');
        end
    end
end
figure(h(2))
xlim(ax2,[1 n])
ylim(ax2,[1 m])
% xlim(ax3,[1 n])
% ylim(ax3,[1 m])
set(ax2,'ydir','reverse')
% set(ax3,'ydir','reverse')
colormap(ax2,'parula')
caxis([0 10])
ax2.Visible = 'off';
% ax3.Visible = 'off';
linkprop([ax1,ax2],{'Position','xlim','ylim'});
hbar = colorbar('fontsize',40,'linewidth',1.5);
ylabel(hbar,['Radii of curvature / ' char(181) 'm'])
if knotFlag == 1
    legend(hKnots,'Spline knots')
    set(gca,'fontsize',40)
end

% calculate the spline width
splineWidth = ((max(xint)-min(xint))/90).*pixScaling;

% if the spline fit and radii of curvature look good, save it and
continue with
% crossing analysis
save(['~/Desktop/Step project 2/edgeSpline/' fn],'rotspDataHolder');

%% load crossingTr data
% find crossing bacteria
crossings = crossingTr(crossingTr(:,6) == 1,:);
% grab id numbers of these bacteria
crossingIDs = unique(crossings(:,end));
% Initialize holder for list of curvatures
RCurvatureList = 0;
% Initialize holder for positive/negative curvatures for each
bacterium
RCurvatureSignList = zeros(size(crossingIDs,1),3);

% go through each id number
for i = 1:size(crossingIDs)
    % grab data
    data = crossingTr(crossingTr(:,end) == crossingIDs(i),:);
    % was this step up or down
    figure(h(2))
    if sum(data(:,7)) > 0
        % step up
```

```
        g(1) = plot(ax2,data(:,1),data(:,2),'ro-
','markersize',10,'markerfacecolor','r');
    elseif sum(data(:,7)) < 0
        % step down
        g(2) = plot(ax2,data(:,1),data(:,2),'bo-
','markersize',10,'markerfacecolor','b');
    end
    % what time points is it crossing?
    % recall that in tr, frames start at 0 so add 1
    crossingFrames = data(data(:,6)== 1,end-1)+1;
    % grab the brightfield images
    tempStack = stackBg(:,:,crossingFrames);
    % grab the fluorescence images
    tempStackF = stackB(:,:,data(:,end-1)+1);
    % make max image of tempStackF
    maxtempStackF = max(tempStackF,[],3);
    maxtempStackF = imadjust(maxtempStackF);
    % get size of tempStack
    [m,n,p] = size(tempStack);
    % for each time point, see if body of bacterium intersects with
the step
    % edge, record the sign of curvature
    nTime = size(data,1);
    % get xy points of the ellipse
    ellipsePoints = ellipseXY(data(:,1:5));
    % initialize counters
    nPositiveTotal = 0;
    nNegativeTotal = 0;
    % loop through each step edge
    for k = 1:numSteps
        % grab the sign and radius of this step edge
        RSign = sign(radii{k,1});
        RCurvature = radii{k,1};
        RDataPoints = rotspDataHolder{k,1};
        % loop through each frame
        for j = 1:nTime
            % grab points of the ellipse
            dataXY = ellipsePoints{j,1};
            % test if any points of the edge line are in the ellipse
            testHolder =
inpolygon(RDataPoints(1,:),RDataPoints(2,:),dataXY(:,1),dataXY(:,2));
            intersectedPoints = RSign(logical(testHolder),1);
            % count the number of positive and negative curavture
points
            nPositive = size(intersectedPoints(intersectedPoints ==
1),1);
            nNegative = size(intersectedPoints(intersectedPoints == -
1),1);
            nPositiveTotal = nPositiveTotal + nPositive;
            nNegativeTotal = nNegativeTotal + nNegative;
            % compile a list of the radii of curvature
            RCurvatureList =
vertcat(RCurvatureList,RCurvature(logical(testHolder),1));
```

```
        end
    end
    RCurvatureSignList(i,:) = [crossingIDs(i) nPositiveTotal
nNegativeTotal];
end
legend(g,'Step up','Step down')
set(gca,'fontsize',40)



save(['~/Desktop/Step project 2/interactionCurvature/'
fn],'RCurvatureList');
save(['~/Desktop/Step project 2/interactionSign/'
fn],'RCurvatureSignList');

%% make histogram of radii of curvature of step and overlay with
crossing radii
w = 0.5;
h(3) = figure;
histogram(abs(vertcat(radii{:,1})).*0.36,0:w:10,'normalization','proba
bility')
title('Radii of curvature of step edge')
xlabel(['R / ' char(181) 'm'])
ylabel('Probability')
make_pretty

w = 0.5;
h(4) = figure;
histogram(abs(vertcat(radii{:,1})).*0.36,0:w:10,'normalization','proba
bility')
hold on
histogram(abs(RCurvatureList).*0.36,0:w:10,'normalization','probabilit
y')
xlabel(['R / ' char(181) 'm'])
ylabel('Probability')
make_pretty
legend('Step edge','Bacteria interactions')
exportFigure('Radii_curvature_interaction_10um_example')



%% load multiple files and plot radii of curvature of step edge and
compare with "interaction radii"
close all
clear all
clc
pathRadii = '~/Desktop/Step project 2/edgeSpline/';
pathInteractions = '~/Desktop/Step project 2/interactionCurvature/';

% find how many files we have
list = dir(pathRadii);
```

```
list = list(~ismember({list.name},{'.','..','.DS_Store'}));
n = size(list,1);

% create holder for radii data
holder = cell(n,1);
radiiList = 0;
for i = 1:n
    % get file name
    fileName = list(i).name;
    % load radii data
    load([pathRadii '/' fileName])
    holder{i,1} = rotspDataHolder;
    data = vertcat(rotspDataHolder{:,1});
    % convert radii data to units of micrometers
    radiiData = data(:,3).*0.36;
    % compile list
    radiiList = vertcat(radiiList,radiiData);
end

% create holder for interaction radii data
holder2 = cell(n,1);
radiiInteractionList = 0;
for i = 1:n
    % get file name
    fileName = list(i).name;
    % load radii interactiondata
    load([pathInteractions '/' fileName])
    holder2{i,1} = rotspDataHolder;
    data = vertcat(rotspDataHolder{:,1});
    % convert radii data to units of micrometers
    radiiData = data(:,3).*0.36;
    % compile list
    radiiList = vertcat(radiiList,radiiData);
end
```

Denoising trajectory data for fast framerate data

```
function denoisedTr = denoise(tr,pixThreshold)

% function to apply denoising algorithm to track data
% denoisedTr = denoise(tr,pixThreshold)
% method based on Jin et al., 2011 PNAS
% denoise x and y centroid data, assume that length, width and
orientation
% are not affected, then calculate poles and re-write tr
% inputs are
%   - tr                track matrix with 11 columns
%   - pixThreshold      choice of pixel threshold to do denoising
procedure
% outputs are
%   - denoisedTr        track matrix with the centroid x y position
%                       denoised

% get the number of ID numbers
ids = unique(tr(:,end));
% create a holder for the new denoised data
denoisedTr = cell(size(ids,1),1);
warning off
% begin looping through each ID number
for i = 1:size(ids,1)
    disp([num2str(i) ' of ' num2str(size(ids,1))])
    % grab data of this ID number
    data = tr(tr(:,end) == ids(i),:);
    n = size(data,1);
    % create a new denoised dataset holder for x and y data
    % denoise the center position
    newData = zeros(n,3);
    % calculate difference between points to determine segments
    point1x = data(1,1);
    indxX = 1;
    for j = 2:n
        delta = abs(data(j,1) - point1x);
        if delta > pixThreshold
            indxX = vertcat(indxX,j);
            point1x = data(j,1);
        end
    end
    indxX = vertcat(indxX,n);
    % do the same for y
    point1y = data(1,2);
    indxY = 1;
    for j = 2:n
        delta = abs(data(j,2) - point1y);
        if delta > pixThreshold
            indxY = vertcat(indxY,j);
            point1y = data(j,2);
        end
```

```
    end
    indxY = vertcat(indxY,n);
    % data inbetween indx points are segments to do linear regression
    for j = 2:size(indxX,1)
        segment = data(indxX(j-1):indxX(j),:);
        fitpara = polyfit(segment(:,end-1),segment(:,1),1);
        fittedY = polyval(fitpara,segment(:,end-1));
        newData(indxX(j-1):indxX(j),1:2) = [segment(:,end-1) fittedY];
    end
    % do the same for y data now
    for j = 2:size(indxY,1)
        segment = data(indxY(j-1):indxY(j),:);
        fitpara = polyfit(segment(:,end-1),segment(:,2),1);
        fittedY = polyval(fitpara,segment(:,end-1));
        newData(indxY(j-1):indxY(j),3) = [fittedY];
    end
    % calculate the poles
    c = ((data(:,3)./2).^2-(data(:,4)./2).^2).^0.5;
    dx = c.*cosd(-data(:,5));
    dy = c.*sind(-data(:,5));
    f1x = newData(:,2)+dx;
    f2x = newData(:,2)-dx;
    f1y = newData(:,3)+dy;
    f2y = newData(:,3)-dy;
    % assign the lead and trailing pole by looking at the overall
    % displacement
    dispFinal = [data(1,1) data(1,2) data(end,1)-data(1,1)
data(end,2)-data(1,2)];
    p1 = [data(1,1) data(1,2) data(1,6)-data(1,1) data(1,7)-
data(1,2)];
    p2 = [data(1,1) data(1,2) data(1,8)-data(1,1) data(1,9)-
data(1,2)];
    p1theta = angle_vector(dispFinal(3:4),p1(3:4));
    if p1theta < 90
        % p1 is the leading pole
        % reconstruct tr matrix
        denoisedTr{i,1} = [newData(:,2) newData(:,3) data(:,3:5) f1x
f1y f2x f2y newData(:,1) ones(n,1).*ids(i)];
    else
        % reconstruct tr matrix
        denoisedTr{i,1} = [newData(:,2) newData(:,3) data(:,3:5) f2x
f2y f1x f1y newData(:,1) ones(n,1).*ids(i)];
    end
end
denoisedTr = vertcat(denoisedTr{:,1});

end
```